Array Signal Processing for Communications from High Altitude Platforms and Other Applications

Zhengyi Xu
Communications Research Group
Department of Electronics
University of York

This thesis is submitted in partial fulfilment of the requirements for Doctor of Philosophy (Ph.D.)

December 2007

Abstract

Digital beamforming (DBF) technology using antenna array has reached a sufficient level of maturity that it can be applied to communications to improve system capacity. In this thesis, the applications to digital beamforming in the communications from high altitude platforms (HAPs) and the high data rate OFDM signal transmission in underwater acoustic channel are respectively investigated.

Both conventional and adaptive beamforming methods are investigated in the application to HAP communications. A three-step footprint optimization method based on planar array and hexagonal cellular structure is proposed to generate arbitrary beampattern footprints. A vertical antenna array forming ring-shaped cells is shown to improve the coverage performance and reduce system complexity. In the adaptive beamforming scenario, the minimum variance distortionless response (MVDR) beamformer is investigated. We show that the robustness of the MVDR beamformer can be improved by applying the Mailloux's null-broadening method in the downlink scenario and propose a modified constrained optimization method, which further improves the performance of Mailloux's method. Finally, a method combining cellular and null-broadening adaptive beamforming is proposed. Simulation results show that the method achieves better coverage performance for cellular communications than when using the same number of aperture antennas. Its advantages in payload reduction are even more significant.

The adaptive beamforming techniques are also applied in the receiver design for high data rate OFDM signal transmission in the fast-varying underwater acoustic channel. This work is based on experimental data obtained in the Pacific Ocean at a distance of 30 km in 1989. Several space-time signal processing techniques are investigated. A variety of direction of arrival (DoA) estimation methods are considered, which are based on signal interpolation and the modified MVDR beamformer. The DoA estimates are used for angle-separation of signals for accurate time-delay compensation. The OFDM signals from different directions are linearly combined after Doppler compensation and channel equalization. An adaptive Doppler filter is applied in frequency domain for removing residual intersymbol interference. The null-broadening beamforming method,

originally proposed in the HAPs communications, is applied to improve the robustness of the MVDR beamformer. Experimental results show that the adaptive beamforming based space-time techniques are efficient and provide the bit-error-rate of 10^{-3} and 10^{-2} respectively for the data efficiency 0.5 bit/s/Hz and 1 bit/s/Hz.

Contents

Acknowledgements

I would like to thank my supervisor, Dr. Yuriy Zakharov, for all his advice, support and encouragement during the course of my Ph.D. study.

I am very grateful to Dr. George White, who used to be my thesis advisor. George provided a lot of ideas and helped me a lot especially during the beginning of my Ph.D. career. I would like express my thanks to Dr. John Thornton for some useful discussions.

Special thanks should be given to Dr. Rodrigo de Lamare and Prof. Andy Nix who are respectively my internal and external examiners. They contribute a lot of good suggestions to this thesis.

I would also like to thank all my colleagues in the Communications Research Group, University of York.

This thesis is dedicated to my parents who always support and encourage me during the last three years of my Ph.D. study in York.

Declaration

Some of the research presented in this thesis has resulted in some publications. These publications are listed at the end of the thesis.

All work presented in this thesis as original is so, to the best knowledge of the author. References and acknowledgements to other researchers have been given as appropriate.

List of Abbreviations and Acronyms

ADF	Adaptive Doppler Filter
ADHT	Angle-Dependent Homothetic Transformation
BER	Bit-error-rate
BPSK	Binary Phase Shift Keying
CDMA	Code-Division Multiple Access
CP	Cyclic Prefix
DBF	Digital Beamforming
DCD	Dichotomous Coordinate Descent
DICANNE	Digital Interference Cancelling Adaptive Null Network Equipment
DoA	Direction of Arrival
DSP	Digital Signal Processing
ESPRIT	Estimation of Signal Parameters via Rotational Invariance Technique
FDMA	Frequency-Division Multiple Access
FSPL	Free Space Path Loss
GEO	Geostationary
HAPs	High Altitude Platforms
HPBW	Half-Power Beamwidth
ICI	Intercarrier Interference
ISI	Intersymbol Interference
LCMV	Linear Constraint Minimum Variance
LEO	Low Earth Orbit
LMS	Least Mean Squares
LOS	Line of Sight
LPM	Linear Prediction Method
LS	Linear System
ML	Maximum Likelihood
MLM	Maximum Likelihood Method
MMIC	Monolithic Microwave Integrated Circuit
MMSE	Minimum Mean Square Error
MRIII	Madaline Rule III
MSE	Mean Square Error
MUSIC	Multiple Signal Classification
MVDR	Minimum Variance Distortionless Response
NAME	Noise-Alone Matrix Inverse
NLMS	Normalized Least Mean Squares
NN	Neural Network
OFDM	Orthogonal Frequency Division Multiplexing

RLS	Recursive Least Squares
SDMA	Space-Division Multiple Access
SDP	Semidefinite Programming
SINR	Signal-to-Interference-Plus-Noise Ratio
SNR	Signal-to-Noise Ratio
SOCP	Second Order Cone Programming
SOI	Signal of Interest
SPNMI	Signal-Plus-Noise Matrix Inverse
TDMA	Time-Division Multiple Access

List of Figures

List of Tables

Chapter 1

Introduction

Contents

1.1 Wireless Communications and Multiple Access

Wireless communications is one of the biggest engineering success stories of the last 20 years [1]. The evolution of telecommunications, from the wired phone to personal communications services, is resulting in availability of wireless services [2]. In providing different types of wireless services, such as fixed, mobile, outdoor, indoor and satellite communications, the wireless communications have changed our working habits, and even more generally the ways we all communicate.

A higher demand in wireless communications calls for higher systems capacities. The capacity of a communication system can be increased directly by enlarging the communications channel bandwidth. However, since the electromagnetic spectrum is limited,

efficient use of the frequency resource is crucial for the increase of the communications system capacity. The techniques of multiple access have been proved to provide high system capacity. Multiple access is a synonym for the channel access method - a scheme that allows several terminals connected to the same physical medium to transmit over it and share its capacity. There are four domains in which capacity sharing can take place: 1) frequency, 2) time, 3) code, or 4) space. These techniques are respectively referred to frequency - division multiple access (FDMA), time - division multiple access (TDMA), code - division multiple access (CDMA) and space - division multiple access (SDMA). FDMA divides the frequency spectrum into segments for different users and it was used to deploy first generation cellular systems in the early 80s [3]. With the arrival of digital techniques in the 90s, the techniques of TDMA and CDMA were widely used for the second generation digital cellular system [3, 4]. For TDMA systems, each user is apportioned the entire transmission resource periodically for a brief period of time, while for CDMA systems, each transmitted signal is modulated with a unique code that identifies the user.

SDMA is another widely used multiple access technique in wireless communications [2]. It allows the same carrier frequency to be reused in different cells. Communication signals that are transmitted at the same carrier frequency in different cells are separated by the minimum reuse distance to reduce the level of cochannel interference. The ultimate form of SDMA is to use steered beams at the same carrier frequency to provide service to an individual cell or user, which refers to the techniques of conventional (or cellular) beamforming and adaptive beamforming, respectively. These techniques have drawn considerable interest from the communications community in the recent 15 years [5–12].

1.2 Digital Beamforming (DBF)

The early concepts underlying digital beamforming (DBF) were first developed for applications in sonar [13] and radar systems [14]. DBF is based on well-established theoretical concepts which are now becoming practically exploitable, largely as a result of recent major advances in areas such as monolithic microwave integrated circuit (MMIC) technology and digital signal processing (DSP) technology [2, 3].

DBF is based on capturing the radio frequency signals at each of the antenna element and converting them into in-phase and quadrature-phase channels. The beamforming is then carried out by weighting the digital signals, thereby adjusting their amplitudes and phases such that when added together they form the desired beam. The antenna array

itself takes on a variety of geometries depending on the applications of interest [15]. The most commonly used configuration is the linear array, in which the antenna elements are spaced along a straight line. Another common configuration is a planar array, in which the elements form a rectangular grid or lie on concentric circles [15, 16]. A DBF antenna can be considered the ultimate antenna in the sense that it can capture all of the information that falls on the antenna elements. Since the beamforming instructions are driven by software routines, there is wide-ranging flexibility in the types of beams that can be produced, including scanned beams, multiple beams, shaped beams and beams with steered nulls. The user can therefore apply whatever signal processing is required to extract the information of interest.

Besides the applications in sonar and radar, DBF is also applied in the area of radio astronomy, seismology, tomography and image reconstruction [17]. However, in recent years, the application of DBF is receiving significant attention in the area of satellite and wireless communications, more specifically, personal communications services [18, 19]. In the following two sections, a brief introduction will be given to the two possible applications that are considered throughout the thesis.

1.3 Communications from High Altitude Platforms

High altitude platform (HAP) systems are aeroplanes or airships, operating in a quasi-stationary position at stratospheric altitudes of about 20 km [20]. The HAPs payload can be a complete base-station, or simply a transparent transponder, akin to the majority of satellites [20]. Since line of sight (LOS) paths can be readily obtained from HAPs, considerably less infrastructure may be required to serve the same coverage area, when compared with terrestrial services [21]. Compared with the satellite systems, HAPs systems suffer less free-space path loss (FSPL) (for the geostationary (GEO) satellite, the stratospheric altitude of 40000 km results in the FSPL of the order of 200 dB [20]). Other advantages of HAPs are that they experience little rain attenuation compared to terrestrial links over the same distance [21]. HAPs can be rapidly deployed and therefore they can be used in the emergency scenarios including natural disasters and military missions; HAPs systems require less cost than GEO satellites or a constellation of low earth orbit (LEO) satellites. Because of these advantages, HAPs have been considered as a possible future communications infrastructure, following terrestrial and satellite systems [22].

The HAP antenna is one of the most important parts in the whole system and it would constitute a significant part of the payload. However, the space and weight

available on a HAP may be limited. Therefore, optimal design of the antenna is crucial. One approach to the antenna design is to employ a set of distinct aperture antennas such as horn, lens or reflector antennas to provide one spot-beam per cell [23, 24]. This results in small sidelobe levels. For example, in [23], a flat -40 dB sidelobe level is achieved by lens antenna operating at a carrier frequency of around 28 GHz. Besides, elliptical beams are proposed to cover the equal-sized hexagonal cells. Hence a high system capacity can be achieved. However, the size and weight of such aperture antennas could be significant, which results in a huge antenna payload. For example, for a 121 cell layout and a 28 GHz carrier frequency, the antenna payload is approximately 40 kg [24]; here, dielectric lens antennas were assumed with an aperture radius up to 80 mm [23]. Any stabilization mechanism for the antenna would lead to an extra payload.

Another approach is based on the use of antenna arrays with beamforming signal processing techniques. This approach is further divided into conventional and adaptive methods, according to whether the beams are steered to cells or to users. Although the use of antenna array and DBF in application to HAPs communications has not been found much in the open literature, there are some related work from the literature for satellite applications [25, 26]. The adaptive beamforming methods may provide better coverage performance than the conventional beamforming methods, however, they require real-time implementation of advanced signal processing techniques, that would be a challenge especially for broadband applications [26]. The conventional beamforming applies weights to the array elements to steer a set of beams in order to form cells on the ground. Unlike the aperture antennas, the array antenna elements can typically be constructed from light weight printed circuits with the weighting around 3.5 kg/m^2, which could be two orders less than that of the dielectric lens antennas [27]. Therefore, the motivation of our work is to optimize the weights of antenna array elements to improve the coverage performance of HAPs communications while reducing the antenna payload. This work is partially supported by CAPANINA (FP6-IST-2003-506745) - an EU project for wireless broadband delivery from HAPs [28].

1.4 High Data Rate OFDM Signal Transmissions in the Underwater Acoustic Channel

As the second part of the work, we apply the DBF techniques in the scenario of underwater high data rate transmissions. The underwater acoustic channel is a challenging environment for reliable coherent communications [29]. The underwater channel is non-stationary because of moving transmitting and receiving antennas, and multiple

reflections of sound waves off the bottom and moving water surface. Communications in a time-varying multipath channel suffer from the intersymbol interference (ISI) which causes severe signal distortion and results in performance degradation in high data rate communications systems.

Orthogonal frequency division multiplexing (OFDM) [30] is one of the techniques for the signals transmission in the time-varying multipath channel. Originally, OFDM is adopted in radio communications systems as an efficient technique for high data rate transmission in frequency-selective channels. It uses a large number of closely-spaced orthogonal sub-carriers. Each sub-carrier is modulated with a conventional modulation scheme at a low symbol rate [31]. OFDM has the ability to cope with severe channel conditions such as multipath and narrowband interference and therefore simplifier the channel equalization and demodulation algorithms. Due to these significant advantages, OFDM signals have been used in the underwater acoustic channel to provide robustness against time-varying selective fading. Multiple experiments with data transmission using OFDM signals were carried out by the Acoustics Institute (Moscow) in 1987-1989 [32, 33]. In recent years, the use of OFDM signals has been considered as a promising technique for high data rate transmission in the underwater acoustic channel [34–36].

Based on the OFDM signal transmission, we apply the adaptive beamforming methods to improve the performance of underwater communications. More specifically, the adaptive beamformers can be used to estimate direction of arrival (DoA) information and separate arriving signals from the multipath. According to the DoA information, time-delay and Doppler can be accurately compensated, which improves the demodulation performance. We use the experimental data obtained in the Pacific Ocean in 1989 [33, 36]. The OFDM signals were transmitted by a fast moving (at a speed of 5 m/s) underwater transducer at a depth of 250 m. A linear vertical antenna array of omnidirectional elements, positioned at a depth of 420, was used for receiving the signals. The transmission data efficiency were 0.5 bit/s/Hz and 1 bit/s/Hz.

1.5 Beamforming Methods Considerations - A Literature Review

Antenna array processing involves manipulation of signals induced on various antenna elements. Its capabilities of steering nulls to reduce cochannel interferences and pointing independent beams toward various mobile users make it attractive to a wireless commu-

nications system designer. The difference between steering antenna array and steering distinct aperture antennas is that the antenna array is electrically steered by weighting each antenna element to change phases, while the aperture antennas are steered mechanically. The wide spread interest in the subject area has been maintained over decades. The first issue of IEEE Transaction on Antennas and Propagation was published in 1964 [37] and was followed by a series of special issues of adaptive antennas, adaptive processing and beamforming [38–40]. In this section, an overview of various beamforming methods is given.

1.5.1 Conventional beamformers

A beamformer is considered as conventional if the weights of the antenna elements are not adaptively updated. Therefore, such beamformer is suitable for the application of fixed cellular communications, for which, every beam for the corresponding fixed cell is generated independently. Any complex signal processing techniques can be accomplished off-line. The simplest conventional beamformer is the delay-and-sum beamformer with all its weights of equal magnitudes. The phases are selected to steer the array antenna in a particular direction, known as the look direction [41]. The array with these weights has unity response in the look direction. This method, however, exhibits high sidelobes, which could result in high co-channel interference.

Various solutions to antenna beampattern synthesizing have been proposed during the last several decades. In [42], the array pattern is optimized by minimizing a cost function built by the terms of the sidelobes levels, pattern directivity and excitation variability. Genetic algorithm [43] is applied to search for the minimum of the cost function due to its ability to escape from local minima and maxima. The searching time required for the genetic algorithm is shown to be less than exhaustive searching. Simulated annealing techniques [44] can be combined with the genetic algorithm to achieve substantial amount of array thinning (beamwidth narrowing) with optimal performance characteristics. Similar work can also be found in [45].

The theory of synthesizing asymmetric beampatterns using an unequally spaced antenna array has been studied in depth and is well documented. The analysis of unequally spaced antenna arrays originated with the work of Unz as early as 1960 [46], who developed a matrix formulation to obtain the current distribution necessary to generate a prescribed radiation pattern from an unequally spaced linear array. Recently, the related work on asymmetric beampattern designs can be found in [47–49]. It is shown in [50] that beampatterns of a linear unequally spaced array can be distinguished for the

steering angles $\pm\pi/2$, which is another advantage of using asymmetric beams, compared with the symmetric ones. By using the simulating annealing scheme, as in [42], it is possible to optimize simultaneously both the positions and the weights of all the array elements to obtain an asymmetric beampattern similar to the desired one. In [51], it is shown that for any fixed set of locations, the beampattern synthesizing problem is a convex programming problem. Taking into account this result, a hybrid approach is further proposed in [52], where convex programming is used to solve the beampattern synthesizing problem for fixed element positions and simulating annealing is used to find the optimal element positions as a global optimization. Sidelobes levels are improved by 5 dB, compared with the results in [50].

Other work have been focused on synthesis of planar array to generate arbitrary 2-dimensional footprint patterns. From the recent literature, such studies are used in the applications of satellite communications. In [53], a modified Woodward-Lawson method is proposed to synthesize arrays for arbitrary footprint shapes. This is followed by a series of methods based on angle-dependent homothetic transformation (ADHT) and sampling a circular Taylor distribution [54–56]. However, the drawback of the modified Woodward-Lawson method is that it requires the array to lie on a rectangular lattice and it approves incapable of synthesizing arrays radiating good rectangular footprints with aspect ratios greater than about $1.3:1$ due to the nonconvex of the array boundaries [57,58]. In [58], it is shown that such limitation can be significantly overcome by introducing a two-stage optimization. The purpose of the first stage is to define the physical configuration of the array as the set of elements and the second stage is the element excitation optimization to reduce ripples and sidelobe levels. As an extension to [57] and [58], a method is proposed, based on defining a spatial masking filter according to the desired beampattern, calculating the antenna aperture distribution which corresponds to this masking filter and the aperture size, and finally spatially sampling the aperture distribution at the antenna element positions [59]. This method allows a planar array with arbitrary geometry to generate arbitrary footprint patterns, which implies that such beampattern optimization technique using a planar array has the potential ability to be used for cellular communications with arbitrary cellular configurations.

1.5.2 Adaptive beamformers

Adaptive beamforming is a technique in which an array of antennas is exploited to achieve maximum reception in a specified direction by estimating the signal arrival from a desired direction (in the presence of noise) while signals of the same frequency from other directions are rejected. The underlying idea is that, though the signals emanating

from different transmitters occupy the same frequency channel, they still arrive from different directions. This spatial separation is exploited to separate the desired signal from the interfering signals. Therefore, beampatterns of adaptive beamformers are optimized only at the directions of desired signal and interferers. This makes an antenna array, to some extend, more 'directive' than when using conventional beamforming methods. However, the computational complexity makes it challenging for adaptive beamformers to be implemented especially for real-time and broadband applications.

A null-steering beamformer (or referred as Digital Interference Cancelling Adaptive Null Network Equipment(DICANNE)) is one of the earliest schemes of adaptive beamformers [60, 61]. It is designed to cancel a plane wave arriving from a known direction and thus produces a null in the response pattern in the DoA of the plane wave. This is achieved by estimating the signal arriving from a known direction by steering a conventional beam in the direction of the source and then subtracting the output of this from each element. The process is very effective for canceling strong interference and could be repeated for multiple interference cancellation. However, it is not designed to minimize the uncorrelated noise at the array output. It is possible to achieve this by selecting weights that minimize the mean output power subject to the above constraints [62].

The null-steering method requires knowledge of the directions of interference sources and the criteria does not maximize the output signal-to-noise-ratio (SNR). The problem is solved in [63, 64]. The weights are generated according to the correlation matrix of the noise without any information about the arriving signals. Such a method is also referred to as noise-alone matrix inverse (NAME) [65]. In practice, when the estimate of the noise-alone matrix is not available, the total correlation matrix (signal plus noise) is used to estimate the weights, which is referred to as the signal-plus-noise matrix inverse method (SPNMI). It is also known as the minimum variance distortionless response (MVDR) beamformer (or also referred to as Capon, Maximum likelihood (ML) filter) [41, 66]. The MVDR beamformer is considered as the optimal beamformer. It minimizes the total noise, including the interferences and uncorrelated noise, while keeping unit power for the desire signal. Therefore, the signal-to-interference-plus-noise ratio (SINR) is maximized.

Different from the methods mentioned above, there is a class of adaptive beamformer that employs reference signals. The reference signal is applied to obtain the error signal, which is further used to control the weights. Weights are adjusted such that the mean square error (MSE) between the array output and the reference signal is minimized. The minimum mean square error (MMSE) processer (also known as the Wiener filter) is the solution to the well known Wiener-Hopf equation [41, 67]. The Wiener filter

provides a higher output SNR than the ML filter, however, at the cost of signal distortion. The least mean squares (LMS) algorithm is one of the most important members of the steepest-descent family [67–69]. The algorithm updates the weights at each iteration by estimating the instant gradient of the quadratic MSE surface and then moving the weights in the negative direction of the gradient by a constant step. A data-dependent step can be substituted for the constant one to achieve better convergence performance and less signal sensitivity, which is referred to as the normalized LMS algorithm (NLMS) [70, 71]. The convergence of the LMS algorithm depends upon the eigenvalues of the correlation matrix. Therefore LMS may converge slow for a correlation matrix with a large eigenvalue spread. This problem is solved by the recursive least squares (RLS) algorithm [67, 72]. However, RLS involves high computational complexity and it may not work properly in finite-precision (fixed point) arithmetic, due to unstable round-off error propagation [73]. A neural network based algorithm - Madaline Rule III (MRIII) method is discussed in [74]. It minimizes the MSE between the reference signal and a modified array output instead of directly the array output as the algorithms mentioned previously. The algorithm is suitable for analog implementation, resulting in fast weight update. However, the global convergence of the MRIII is not guaranteed [74].

Most of the adaptive algorithms described above are computationally complex due to the reason that the inversion of the correlation matrix is required, such as NAME, MVDR, MMSE and RLS. Recently, a Dichotomous Coordinate Descent (DCD) algorithm is proposed to solve the linear systems (LS) equations [75, 76]. Without the operation of multiplication and division, the DCD algorithm provides a simple and efficient alternative to the current LMS and RLS algorithms. Due to the advantages of computational complexity reduction, the DCD algorithm is especially suitable for hardware implementation (on FPGA or ASIC platforms). Its FPGA implementation is discussed in [77]. In [78], the DCD algorithm is applied in the MVDR beamformer and implemented in FPGA. Instead of directly calculating the inversion of the correlation matrix, the new method estimates the multiplication of the inverse correlation matrix and the snapshots received by the antenna elements in order to avoid the bulky computational burden for the hardware implementation. This work shows the potential feasibility of the classical optimal beamformer (MVDR) for real-time applications.

It is well known that the data-dependent MVDR beamformer has better resolution and much better interference rejection capability than the conventional data-independent beamformers, provided that the steering vector corresponding to the signal of interest (SOI) is accurately known. However, the knowledge of the SOI steering vector can be imprecise, which is often the case in practice due to the differences between the assumed signal arrival angle and the true arrival angle. This makes the SINR of the MVDR method

degrade catastrophically. Many approaches have been proposed during the past three decades to improve the robustness of the MVDR beamformer. To account for the array steering errors, additional linear constraints, including point and derivative constraints, can be imposed to improve the robustness of the MVDR beamformer [79–81]. However, these constraints are not explicitly related to the uncertainty of the array steering vector. Diagonal loading is one of the most popular approaches in the literature. It chooses the beamformer to minimize the sum of the weighted array output power plus a penalty term, proportional to the square of the norm of the weight vector [82–84]. However, the loading factor is chosen in a more *ad hoc* way in these papers, typically about ten times of the noise power in a single antenna element [85]. In [85], a robust beamforming method is proposed to optimize the worst-case performance. This is achieved by minimizing the output interference-plus-noise power while maintaining a distortionless response for the worst-case (mismatched) signal steering vector. It is shown that the proposed beamformer can be interpreted as a diagonal loading approach and is solved by the second-order cone programming (SOCP). In the method presented in [86], uncertainty in the array manifold is modeled via an ellipsoid that gives the possible values of the array for a particular look direction. Weights are chosen that minimize the total weighted power output of the array, subject to the constraint that the gain should exceed unity for all array response in this ellipsoid. As in [85], the optimization problem can be cast as a SOCP problem and it is solved by the techniques of Lagrange multiplier. In [87], it is presented that the diagonal loading factor can be precisely calculated based on the ellipsoidal uncertainty set of the steering vector. The steering vector in the standard MVDR beamformer is then substituted by the estimated one based on the calculated loading factor and the same optimal weights are obtained as in [85]. Methods described in [85–87] can be considered as an extension of diagonal loading. However, the robust adaptive beamforming methods mentioned above are all designed for uplink scenario. To our best knowledge, the diagonal loading (and its extension form) based robust adaptive beamforming methods can not be applied in the downlink scenario. In recent literature, there are several, although not a lot, publications on robust downlink beamforming [88, 89]. In [88], a method is proposed which is based on the optimization criteria that minimizes the total transmit power while maintaining a certain level of downlink SINR. In [89], the statistical distribution of the uncertainty is exploited to minimize the total transmit power under the condition that the non-outage probability of each user in downlink is greater than a certain threshold. However, both methods achieve quite low performance (in terms of extremely high transmit power in total) when users are closely separated. Furthermore, the selection of the constrained parameter is still in an *ad hoc* way.

The MVDR beamformer places sharp nulls in the directions of interferers. Therefore, the presence of interferer motion does not provide sufficient nulling of the interferer

given the number of snapshots available. Different from the robust techniques described above, another efficient method is null-broadening [90–93]. The null-broadening concept was originally developed by Mailloux for beampattern synthesis [90]. A cluster of equal-strength incoherent artificial sources are distributed around each original source in order to generate a trough like beampattern. The null-broadening method requires DoA estimation to obtain steering knowledge. The main advantages of the null-broadening method are that it provides robustness for the inaccuracy of the DoA estimation and it can be simply implemented.

Although a lot of DBF schemes (both conventional and adaptive) have been developed in the literature, little work has been done in evaluating and comparing the conventional and adaptive beamformers in the same communications scenario. The only work we found from the literature is the DBF performance evaluation for satellite communications [26]. A 136×136 planar array is proposed to provide a coverage over the U.S. System capacity, SINR and computation complexity of several DBF strategies are compared. The neural network (NN) adaptive beamformer achieves better system capacity than that of other conventional beamformers. However, it results in higher computation complexity and requires higher memory. The dynamic Chebyshev beamforming strategy has varying system capacity due to its controllable sidelobes levels. The computation complexity is much lower than in the adaptive beamformer. Therefore, it is considered as the most practical solution for current satellite systems. However, the accuracy of the coverage performance comparison between conventional and adaptive beamformers can be further improved when the ground user distribution is taken into account.

1.6 Motivation and Contribution

1.6.1 Challenge and motivation

The antenna array strategy for HAP communications can be the same as that in [26] for satellite communications. That is to use a planar antenna array to provide a circular coverage on the ground. In the case of conventional beamforming strategies, the coverage area is divided into equal-sized hexagonal cells and the beamforming methods are designed in order to make the mainlobe footprint cover the desired cell while suppressing sidelobes levels. From the literature [37]-[41], antenna element spacing is optimized for a particular steering position beam. Therefore, these methods are not designed to generate

multi-beams simultaneously. In our scenario, a fixed antenna element spacing is applied. The method of generating arbitrary footprint beampatterns in [59] can be applied in our scenario. However, this method is very sensitive to the choice of the masking filter. In particular, masking filters with sharp boundaries may result in poor performance. From the literature, performance of almost all optimization methods are evaluated when the array antenna is steered to the broadside, which means the footprint distortion problem is not taken into account. For a planar antenna array, the footprint could be wide elliptical when the antenna array is steered to the endfire. This results in high co-channel interference and it is challenging to provide equal-sized cellular communications [23].

In the case of adaptive beamforming, the MVDR beamformer has strong interference rejection capability. In the downlink HAPs scenario, the method can be used to improve the SIR by steering nulls to the cochannel interferers. In the scenario of underwater acoustic communications, the MVDR beamformer can be applied to separate arriving signals from the multipath in order to compensate for time-delay and Doppler accurately. However, the MVDR beamformer is very sensitive to the steering errors and results in performance degradation for both scenarios. Null-broadening [90] is a simple and robust adaptive beamforming method. However, this method has not been fully explored due to its undesirable effects. For instance, the mainlobe is not broadened. This may result in a poor performance when the system is suffering high steering errors while the mainlobe of the beampattern is unacceptably narrow (the beamwidth relates to the number of antenna elements and steering positions). Furthermore, arranging equal number of additive sources for each interferer and applying rectangular window as power distribution evidently limit the system capacity.

1.6.2 Thesis contribution

The contribution of this thesis is summarized as follows:

- A footprint optimization method is proposed for HAPs communications that is based on planar antenna array and hexagonal cellular configuration. The method generates equal-sized circular footprints no matter where the antenna is steered within the coverage area. Therefore, co-channel interference is reduced.
- A vertical antenna array forming ring-shaped cells is proposed for HAPs communications. Such antenna configuration generates symmetric cylinder footprint and gets rid of the footprint distortion problem, which provides more optimization free-

dom for sidelobes suppression. As a result, the method simplifies system design while improving the coverage performance.

- A modified null-broadening adaptive beamforming method is proposed for HAPs communications. The method improves the robustness of Mailloux's method by broadening the mainlobe as well as the interference positions. Taking into account the varying beamwidth for different steering positions, the total number of fictitious sources is reduced to improve the optimization freedom, which results in a better coverage performance.

- Based on the modified null-broadening method, a constrained optimization method is proposed to improve the coverage performance of conventional beamforming in the HAPs communications scenario. The method optimizes the beampattern only at the cochannel cells positions. The method allows a linear vertical antenna array achieving better coverage performance than that of using a set of distinct aperture antennas with the same number of antenna elements.

- A methodology is proposed to evaluate and compare the coverage performance between conventional and adaptive beamformers. The comparison methodology takes into account the ground user random distribution and allows the two kinds of beamforming systems occupying the same amount of multiple access resources in order to improve the accuracy of the performance comparison. Simulation results suggest the conditions at which the adaptive beamformer achieves better or worse coverage performance than the conventional beamformer.

- An adaptive beamforming based receiver is proposed for high data rate OFDM transmission in the underwater acoustic channel. Several DoA estimation methods are investigated, which are based on signal interpolation and modified MVDR beamforming. The DoA information is used to separate arriving angles and therefore time-delay and Doppler effect can be accurately compensated. The modified null-broadening method proposed in the HAPs communications scenario is applied to improve the robustness of the MVDR beamformer. Experimental results show that the proposed signal processing techniques improve the performance of high data rate OFDM transmission in the underwater acoustic channel.

1.7 Thesis Outline

This thesis explores the techniques of DBF using antenna array in the applications of communications from HAPs and high data rate OFDM signal transmission in the

underwater acoustic channel. In the HAPs scenario, the solutions of both conventional and adaptive beamforming methods are considered in order to improve the coverage performance while keeping low antenna payload. The proposed adaptive beamforming methods are also applied in the more sophisticated underwater acoustic channel. The techniques are efficient for accurate time-delay and Doppler effect compensation, which improves the performance of OFDM signal transmission in the underwater channel.

Following the introduction and literature review, Chapter 2 describes the fundamentals of DBF including antenna array characteristics, antenna array geometry and beampattern generation. Then the thesis is divided into two parts. Chapters $3 \sim 7$ investigate the beamforming methods in the scenario of HAP communications while Chapters 8 and 9 focus on the beamforming for underwater communications.

Chapter 3 presents a footprint optimization method based on planar antenna array and hexagonal cellular structure on the ground. The method is constitute of designing masking filters, calculating continuous aperture distributions and space-sampling at antenna elements. This method is effective to generate arbitrary beampattern footprints to cover the corresponding cells in order to reduce the performance degradation from co-channel interference.

Chapter 4 introduces a novel antenna array and cellular configuration. That is to use a linear vertical antenna array to form a ring-shaped cellular structure. Such a configuration solves the problem of footprint distortion and simplifies the antenna system design. We show that, compared with a planar antenna array, a vertical antenna array allows 6 dB SIR improvement while requiring approximately 2.5 times less antenna elements by even applying simple window weights to antenna elements.

In Chapter 5, the MVDR adaptive beamforming and its diagonal loading form are investigated. Mailloux's null-broadening method is applied in the downlink HAP communication scenario, which significantly improves the robustness of the traditional MVDR beamformer. We show that the Mailloux's method can be improved by solving a constrained optimization problem. This allows the mainlobe of the beampattern to be broadened as well as the nulls. As a result, the coverage performance can be further improved.

In Chapter 6, based on the methods proposed in Chapter 5, the constrained optimization technique is proposed in the cellular beamforming scenario, which takes advantages of both cellular and adaptive beamformers. Simulation results show that this technique allows a linear antenna array of omnidirectional antenna elements to achieve

better coverage performance than that of using the same number of aperture antennas. Its advantages in antenna payload reduction are even more significant.

Chapter 7 compares the coverage performance of conventional beamforming and adaptive beamforming in the downlink HAP communications scenario. In order to make the performance of these two beamformers to be comparable, a methodology is proposed, which takes into account the random user distribution and allows the two beamforming systems occupying the same amount of multiple access resources. Simulation results suggest the conditions at which the conventional and adaptive beamformers achieve the same coverage performance in the HAPs communication scenario.

Chapter 8 and 9 investigate the application of DBF methods in high data rate transmission in underwater acoustic channel. Chapter 8 describes the system model including OFDM signal transmission, Doppler compensation and time synchronization, channel equalization and demodulation. An adaptive Doppler filter (ADF) is used in the frequency domain for removing residual intercarrier interference (ICI). Performance of using one receiver antenna and using the technique of combining signals from multiple antennas are evaluated, based on the experimental data obtained in the Pacific Ocean in 1989. In Chapter 9, a linear antenna array and adaptive beamforming methods are applied to improve the high data rate OFDM transmission in the underwater channel. Several DoA estimation methods are considered based on signal interpolation and a modified MVDR beamforming. Especially, the constrained null-broadening method that is proposed previously for HAPs communications is applied to improve the robustness of the MVDR beamformer, which shows its effectiveness for accurate time-Doppler compensation in such a fast time-varying channel.

Finally, Chapter 10 presents the main conclusions of the thesis and ideas for future work are discussed.

Chapter 2

Preliminaries of Digital Beamforming

Contents

2.1 Introduction

Arrays of antennas are used to direct radiated power towards a desired angular sector. The number, geometrical arrangement, relative amplitudes and phases of the array elements depend on the angular pattern that must be achieved. Once an array has been designed to focus towards a particular direction, it becomes a simple matter to steer it towards some other direction by changing the relative phases of the array elements - a process called steering or scanning [17].

In this chapter we discuss some fundamentals of the antenna array and consider various design issues including the array factor generation for various antenna geometries, the tradeoff between beamwidth and sidelobes level, the grating lobe problem and the footprint distortion problem.

2.2 Antenna Array Geometry

2.2.1 Linear antenna array

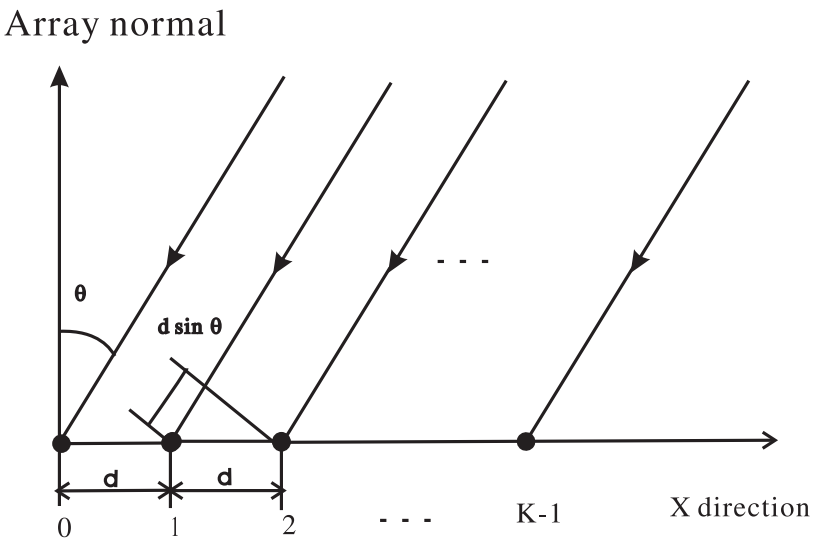

Figure 2.1: A uniform spaced linear array model

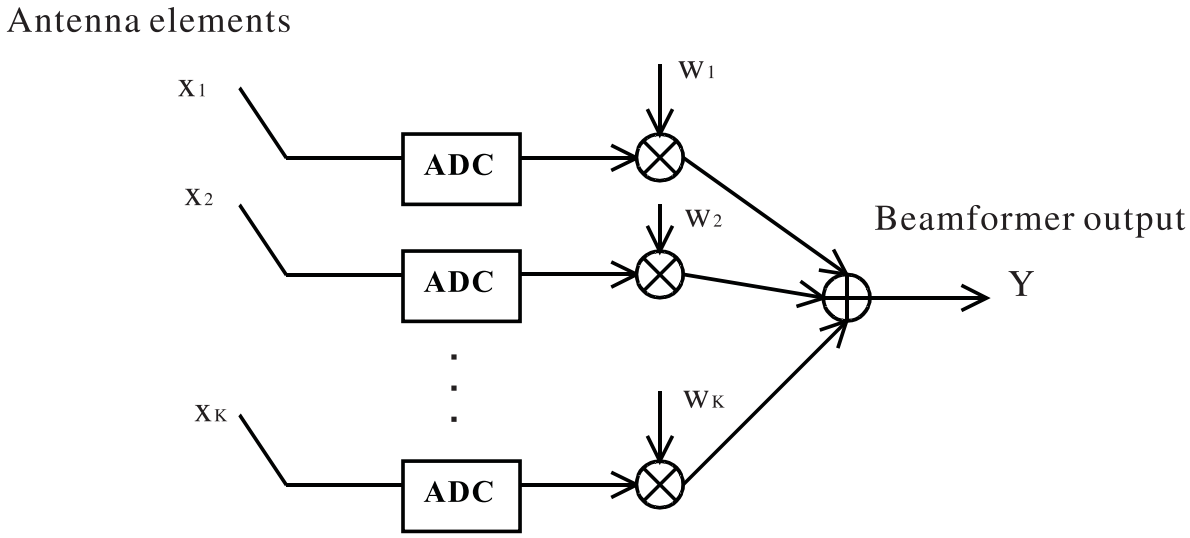

Figure 2.2: A simplified DBF model.

Fig.2.1 illustrates a uniformly spaced linear array with K identical omnidirectional antenna elements, located along the X direction. The inter-element spacing is denoted by d. Fig.2.2 depicts a simple narrow band DBF structure. Let's denote $x_k(t)$ as the signal received by the kth antenna element at time index t. These signals are then weighted by complex weights w_k with $k = 0, 1, \cdots K-1$. The output of the beamformer $y(t)$ is the

linear combination of the data at the K antenna elements at time n:

$$y(t) = \sum_{k=0}^{K-1} w_k^* x_k(t), \tag{2.1}$$

where $(\cdot)^*$ represents a complex conjugate. One of the most important antenna array parameters is the array factor. It represents the far-field radiation pattern of an array of isotropically radiating elements. If a plane wave impinges upon the array at an angle θ with respect to the array normal, as shown in Fig.2.1, the wave front arrives at the element $k+1$ sooner than at element k, since the differential distance along the two ray paths is $d\sin\theta$. By setting the phase of the signal at the origin arbitrarily to zero, the phase leads of the signal at element k relative to that at element 0 is $\frac{2\pi}{\lambda}kd\sin\theta$, where λ is the wave length. All the element outputs can be summed to provide the total array factor $F(\theta)$ [2]:

$$F(\theta) = \sum_{k=0}^{K-1} w_k e^{j\frac{2\pi}{\lambda}kd\sin\theta}. \tag{2.2}$$

The complex weight can be represented as,

$$w_k = A(k)e^{jk\alpha}, \tag{2.3}$$

where the phase of the kth element leads that of the $(k-1)$th element by α, the array factor becomes

$$F(\theta) = \sum_{k=0}^{K-1} A(k)e^{jk\frac{2\pi}{\lambda}d\sin\theta + k\alpha}. \tag{2.4}$$

If $\alpha = -j\frac{2\pi}{\lambda}d\sin\theta_0$, θ_0 the angle direction the antenna array is steered, a maximum response of $F(\theta)$ will result at θ_0. That is, the antenna beam has been steered towards the wave source. It is found that, in (2.1), if $x_k(n) = e^{j\frac{2\pi}{\lambda}kd\sin\theta}$ and $w_k = -\frac{2\pi}{\lambda}d\sin\theta_0$, the beamformer output is equal to the array factor in (2.4). Fig.2.3 is an example of array factor of an 8-element linear antenna array with $d = \frac{\lambda}{2}$, steering at $\theta_0 = 0^\circ$. The amplitude of the weights $A(k) = 1/8$ (or refer to the uniform amplitude weighting). Sidelobe level is about -12.8 dB and the 3-dB beamwidth, or half-power beamwidth (HPBW), is about 12.78°.

2.2.2 Rectangular array

In addition to placing elements along a line to form a linear array, one can position them on a plane to form a planar array. Planar arrays provide additional variables which can be used to control and shape the array's beampattern. The main beam of the array can be steered towards any point in its half space. The 3-dimensional beampattern generated

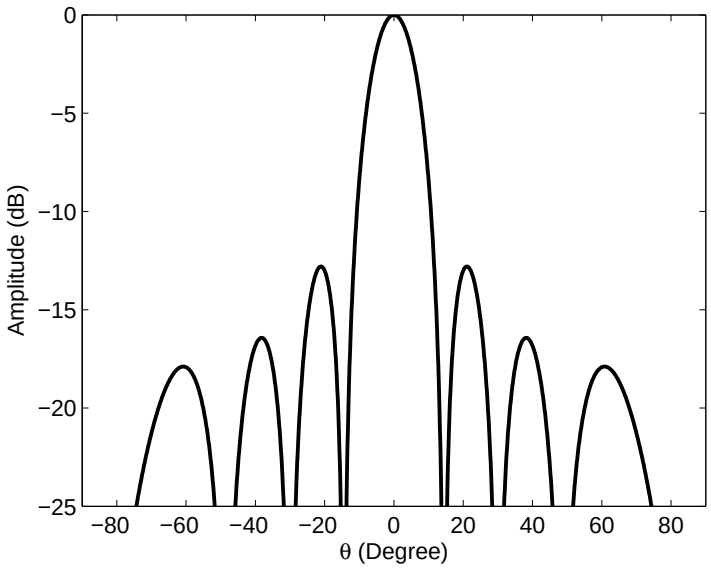

Figure 2.3: The beampattern of an eight-element linear array steered at 0 degree, element spacing equals 0.5 λ.

by a planar array can be used to cover a 2-dimensional ground area, as in applications of satellite communications [26, 57–59]. A rectangular array configuration is shown in Fig.2.4. The array factor of a rectangular array can be viewed as a pattern multiplication of the two linear arrays along X and Y coordinates. Suppose that there are K elements along the X coordinate, then the array factor can be represented as

$$F_x(u) = \sum_{k=0}^{K-1} A_x(k) e^{j\frac{2\pi}{\lambda} k d_x \sin u + k\alpha}, \tag{2.5}$$

where $\sin u = \sin\theta\cos\phi$ and $\alpha = -\frac{2\pi}{\lambda} d_x \sin u_0 = -\frac{2\pi}{\lambda} d_x \sin\theta_0 \cos\phi_0$, θ_0 and ϕ_0 represent the complementary elevation and azimuth angles, defining the steering position for a given beam. Array factor along Y coordinate has a similar form. Suppose that there are L elements, then the array factor can be represented as

$$F_y(v) = \sum_{l=0}^{L-1} A_y(l) e^{j\frac{2\pi}{\lambda} l d_y \sin v + l\beta}, \tag{2.6}$$

where $\sin v = \sin\theta\sin\phi$ and $\beta = -\frac{2\pi}{\lambda} d_y \sin v_0 = -\frac{2\pi}{\lambda} d_y \sin\theta_0 \sin\phi_0$. The overall array factor is the multiplication of F_x and F_y,

$$F(\theta,\phi) = F_x(u)F_y(v) = \sum_{k=0}^{K-1}\sum_{l=0}^{L-1} A_x(k)B_y(l) e^{j\frac{2\pi}{\lambda} k d_x \sin u + k\alpha} e^{j\frac{2\pi}{\lambda} l d_y \sin v + l\beta}. \tag{2.7}$$

It is some times more convenient to view the 3D array factor in the X-Y distance co-

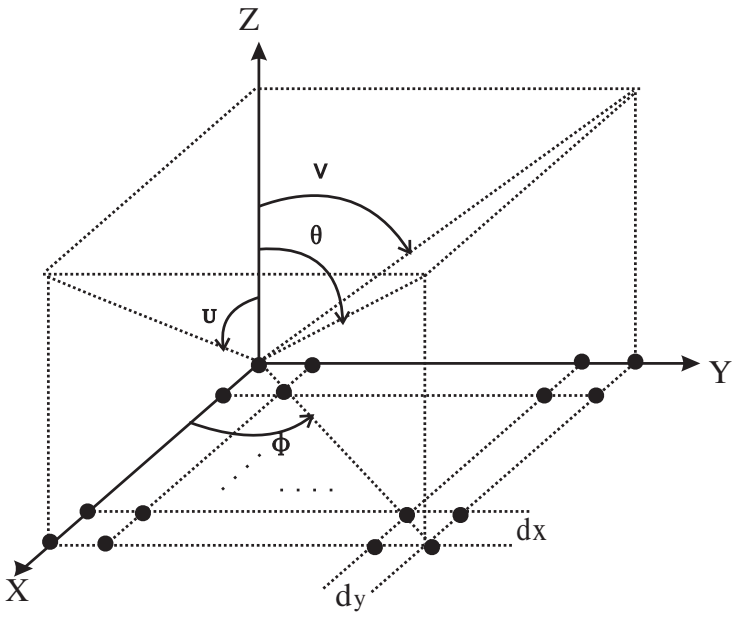

Figure 2.4: A rectangular planar array geometry

ordinates instead of in θ - ϕ co-ordinates. Therefore, the following function is frequently used,

$$F_1(X, Y) = |F(\theta, \phi)|, \tag{2.8}$$

where $\phi = \arctan(Y/X)$, $\theta = \arctan(\sqrt{X^2 + Y^2}/H)$ and H is the antenna array altitude to the ground. Fig.2.5 gives the 2D contour plot of the array factor of an 8 by 8 rectangular array with element spacing $d_x = d_y = \frac{\lambda}{2}$, $A_x(k) = B_y(l) = 1/8$, $H = 20$ km, steering at the ground location $(0, 0)$ km. The maximum power (or mainlobe) is represented in dark red. The sidelobe level and mainlobe beamwidth are approximately the same as that of an 8-element linear array.

2.2.3 Other antenna array configurations

In Sec.2.2.1 and Sec.2.2.2, we have shown the array factor calculation for the most common antenna array configurations. However, for many applications, one may need to apply an arbitrary geometry planar array, such as circular, hexagonal, truncated rectangular or even randomly positioned planar array. Generation the array factor for these antenna array is more complicated. In this section, a common solution is given, which can be used to calculate the planar antenna array with any geometry configuration.

Consider an antenna array in an $X - Y$ plane with K elements, the positions of all the elements should be recorded, each having coordinates [$x(k)$, $y(k)$] and a complex

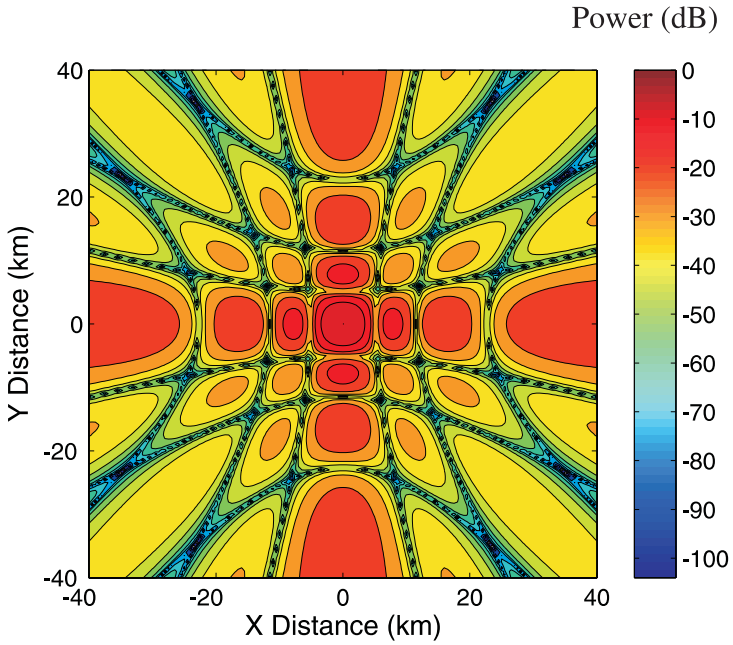

Figure 2.5: 2D Array factor of an 8×8 rectangular array, steering at (+0,+0)km

weight w_k. The array factor is then given by [17],

$$F(\theta,\phi)=\sum_{k=0}^{K-1} w_k e^{j\frac{2\pi}{\lambda}[x(k)\sin\theta\cos\phi+y(k)\sin\theta\sin\phi]}. \tag{2.9}$$

For the uniform amplitude weighting method, weights are given by:

$$w_k=\frac{1}{K}e^{-j\frac{2\pi}{\lambda}[x(k)\sin\theta_0\cos\phi_0+y(k)\sin\theta_0\sin\phi_0]}. \tag{2.10}$$

2.3 Visible Region and Grating Lobes

In an antenna array, if the element spacing is too large, several lobes of the same height as the mainlobe are formed in visible space on each side of the array plane. The extra mainlobes formed due to large element spacings are referred to as grating lobes.

The array factor $F(\theta)$ in (2.2) is periodic in θ with period 2π. However, the actual range of variation of θ depends on the value of the quantity $k_0 d$, where $k_0 = 2\pi/\lambda$ is the wave number. The overall range of variation Ω, defined as the visible region, is $-k_0 d \leq \Omega \leq k_0 d$ [94]. The total width of this region is $\Omega_{vis} = 2k_0 d$. Since the Nyquist interval is

$[-\pi, \pi]$, according to the different antenna element spacing, we obtain,

$$\begin{cases} d < \lambda/2 \Rightarrow k_0 d < \pi \Rightarrow \Omega_{vis} < 2\pi & \text{less than Nyquist} \\ d = \lambda/2 \Rightarrow k_0 d = \pi \Rightarrow \Omega_{vis} = 2\pi & \text{full Nyquist} \\ d > \lambda/2 \Rightarrow k_0 d > \pi \Rightarrow \Omega_{vis} > 2\pi & \text{more than Nyquist} \end{cases}$$

In the case $d > \lambda/2$, the values of the array factor are over-specified and repeated over the visible region. This can give rise to grating lobes or fringes, which are mainbeam lobes in directions other than the desired one. The number of grating lobes in an array pattern is the number of complete Nyquist intervals fitting within the visible region. The number can be calculated by [95]

$$N_g = \frac{\Omega_{vis}}{2\pi} = \frac{k_0 d}{\pi} = \frac{2d}{\lambda}. \tag{2.11}$$

Grating lobes occur at angles θ_g satisfying the equation [94]

$$\cos\theta_g = \cos\theta_0 + \rho\lambda/d, \tag{2.12}$$

for such integer $\rho \neq 0$ that $|\cos\theta_0 + \rho\lambda/d| \leq 1$.

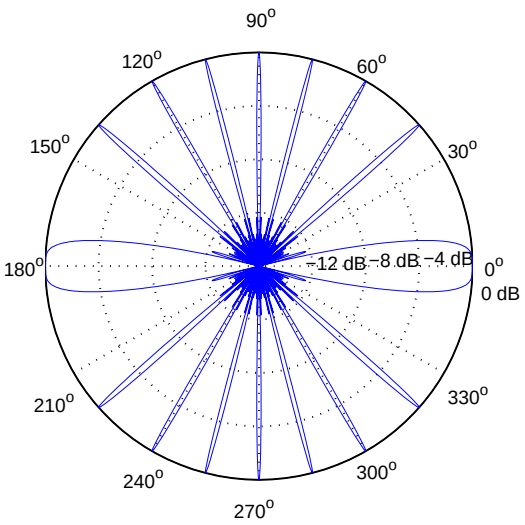

Figure 2.6: Array factor of 8 element linear array and 4 λ element spacing

Fig. 2.6 shows the array factor of an 8-element linear array and the element spacing is 4λ. From $-90°$ (or $270°$) to $90°$, there are 8 grating lobes and one mainlobe. Grating lobes are positioned at $\pm 41.4°, \pm 60°, \pm 75.5°$ and $\pm 90°$, just as the results that can be calculated by (2.11) and (2.12). These lobes result in undesirable interference within the visible region. However, it is found that the increase of the element spacing

reduces the 3 dB beamwidth of the mainlobe (eg. the antenna array with 4λ element spacing generates a beampattern with mainlobe beamwidth 1.6°, exactly 8 times less than that of $\lambda/2$ element spacing). This implies that the the system capacity is improved since more users can be supported. Therefore, in order to improve the coverage performance, one can enlarge the element spacing while avoiding grating lobes within the coverage area $\mid \theta \mid < \theta_n$. From (2.12), the maximum element spacing d_{max} is obtained as

$$d_{max} = \frac{\lambda}{1 - \cos\theta_n}, \tag{2.13}$$

2.4 Beampattern Optimization by Window Functions

Design of antenna element weights is important for beampattern optimization. It is shown in Fig. 2.3 that uniform amplitude weighting results in relatively high sidelobes levels. By applying a non-uniform amplitude weighting to the conventional beamforming, sidelobe level can be reduced. The simplest method is to apply window functions.

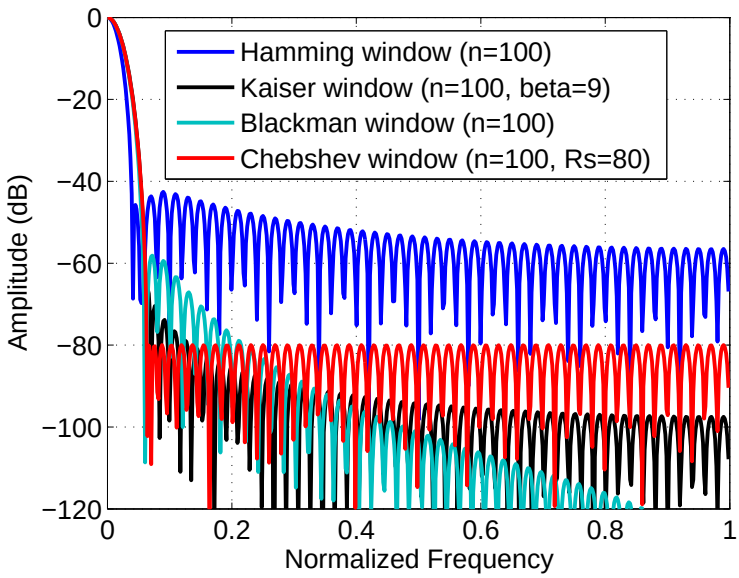

Figure 2.7: Frequency domain comparison of several window functions

Fig. 2.7 gives the frequency response of 4 kinds of window functions: Hamming, Blackman, Kaiser and Chebyshev window. Hamming window can suppress the sidelobe level to be lower than -40 dB. Blackman window can achieve -58 dB sidelobe level, however, its beamwidth is wider than that of the Hamming window. Kaiser window

and Chebyshev window are controllable. A Lower sidelobe level can be achieved at the expense of wider beamwidth. Beampatterns optimized by Hamming window are shown

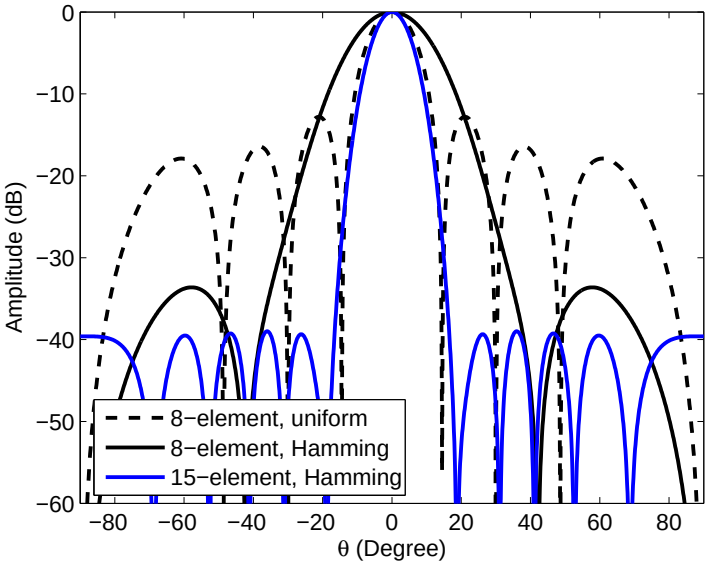

Figure 2.8: Beampattern optimized by Hamming weighting.

in Fig. 2.8. Sidelobe level is significantly reduced. However, the 3 dB beamwidth, when applying Hamming weights, becomes wider than that of the uniform amplitude weights. It is shown that approximately 2 times more elements are required when using Hamming weight to achieve the same 3 dB beamwidth as that of the uniform amplitude weights. In Chapters 3, 5 and 6, more sophisticated methods will be described to improve the system capacity.

2.5 Footprint Distortion

The discussions in the previous section have considered arrays whose maximum response axis were at broadside, or $\theta_0 = 0°$. When the array is steered towards the endfire, the mainlobe beamwidth is broadened, as shown in Fig.2.9. Fig.2.10 is an example of a planar array footprint distortion. It is found that the shape of the footprint is more like ellipse and the mainlobe beamwidth is significantly broadened, compared with the footprint in Fig.2.5. The problem is referred to as scan limit by Elliott in [96]. It is shown in Fig.2.11 that the window method can not solve the problem of footprint distortion. Although sidelobes are significantly reduced, the mainlobe beamwidth turns out to be even wider.

In the HAPs communications, the traditional cellular beamforming strategy is to deploy a planar array to cover hexagonal cells on the ground. This requires multi-beams with equal-sized circular footprints to be generated. Unfortunately, the footprint distortion problem makes such requirement challenging. It causes high co-channel interference and deteriorates the system capacity.

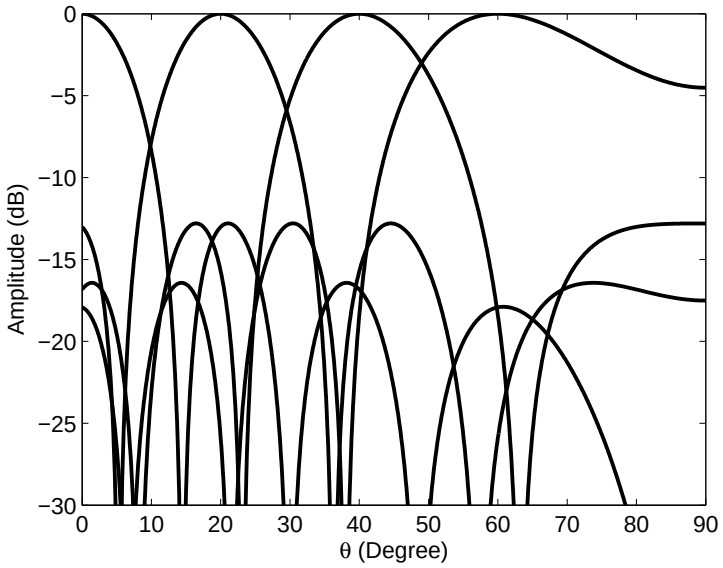

Figure 2.9: Multi-beams of an eight-element antenna array, steered at $0°$, $20°$, $40°$ and $60°$, 0.5λ spacing.

2.6 Summary

In this chapter, some basic antenna array characteristics have been discussed. The array factor of a linear array can be considered as the sum of the element responses distinguished by their relative difference of signal arriving. Such method can be simply extended to 2D rectangular planar array and even arbitrary complicated geometry according to specific applications.

Elements spacing can be adjusted to control the mainlobe beamwidth. However, this can cause grating lobes when the element spacing is larger than the wavelength. Grating lobes are the result of over-sampling within one Nyquist interval. These signals cause high interference and result in low system capacity. However, since the positions of grating lobes are forecasted for an equally-spaced antenna array, the mainlobe beamwidth can be reduced by increasing the element spacing while avoiding

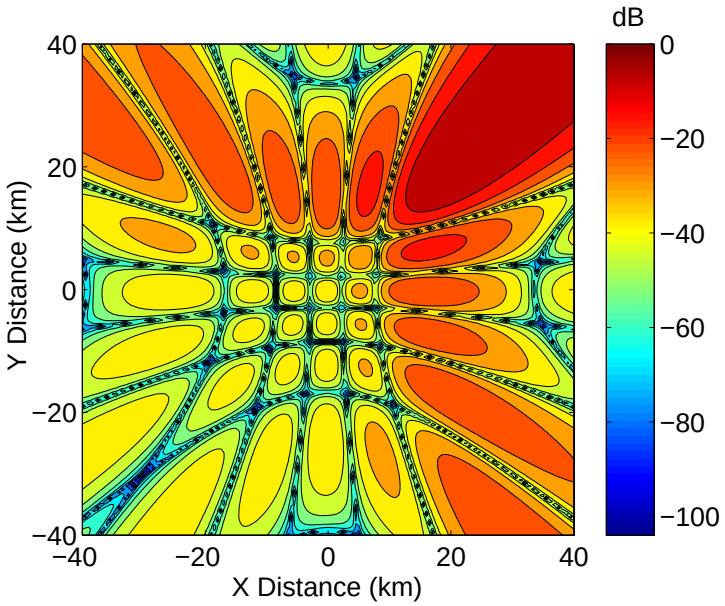

Figure 2.10: Steering the beam to (+24,+24)km, using an 8×8 rectangular array and uniform weights

grating lobes within the pre-defined coverage area in order to improve the system capacity.

Several window functions have been analyzed as the array elements weights. It is shown that window functions have quite good effect on sidelobe suppressing. However that is at the expense of broadening beamwidth. Moreover, such methods can not solve the problem of footprint distortion (scan limit) especially when the antenna is steered towards the endfire. The effect of scan limit is one of the most challenging problems for cellular beamforming scenario, which degrades the system capacity to a large extent.

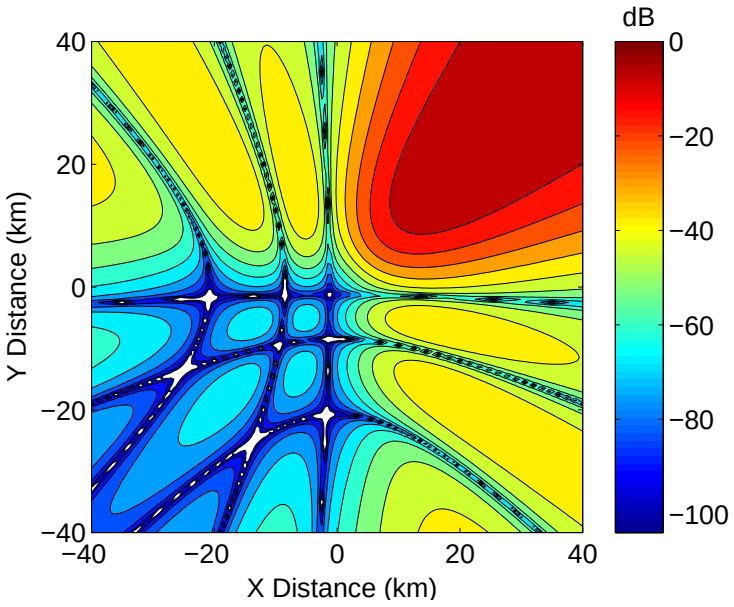

Figure 2.11: Steering the beam to (+24,+24)km, using an 8×8 rectangular array and Hamming weights

Chapter 3

The Three-Step Beampattern Optimization Method for HAPs Communications

Contents

3.1 Introduction

In many applications of antennas, point-to-point communications are of interest. A highly directive antenna beam can be advantageous where these links are over large distance, for example, in a HAPs communications scenario. As the directivity of the antenna increases, the gain also increases. At the receiver end of the communications link, the increase in directivity means that the antenna receives less interference from its signal environment.

Employing a set distinct aperture antennas, such as horn, lens or reflector antennas is one feasible approach for HAPs application [23, 24, 97]. These highly directive

antennas can be used to provide one spot beam per cell [24]. Elliptical beams are generated to reshape the footprints to be circular to cover the corresponding cells on the ground. A flat -40 dB sidelobes are achieved using 121 aperture antennas, which leads to an overall 18 dB SIR level. However, the space and weight available on a HAP are limited [20]. For a 121-cell layout and a 28 GHz carrier frequency, the 121 dielectric lens antennas are assumed with an aperture radius up to 80 mm and approximately 40 kg antenna payload [23]. Therefore such antenna approach results in bulky antenna payload.

Another approach is based on the use of antenna arrays with beamforming signal processing techniques. This approach can be further divided into conventional (or cellular) and adaptive methods. The adaptive beamforming algorithms maximize the power for the desired user while minimizing the power for interferers in order to maximize the SINR. However, these techniques require real-time signal processing and are challenging for current hardware implementation [26]. Moreover, more complicated robust adaptive beamforming methods are required since the traditional adaptive beamformers are very sensitive to the steering errors. The adaptive beamforming techniques will be investigated in detail in Chapter 5. For conventional beamforming, the ground area is divided into cells and beampatterns footprints are optimized to cover the fixed cells. The motivation for this is the development of a tessellated structure of cells that maximizes the coverage, while simplifying bandwidth reuse planning [97]. Also, every beam can be calculated off-line and there requires no real-time signal processing. This is the same as that of using aperture antennas. However, the payload of an antenna array is much smaller than that of aperture antennas. The array antenna elements can typically be constructed from lightweight printed circuits with the weighting around 3.5 kg/m^2. For a 424-element antenna array, as will be discussed in this chapter, the aperture radius is 60 mm and the antenna mass is expected to be less than 0.4 kg [27], which is around two orders less than that of the dielectric lens antennas. Although, more antenna elements will result in more wires, the total antenna weight can still be reduced. For cellular beamforming, due to the problem of scan limit, it is challenging to generate equal-sized circular footprint for every cell while keeping relatively low sidelobe level. From the literature, a potential solution to the above problem is found in [59]. The method is based on defining a spatial masking filter according to the desired beampattern, calculating the antenna aperture distribution which corresponds to this masking filter and the aperture size, and finally spatially sampling the aperture distribution at the antenna-element positions. However, this method is not completely suited for the HAPs scenarios and the most disadvantage is that results produced by this method are very sensitive to the choice of the masking filter. In particular, when masking filters with sharp boundaries as in [59] are applied for the HAPs scenarios, the results are poor. Although the method can generate footprint with arbitrary geometry, this is only the case when the planar antenna array is steered to its

broadside. The performance is poor when it is steered to the endfire. Therefore, the scan limit problem is not thoroughly solved.

In this chapter, we apply the method in [59] for optimizing antenna array weights, to obtain arbitrary cell shapes (as defined by beam footprints on the ground) and low sidelobe levels. Specifically, the following refinements to the method are introduced:

- A ground masking filter corresponding to the desired cell shape, is defined and then it is transformed to an angle masking filter.
- A two-dimensional Gaussian function is used as the ground masking filter to reduce the Gibbs effect due to designing the masking filter with sharp boundaries.
- The parameters of the masking filter are adjusted to achieve footprints close to circular at arbitrary steering location while obtaining a good compromise between mainlobe width and sidelobe levels.

From the simulation, we show that this approach allows a 424-element antenna array to achieve a coverage performance similar to that previously reported for 121 lens aperture antennas [23] with an expected reduction in mass antenna payload. The related material has been published in [27].

3.2 Communications Scenario

Fig. 3.1 illustrates a communication scenario with a HAP at an altitude of $H = 20$ km providing coverage over a circular area with radius of 32.7 km. This coverage area is divided into cells in order to maximize spectral efficiency. In Fig. 3.1, θ is the complementary elevation angle, while ϕ is the azimuth angle and $\phi = \arctan(\frac{Y}{X})$, $\theta = \arctan(\frac{\sqrt{X^2+Y^2}}{H})$, X and Y representing the distance coordinates.

An example of communication parameters is presented in Table.3.1. The ITU recommended frequency for HAPs worldwide is 47/48 GHz [98], but, as there has been subsequent growing interest in the 28/31 GHz band [99], we have assumed a carrier frequency 30 GHz for the present work. The number of cells is 121 with the radius of the cells being equal to 3.15 km. We also assume that the communication system exploits a spectral re-use plan with re-use factor 4. This particular scenario has been chosen in order to compare the performance of the antenna array with that of a set of directive aperture

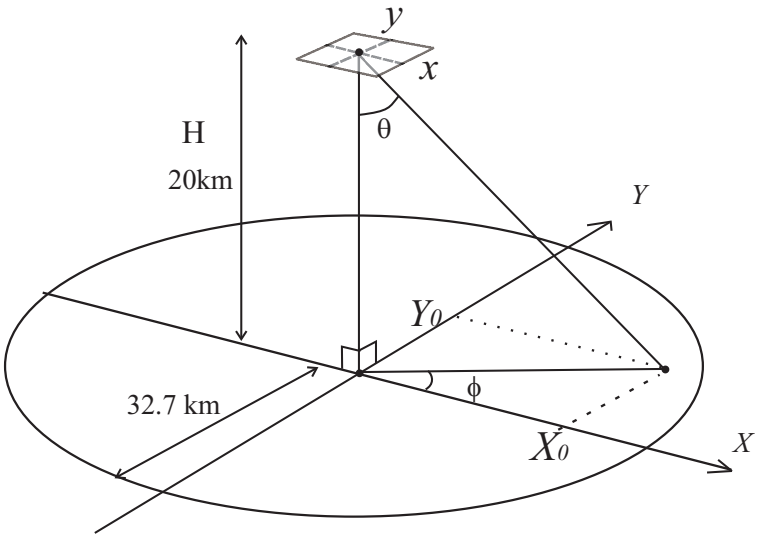

Figure 3.1: Steering a planar antenna array to a desired position from a HAP to the ground

antennas in [23]. The parameters (besides the antenna parameters) shown in Table.3.1 are the same as in [23]. Fig. 3.2 is the 424-element antenna array configuration. Element spacing is set to be $\lambda/2$.

3.3 Method Description

Consider an antenna array on an X-Y plane with K elements, each having co-ordinates $[x(k), y(k)]$ and a complex weight w_k. Let's rewrite the array factor:

$$F(\theta, \phi) = \sum_{k=0}^{K-1} w_k e^{j\frac{2\pi}{\lambda}[x(k)\sin\theta\cos\phi + y(k)\sin\theta\sin\phi]}. \tag{3.1}$$

It is sometimes more convenient to view the 3D array factor in the X-Y distance co-ordinates instead of in θ - ϕ co-ordinates. Therefore, we use,

$$F_1(X, Y) = |F(\theta, \phi)|, \tag{3.2}$$

where $\phi = \arctan(Y/X)$, $\theta = \arctan(\sqrt{X^2 + Y^2}/H)$. We now describe an optimisation method of calculating antenna element weights to improve the footprint beampattern and SIR performance.

Table 3.1: Communications Scenario

Wavelength	1 cm
Frequency band	30 GHz
HAPs altitude	20 km
Minimum elevation angle	31.45°
Radius of coverage area	32.7 km
Number of antennas elements	424
Radius of antenna aperture	6 cm
Antenna array configuration	Planar array
Element distance	0.5λ
Type of cellular design	Hexagonal plan
Radius of each cell	3.15 km
Frequency re-use plan	4
Number of cells	121

3.3.1 Step 1: Generating a ground masking filter and transforming it to an angle masking filter

Hexagonal cellular structure is applied over the ground coverage area. Every cell should be covered by approximately circular beampattern footprints. Therefore, we propose to use the two-dimensional Gaussian function

$$P(X', Y') = \exp\left[-\frac{(X')^2}{2\sigma_X^2} - \frac{(Y')^2}{2\sigma_Y^2}\right] \tag{3.3}$$

in order to define the desired circular cell footprint; σ_X and σ_Y are scaling factors defining the cell size along X and Y directions. This Gaussian function is moved to a steering point (X_0, Y_0) km and then rotated by an angle ϕ', thus providing a ground masking filter for a specific cell. Mathematically, the ground masking filter is described by

$$P_G(X, Y) = P(X', Y') \tag{3.4}$$

with the vector rotation

$$\begin{bmatrix} X' \\ Y' \end{bmatrix} = \begin{bmatrix} \cos\phi' & \sin\phi' \\ -\sin\phi' & \cos\phi' \end{bmatrix} \begin{bmatrix} X - X_0 \\ Y - Y_0 \end{bmatrix}. \tag{3.5}$$

In order to compensate the effect of scan limit, the azimuth angle of the masking filter ϕ' is defined as an angle orthogonal to the azimuth angle $\phi_0 = \arctan\frac{Y_0}{X_0}$, as shown in Fig.3.3. Mathematically, it is represented as

$$\phi' = \begin{cases} \phi_0 + 90^\circ & 0^\circ \le \phi_0 < 90^\circ \\ \phi_0 - 90^\circ & 90^\circ \le \phi_0 < 270^\circ \\ \phi_0 - 270^\circ & 270^\circ \le \phi_0 < 360^\circ \end{cases}$$

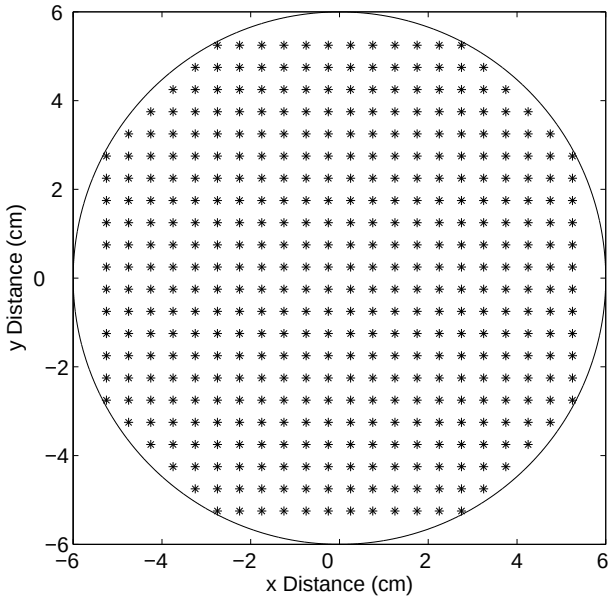

Figure 3.2: 424 Planar antenna array configuration

The transform of the ground masking filter to the angle masking filter is given by

$$P_A(\theta, \phi) = P_G(X, Y) \tag{3.6}$$

The shape and size of the beampattern footprint depends on the selection of the parameters σ_X and σ_Y of the ground masking filter. An algorithm for the selection is described later in Section 3.3.3.

3.3.2 Step 2: Calculation of continuous aperture distribution

The aperture distribution $\chi(\rho, \beta)$ can be expressed by the Fourier series:

$$\chi(\rho, \beta) = \sum_{n=-\infty}^{\infty} \chi_n(\rho) e^{jn\beta} \quad (0 \leq \rho \leq r\ ,\ 0 \leq \beta \leq 2\pi), \tag{3.7}$$

where ρ and β are the radial and angular coordinates of a circular aperture with radius r. The Fourier coefficients $\chi_n(\rho)$ can be derived as [59]:

$$\chi_n(\rho) = \frac{\pi}{2r^2(j)^n} \int_0^{2r/\lambda} \widetilde{\phi}_n(\omega) J_n(\omega\rho) \omega d\omega, \tag{3.8}$$

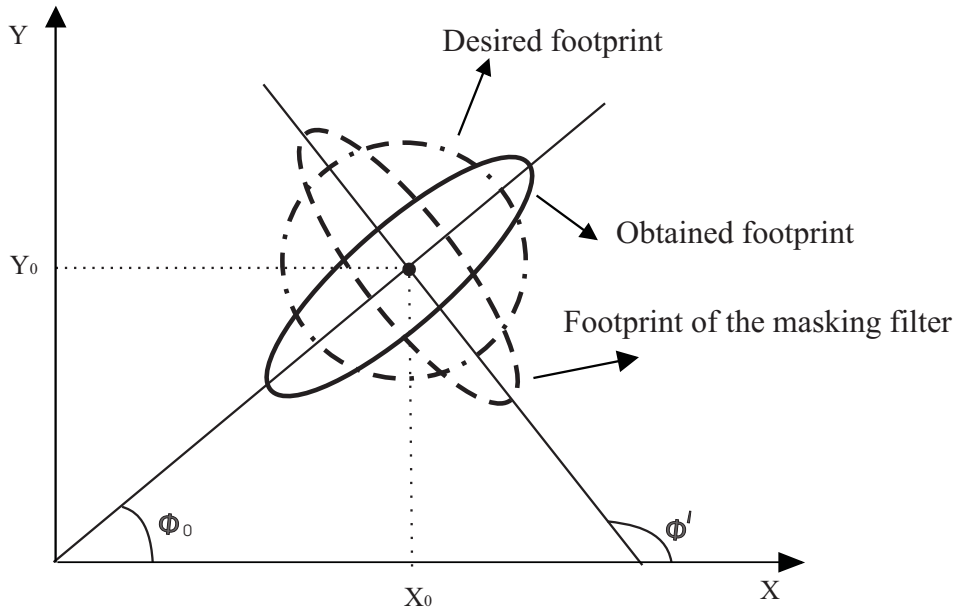

Figure 3.3: Scan limit compensation

where $\omega = \frac{2r}{\lambda}\sin\theta$, $J_n(\cdot)$ is the nth order Bessel function of the first kind and $\tilde{\phi}_n(\omega)$ is the Fourier transform of the Gaussian masking filter designed in Step I,

$$\widetilde{\phi}_n(\omega) = \frac{1}{2\pi}\int_{-\pi}^{\pi} P_A(\theta,\phi)e^{jn\phi}d\phi, \tag{3.9}$$

where $P_A(\theta,\phi)$ is given by (3.6). Since we can not calculate the infinite number of Fourier terms in (3.7), the series should be truncated to obtain an approximation $\widetilde{\chi}(\rho,\beta)$. Then (3.7) can be rewritten as a finite Fourier series

$$\widetilde{\chi}(\rho,\beta) = \sum_{n=-M}^{+M} \chi_n(\rho)e^{jn\beta}. \tag{3.10}$$

In general, an increase in M leads to a better approximation accuracy but it also significantly increases the computation time. In our simulation below, where the number of elements of the antenna array is 424, M is set to be 500; this is enough for our scenario to provide sufficient approximation accuracy.

3.3.3 Step 3: Sampling the aperture distribution onto a pre-designed planar array

Each antenna element is then assigned a complex weight by spatial sampling the estimated aperture distribution:

$$w_k = \widetilde{\chi}(\rho_k,\beta_k), \quad k = 1,\ldots,K, \tag{3.11}$$

where the position of each antenna element is defined within an aperture of radius r.

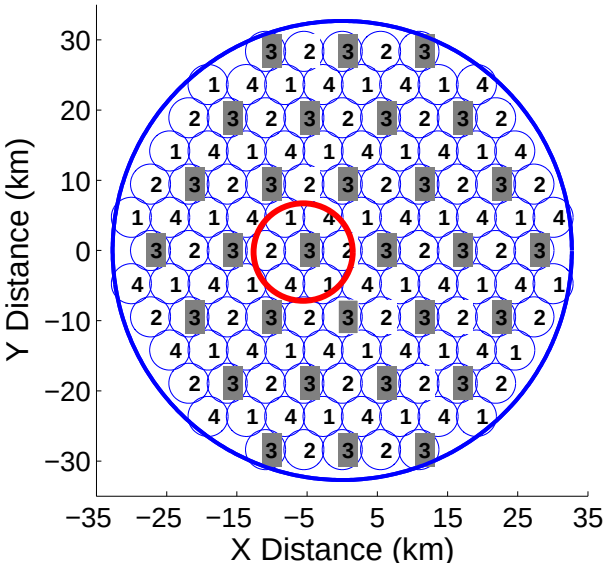

Figure 3.4: 121 Hexagonal cellular configuration

Efficient spectral re-use in wireless telecommunications systems is often achieved by using a cellular coverage strategy. Fig. 3.4 is an example of 121 cells with hexagonal cellular configuration. Frequency re-use factor is 4. Cells that share the same spectral channel are marked by the same number and are termed as co-channel cells; Each cell has a different spectral channel to its neighbors. The shadowed cells are those that share channel 3. They are selected to investigate the performance of the antenna array using the proposed method. We assume that all channels share the same coverage performance, so one channel only is analyzed. Both sidelobes and the size of the mainlobe affect the system performance. The red circle sets the limitation of the size of the mainlobe footprint. If the mainlobe footprint surpasses this limitation, users at those neighbor co-channel cells may receive high interference, which significantly reduces the system capacity.

We now propose a method for selecting the parameters of the 2D Gaussian function (3.3), defining the ground masking filter for a specific cell. Firstly, the maximum of the Gaussian function is positioned in the center of the cell; this defines the parameters X_0 and Y_0 in (3.5). Secondly, we aim to select values of σ_X and σ_Y, controlling the beamwidth and sidelobe levels, to reduce co-channel interference. The relationship between σ_X and σ_Y affects the shape of the cell footprint. This relationship depends only on the distance between the cell center and the center of the HAP coverage area. In the center point of the coverage area, σ_X and σ_Y should be equal to achieve a circular

cell shape. Computational experiments have shown that for a 424-element antenna array arranged as a circular planar array, providing communications for a coverage area with radius 32.7km, σ_Y should be 1.2 times larger than σ_X at the boundary of the coverage area. At other positions, this relationship can be approximated by a linear function of the distance. Thus, the shape of the cell footprints can be approximately controlled to be circular for all cells. Taking this into account, the only parameter to be found is σ_X (or σ_Y). Let σ_0 be an initial value of σ_X, and ε be an accuracy metric for determining the optimal value of σ_X. The algorithm for optimizing σ_X is described by the following steps:

1. Initialize $\sigma_X = \sigma_0$ and a parameter Δ=σ_0/2.

2. If $\Delta \leq \varepsilon$, choose σ_X and end this process. Otherwise, calculate $\sigma_X + \Delta$ and $\sigma_X - \Delta$ and determine the average power at all co-channel cells except the steering cell.

3. Compare the average powers for $\sigma_X + \Delta$, σ_X and $\sigma_X - \Delta$ and find a minimum P_{min} among them. If σ_X provides the minimum power, go to step 5; if $\sigma_X + \Delta$ or $\sigma_X - \Delta$ provides the minimum, go, respectively, to step 4a or step 4b.

4a. Increase σ_X, $\sigma_X + n\Delta$ ($n = 1, 2, \cdots$), calculate the average power in co-channel cells and update the minimum P_{min} until the average power becomes larger than the current minimum value.

4b. Decrease σ_X, $\sigma_X - n\Delta$ ($n = 1, 2, \cdots$), calculate the average power in co-channel cells and update the minimum P_{min} until the average power becomes larger than the current minimum value.

5. Reduce Δ, $\Delta = \Delta/2$, and go to step 2.

This algorithm finds the optimum parameters for the masking filter to achieve minimum average sidelobe levels in ground co-channel cells.

3.4 Simulation Results

First, we use the antenna array shown in Fig.3.2 and steer the power to the cell with the center at $X_0 = -5.46$ km and $Y_0 = 0$ km. The footprint of the beampattern is shown in Fig.3.5. Fig.3.6 compares a section of the footprint along the X axis at $Y = Y_0$ with

that of the array with the uniform amplitude weighting. The proposed method allows a significantly lower sidelobe level (-67 dB) with respect to the case of the uniform weighting. However, the beamwidth is increased, the effects of which can be mitigated through appropriate choice of spectral re-use factor.

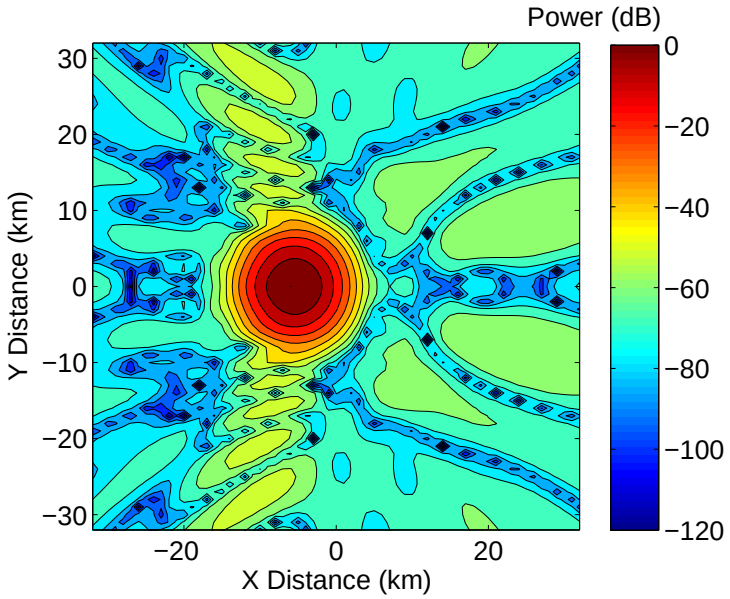

Figure 3.5: Optimized beampattern of a 424-element antenna array, steered at (-5.46,+0)km

Next we consider a situation when the cell is further away from the center of the coverage area; the cell center is at $X_0 = -16.38$ km and $Y_0 = +18.914$ km. Fig. 3.7 is the result of uniform weighting and it is used to be compared with optimized result, shown in Fig. 3.8 and Fig. 3.9. Sidelobes are suppressed to approximately -39 dB. Although the overall performance is worse than for the previous example, where the cell was close to the center of the coverage area, the proposed method provides a significantly better sidelobe suppression than the uniform magnitude weighting. The footprint shape in Fig. 3.8 is also closer to circular when compared with the uniform amplitude weighting in Fig. 3.7.

Fig.3.10 shows footprints of all channel-3 cells. It is seen that the footprints are approximately circular at most ground location within the coverage area.

We now investigate the communications performance by analyzing the relationship between coverage and SIR. First, cells are assigned by different channels, known as the process of frequency re-use. Assume that there are N_c cells that share the same channel and users are randomly positioned in these co-channel cells. Then a HAP antenna steers

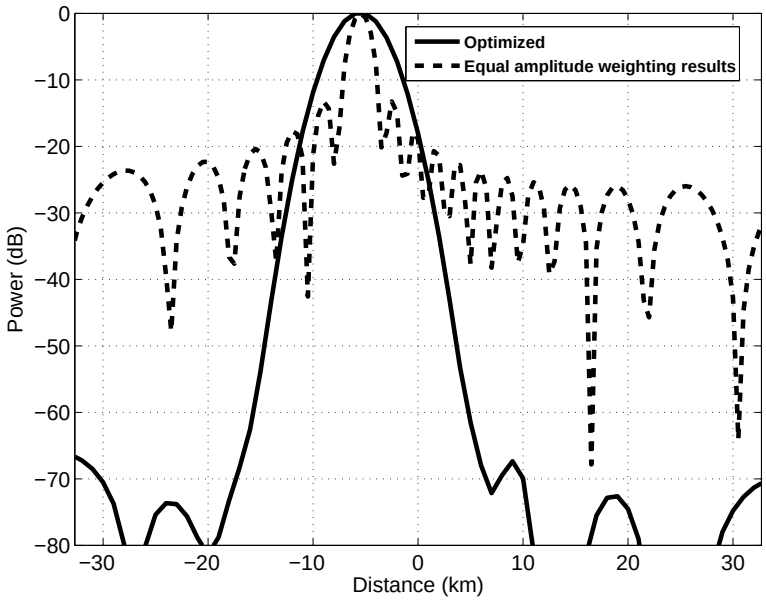

Figure 3.6: One section in Fig.3.5 along the X-axis at Y=Y_0=0 km; solid line: optimized beampattern using 3-stage method; dash line: equal amplitude weighting method

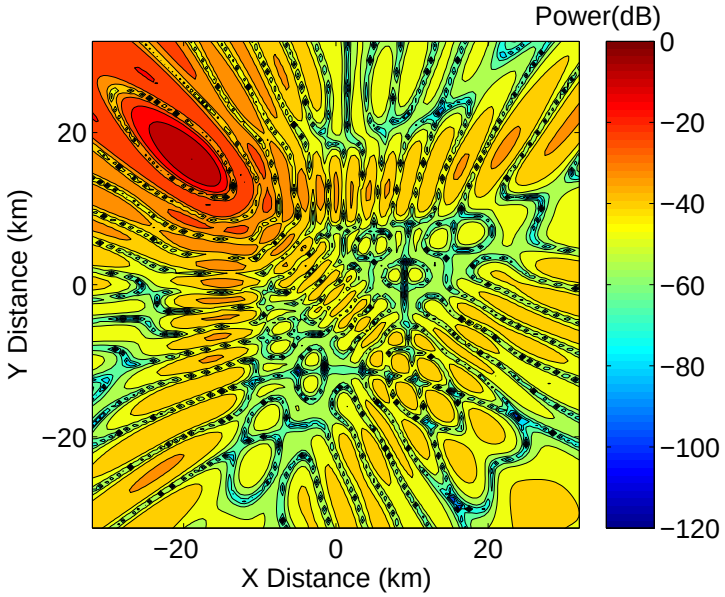

Figure 3.7: Beampattern of a 424-element antenna array, steered at (-16.38,+18.914)km, using uniform weighting

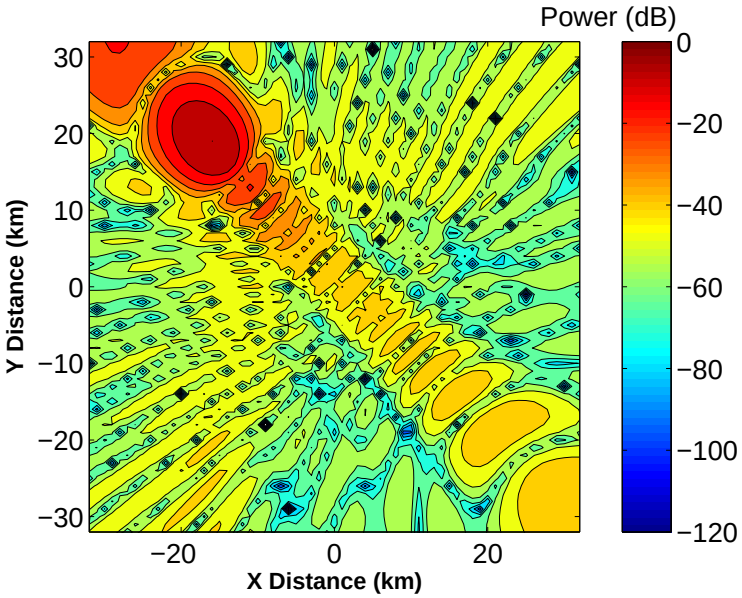

Figure 3.8: Optimized beampattern of a 424-element antenna array, steered at (-16.38,+18.914)km

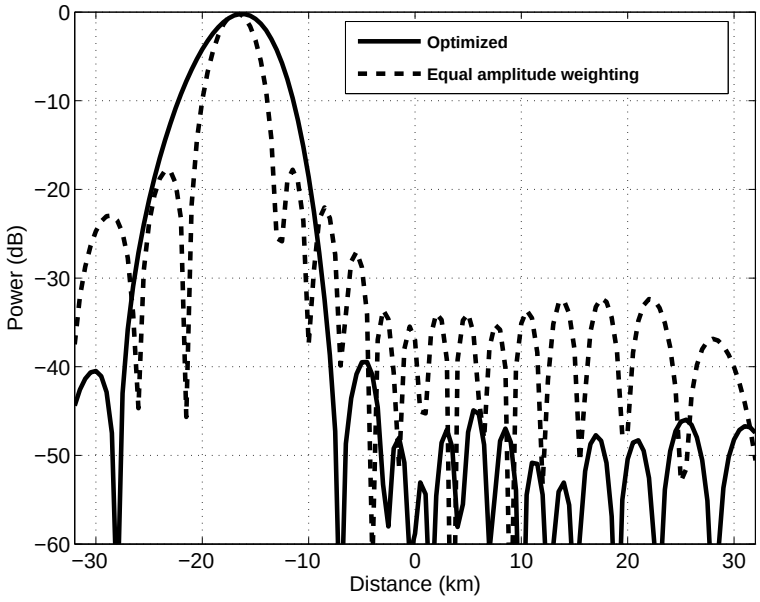

Figure 3.9: One section of the function $F_1(X, Y)$ in Fig.3.8 along the X-axis at Y=Y_0=18.914 km

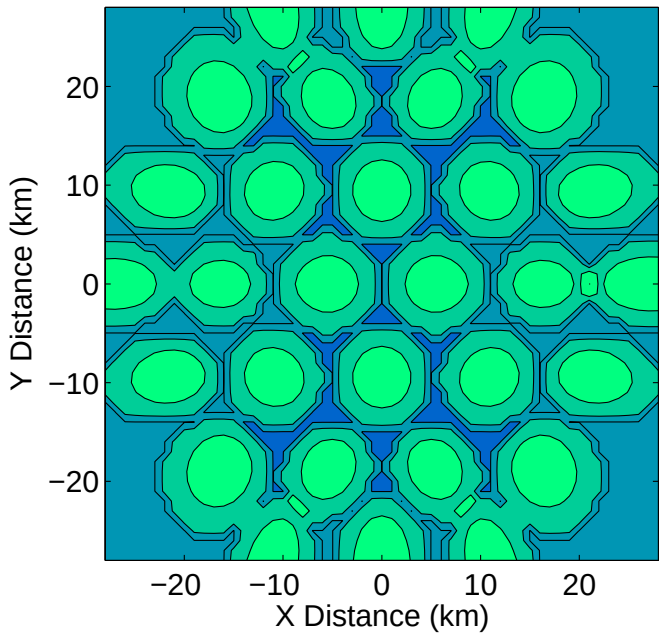

Figure 3.10: Multi-beam steering to all cells of channel 3

N_c beams to these co-channel cells. The user of interest at the ground position (X, Y) receives powers $P_i(X, Y), i = 1, \cdots, N_c$, from these beams, one forms the cell with the user of interest, the power of which is denoted by $P_m(X, Y)$. For the user of interest, the SIR can be defined by:

$$SIR(X, Y) = \frac{P_m(X, Y)}{\sum_{i=1, i \neq m}^{N_c} P_i(X, Y).} \tag{3.12}$$

To estimate the coverage performance, we run a set of simulation trials. In one trial, the SIR for every user is calculated by using (3.12), i.e., N_c SIR values are found. From these values obtained in all the trials, the function $C(\rho) = Pr\{SIR > \rho\}$, representing the coverage performance, is estimated and plotted. Coverage can be quantified as the fractional area of the co-channel cell group served at a given SIR threshold. Then, such coverage curves corresponding to 'best' and 'worst' cells (cells with highest and lowest SIRs, respectively) are identified. The average performance over all cells is also calculated.

Fig. 3.11 shows the coverage performance of the 424-element antenna array shown in Fig. 3.2 and compares the performance with results achieved by directive aperture antennas in [23]. In Fig. 3.11, the solid line from [23] corresponds to the coverage performance provided by 121 lens aperture antennas under the assumption that the sidelobes are modeled as a flat floor at -40 dB for all antennas including those directed to the cell at the edge of the coverage area. Other curves represent the best, worst and

average coverage performance achieved by the 424-element antenna array. Using the three step optimization, the best cell can provide 6 dB better SIR than that of the aperture antennas [23] for the 95% coverage. However, the worst cell provides 2 dB lower SIR than that of aperture antennas. Finally, it is found that the average cell coverage performance is very close to that of aperture antennas.

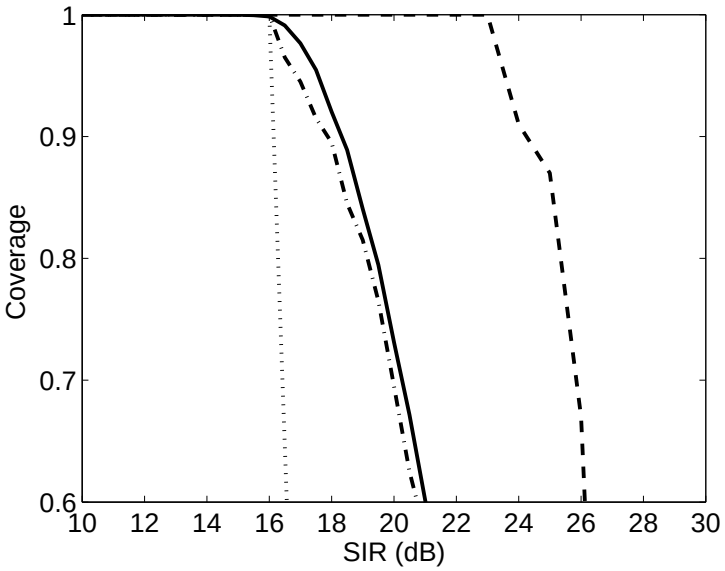

Figure 3.11: Coverage performance: (1) 424-best: best cell performance of the 424-element antenna array (dashed line); (2) 424-worst: worst cell performance of the 424-element antenna array (dotted line); (3) 424-ave: average cell performance of the 424-element antenna array (dot-dashed line) (4) 121-aper: array of lens aperture antennas [13] (solid line)

Thus, when using a 424-element circular antenna array, the proposed method allows synthesis of antenna weights to achieve a performance similar to that of 121 aperture antennas in [23]. Hence, only 4 omnidirectional antenna elements per cell are required to get the same performance as that of one narrow beam aperture antenna per cell. Considering that a large set of aperture antennas would constitute a significant payload with bulky size and weight and cause the problem of mechanical steering, the conventional planar antenna array with simple omnidirectional elements whose element weights are optimized by the proposed method allows a simplified solution for the HAPs antenna.

3.5 Summary

In this chapter, we have proposed a method for optimizing weight coefficients of a HAP antenna array to form a customized cell footprint within a circular coverage area on the ground. The method includes designing a ground masking filter, which describes the desired footprint; transforming it to an angle masking filter; calculating a continuous aperture distribution on a predefined circular antenna aperture and sampling the continuous distribution onto the antenna elements. The proposed method, as a development of the approach in [59], can be used to generate arbitrary beampattern footprint at any steering location on the ground. Therefore, the undesired effect of scan limit is reduced. Furthermore, we propose to use Gaussian masking filters as these result in a better coverage performance compared to masking filters with sharp boundaries, as been proposed in [59]. An algorithm has been proposed to select optimum parameters of the Gaussian masking filter. The proposed method allows controlling cell footprints as well as providing a relatively low level of sidelobes.

It has been shown that this technique allows a 424-element antenna array to achieve a coverage performance similar to that of 121 directive aperture antennas (the SIR difference for 95% coverage is within 1 dB), which provides benefits in terms of antenna payload reduction, the flexibility of electrical steering and expandability. Thus using 4 omnidirectional antenna elements per cell is enough to get the same performance as that of one narrow beam aperture antenna per cell.

Chapter 4

Vertical Antenna Arrays and Ring-shaped Cellular Configuration for HAPs Communications

Contents

4.1 Introduction

In the previous chapter, we have proposed a method to optimize the beampattern of planar antenna array. The main advantage of this method is that one can generate a footprint with arbitrary beampattern footprint shape and still maintain relatively low sidelobe levels. The shape of the footprint should correspond to the shape of the cell on the ground. We are applying the traditional hexagonal cellular configuration on the ground, which means equal-sized circular footprints are required by deploying a two-dimensional planar antenna array.

Although it has been indicated that the method can provide similar coverage per-

formance as that of using a set of distinct aperture antennas with a reduced antenna payload, there remains several points requiring improvement. For instance, footprints haven't been optimized to be perfectly circular at arbitrary position on the ground, especially at the boundary of the coverage area. This implies that part of the cells are not perfectly covered by their corresponding footprints, which results in significant fluctuation of SIR values for different cells at various locations. As it is shown in the simulations, the SIR performance difference between the 'best' and 'worst' cells could be as large as 8 dB. Furthermore, scan limit is one of the properties of the electrically steerable antenna array. The three step method loss some optimization freedom for sidelobe suppression at the time it optimizes the shape of the footprints. It is found that sidelobe levels of the beampatterns steered at the boundary position are about -39 dB using a 424-element antenna array [27]. The overall sidelobe levels are not low enough when, for some scenarios, a higher SIR performance is desirable for reliable communications. Sidelobes can be further suppressed by adjusting the parameters of the Gaussian masking filter. This process, however, enlarges the size of the footprint and increases the co-channel interference.

The disadvantages mentioned above result in the requirement of 4 times more antenna elements than the aperture antennas in order to achieve the same capacity performance. However, whilst hexagonal cells are typically assumed for terrestrial communications, they are not necessarily best for communications from HAPs. Our motivation is to develop a configuration of antenna array and cellular structure that allow every cell to be well covered by the antenna footprints. Therefore, complicated footprint optimization is avoided, which saves the optimization freedom for sidelobe suppression and a significant capacity performance improvement for such cellular beamforming is expected. Recently a novel ring-shaped cell configuration has been proposed in [100] for HAPs communications. Multibeams that generated by a two dimensional rectangular planar array are employed in the scanning operation for each ring cell. Such cellular structure requires no rotational motion monitoring and corrections as well as minimizes the traffic resulting from location updating. Other major advantages lie in power reduction and allowing the implementation of TDMA techniques, which can not be implemented when applying hexagonal cellular configuration [101, 102]. However, it requires high data rates for multibeams scanning for one cell and it could be even worse when each beam is optimized by complex signal processing methods. Furthermore, planar antenna array is applied in their scenario, which means sophisticated optimization methods still have to be considered in order to reduce the sidelobe levels and solve the problem of scan limit discussed in Chapter 3.

In this chapter, applying the ring-shaped cellular configuration, we propose to use

vertical linear antenna array to generate ring-shaped beampatterns. Because of the circular symmetrical properties of vertical linear antenna array beampatterns, ring-shaped footprints can be easily generated at any location on the ground, which means complex footprint optimization techniques are not required. This significantly simplifies the optimum weighting design. The proposed one dimensional antenna shows improvement in the reduction of both antenna payload and implementation complexity, compared with the two dimensional planar antenna array and aperture antennas. Moreover, simulation results show that a significant improvement in coverage performance is achieved when compared with using planar antenna array. The chapter is organized as follows. In Section 4.2, the system model is described. Section 4.3 describes an algorithm to determine the number and sizes of cells that can be supported. Numerical results are given in Section 4.4 and finally, conclusions are given in Section 4.5. The related material has been published in [103].

4.2 System Model Description

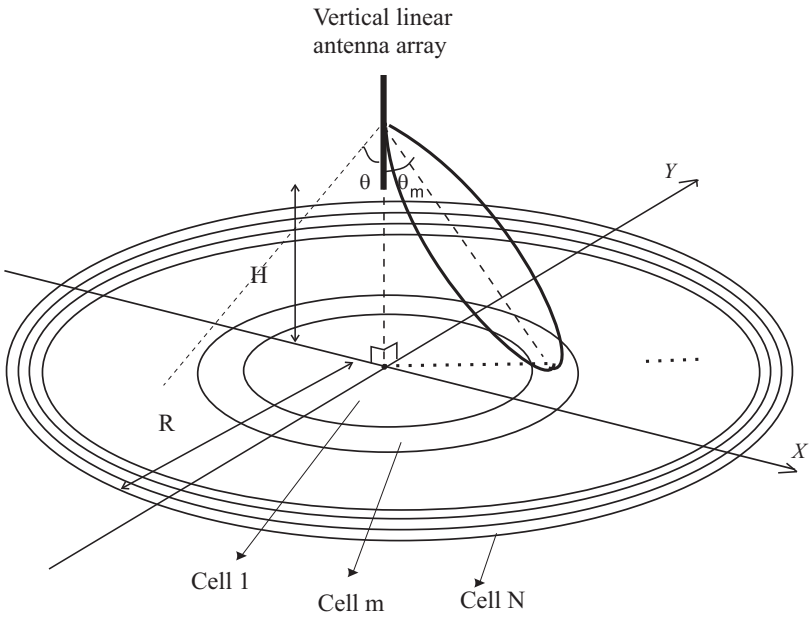

Figure 4.1: Vertical antenna array and ring-shaped cells for HAPs communications.

Fig.4.1 illustrates the communications scenario with a vertical linear antenna array at altitude H providing coverage over a circular area of radius R. This area is divided into N ring-shaped cells. The array factor of a conventional linear antenna array with K

elements steered at the angle θ_m for the mth cell is given by:

$$F^{(m)}(\theta) = \sum_{k=0}^{K-1} w_k e^{jk_0 kd(\cos\theta - \cos\theta_m)} \tag{4.1}$$

where θ is the complementary elevation angle as shown in Fig.4.1, $j = \sqrt{-1}$, $k_0 = 2\pi/\lambda$ the wave number, λ the wavelength, d the element spacing, w_k the weight of the kth antenna element. Fig.4.2 is an example of the beampattern generated by a 170-element linear vertical antenna array, $\theta_m = 45°$. The mainlobe of the beampattern has a cylinder shape and can well cover the corresponding ring-shape cell. Therefore the planar array footprint distortion problems discussed in the previous chapters are avoided.

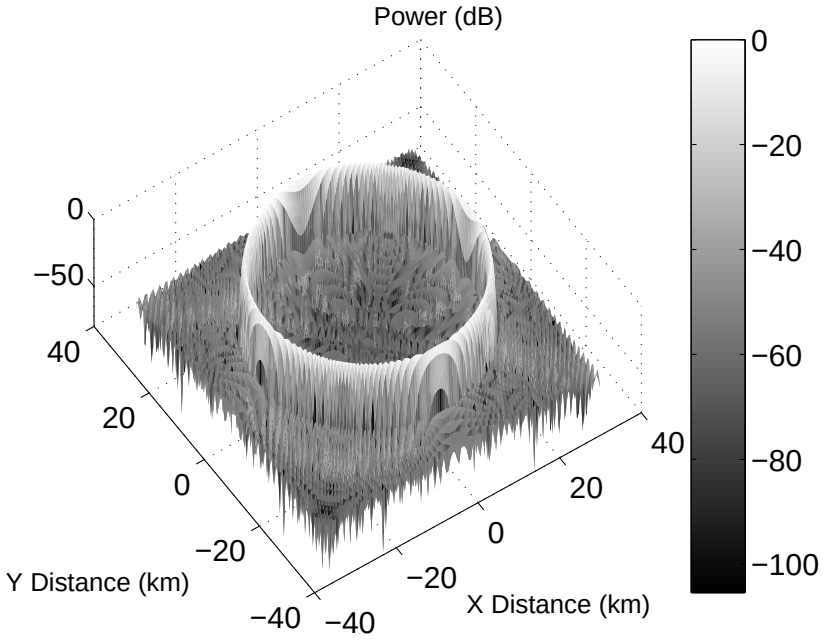

Figure 4.2: The Three dimensional beampattern of a 170-element linear vertical antenna array.

The larger the element spacing d, the narrower the mainlobe beamwidth can be made; this allows more cells to be supported. However, the increase of the element spacing may result in the appearance of grating lobes. One can let $d = \lambda$, in which case, by (2.11), gratinglobes occur at $\pm 90°$. Or one can let $d = \lambda/(1 - \cos\theta_n)$, θ_n the pre-defined coverage boundary, in order to avoid the appearance of the grating lobes within the coverage area. However, the grating lobes may cause severe interference to communication systems outside the coverage area.

An alternative solution to overcome grating lobes and reduce antenna complexity

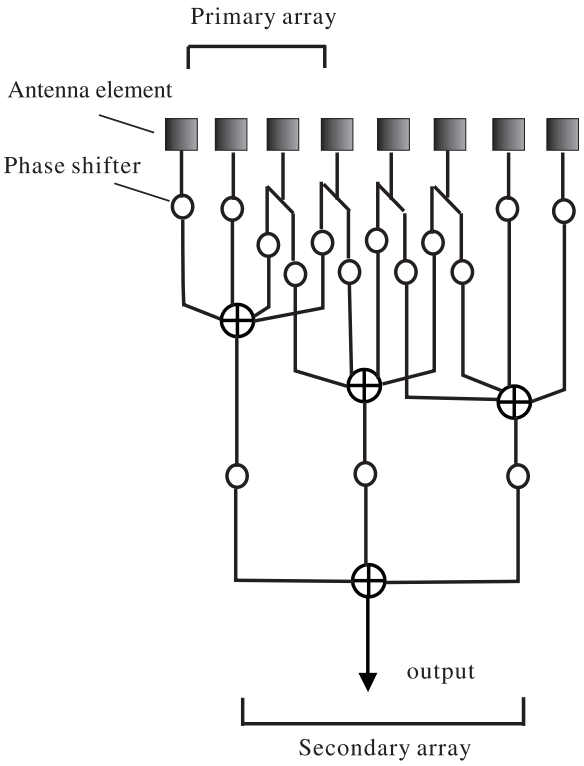

Figure 4.3: An 8-element overlapped subarray antenna example: 4 elements for primary array and 3 elements for secondary array.

is to apply subarray antennas [104]. In such an antenna, elements of the antenna array are divided into subarrays. Array elements can be shared by neighbor subarrays (or named as overlapped subarray, as shown in Fig.4.3. The subarrays are referred to as primary arrays and their respective outputs constitute secondary array. The overall array factor of a subarray antenna is given by [104]

$$\begin{aligned} F^{(m)}(\theta) &= F_1^{(m)}(\theta) F_2^{(m)}(\theta) \\ &= \sum_{k_1=0}^{K_1-1} \sum_{k_2=0}^{K_2-1} w_{k_1} w_{k_2} e^{jk_0(\cos\theta - \cos\theta_m)(k_1 d_1 + k_2 d_2)}, \end{aligned} \tag{4.2}$$

where $F_1(\theta)$ and $F_2(\theta)$ are primary and secondary array factors, K_1 and K_2 define the number of antenna elements in the primary array and secondary array, w_{k_1} and w_{k_2} are element weights of the two arrays, and d_1 and d_2 are their respective element spacings.

The design of the two arrays can be essentially separated. The primary array, described by the parameters d_1, K_1, and w_{k_1}, is designed to suppress the grating lobes without significant attenuation of $F_1(\theta)$ within the coverage area. The weights w_{k_1} are kept the same for all sub-arrays and all directions θ_m, $m = 1, \ldots, N$. The number of elements K_1 is usually small and the element spacing d_1 can be made equal to λ to avoid grating lobes. The secondary array, described by the parameters d_2, K_2, and w_{k_2}, is designed to provide narrow mainlobes and low sidelobes. The weights w_{k_2} are kept the same for all directions θ_m, $m = 1, \ldots, N$. When d_2 is chosen as a multiple of d_1, elements of neighboring subarrays can be shared, thus reducing the antenna complexity and weight. It can be seen that a significant part of the antenna beamforming (the weighting in sub-arrays and weighting by w_{k_2} in the secondary array) is shared by all N antenna beams. The beamforming in a subarray antenna requires only NK_2 multiplications by complex weights $e^{-jk_0 \cos\theta_m k_2 d_2}$ and additions against NK multiplications and additions in the conventional array. Note that for the particular case of $K_1 = 0$, $K_2 = K$, $d_2 = d$, $w_{k_1} = 1$, and $w_{k_2} = w_k$, the sub-array antenna corresponds to the conventional antenna array.

We consider downlink transmission with equal power transmitted to all cells. The cells are allocated frequency channels according to a frequency reuse plan. With the hexagonal cellular configuration, the allowable frequency reuse plans are 1-cell, 3-cell, 4-cell, 7-cell, etc. [105]. With the ring-shaped cellular configuration, any frequency reuse plan more than one is allowable. This makes the design of the cellular structure more flexible and is another advantage of using the ring-shaped cells. In our simulation below, 2 and 3 frequency reuse plans are respectively used.

Coverage performance estimation method is almost the same as that of planar antenna array in Chapter 5. Assume that there are N_c cells that share the same channel and

users are randomly positioned in these co-channel cells, with one user per cell. The HAP antenna steers N_c beams to these co-channel cells. The user of interest at the position θ (defined by the complementary elevation angle) receives powers $P_i(\theta), i = 1, \cdots, N_c$, from these beams, one forms the cell with the user of interest, the power of which is denoted by $P_m(\theta)$. For the user of interest, the SIR can be defined by:

$$SIR(\theta) = \frac{P_m(\theta)}{\sum_{i=1, i\neq m}^{N_c} P_i(\theta)}. \tag{4.3}$$

We run a set of simulation trials. In a trial, the SIR for every user is calculated, i.e., N_c SIR values are obtained. From these values obtained in all the trials, the function $C(\rho) = Pr\{SIR > \rho\}$, representing the cumulative distribution function, is estimated and plotted. Again, we assume that the performance is the same for all frequency channels. Therefore, simulation for one frequency channel only is performed.

4.3 Cells Number and Size Determination

In order to analyze the coverage performance, the number and size of cells should be primarily determined. An algorithm has been proposed to define the center position and the width of each cell. The algorithm aims to make each cell size to be the same as the beamwidth of the corresponding beampattern (defined as the 3 dB beamwidth or HPBW). It has been indicated that the beamwidth of the beampattern varies with the steering position, number of antenna elements, elements spacing and elements weights. For a given scenario of these parameters, the size of the beampattern footprints can be determined at any location on the ground. We steer beams from the center of the coverage area to its boundary and accurately connect each cell on the ground, shown in Fig.4.4. Thus the cells number, cells position and every cell size can be determined. The algorithm flow chart is shown in Fig.4.5 and characters description is given in Table.4.1.

Table 4.1: Characters Description

C_i	Center position of the ith cell
$B_l(i)$	Left boundary of the ith cell
$B_r(i)$	Right boundary of the ith cell
$B(i)$	$B_r(i) - B_l(i)$
R	Radius of the coverage area
$\delta(i)$	$\lvert B_l(i) - B_r(i-1)\rvert$
ε	An accuracy metric
σ	Step size

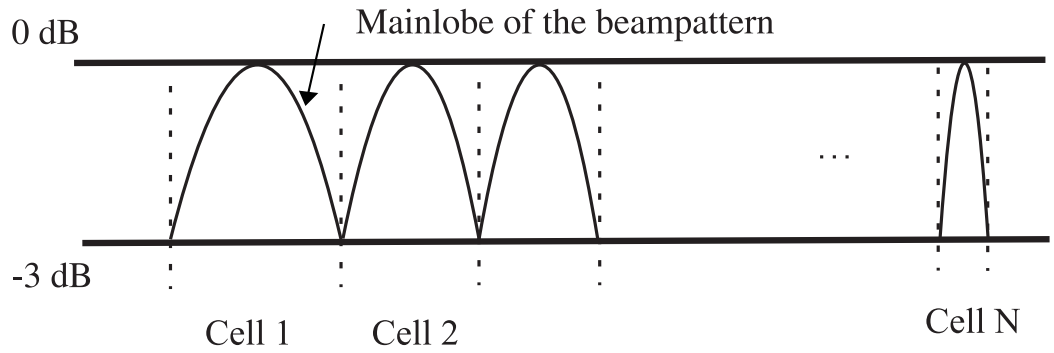

Figure 4.4: Beampattern connection to form cells.

4.4 Numerical Results

Fig.4.6 compares the beampatterns of non-subarray and subarray vertical linear antennas. The number of array elements is 170 for both cases. For non-subarray structure, Hamming window weights and 2λ elements spacing are used, which produces grating lobes at $\pm 60^{\circ}$ and $\pm 90^{\circ}$. For the subarray structure, we use $K_1 = 4$, $K_2 = 84$, $d_1 = \lambda$, $d_2 = 2\lambda$ and Hamming window weights for both primary and secondary arrays. It is shown that grating lobes are suppressed to be approximately 54 dB lower than the main lobe level.

Then we compare the coverage performance of three designs: 1) a set of aperture antennas with hexagonal cells [23]; 2) a planar antenna array with hexagonal cells [27]; and 3) proposed vertical linear antenna arrays with ring-shaped cells. We assume that 3 dB mainlobe beamwidth of each beampattern is used to cover the corresponding cell.

Fig.4.7 shows the coverage performance of 121 narrowbeam (5°-beamwidth) aperture antennas at an altitude of $H = 20$ km, forming 121 hexagonal ground cells in the coverage area of a radius $R = 32.7$ km, with 4-cell frequency reuse plan (30 cells/channel) [23]. Fig.4.7 also shows the coverage performance of a circular planar antenna array with 424 omnidirectional antenna elements [27]; the HAP altitude, cellular structure, coverage area, and the frequency reuse plan are the same as for the aperture antennas. The designs provide very similar performance: 17.6 dB and 17 dB SIRs for 95% coverage, respectively. Thus, the planar antenna array requires less than 4 omnidirectional antenna elements per cell to provide approximately the same performance as the narrowbeam aperture antennas.

A vertical linear antenna array with $K = 121$ elements, Hamming window ele-

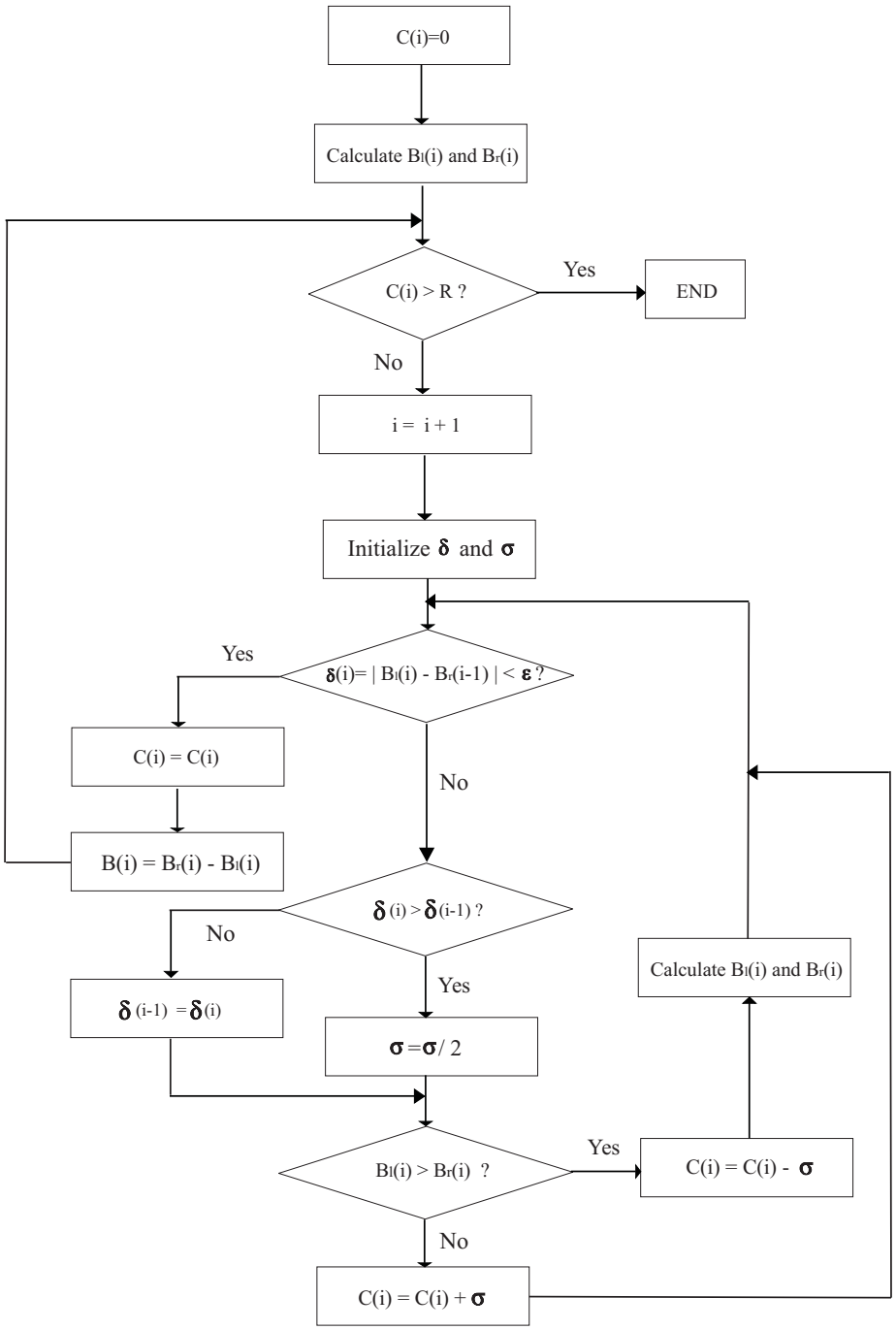

Figure 4.5: An algorithm of connecting beampatterns in order to determine the number, the position and the size of cells.

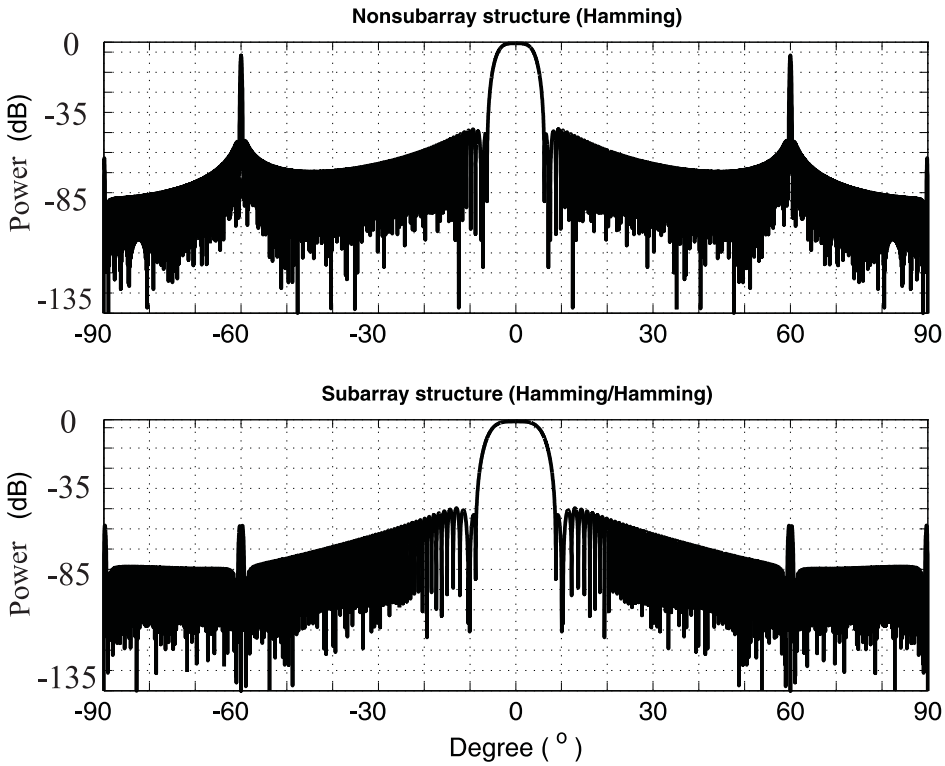

Figure 4.6: Comparison of 170-element linear vertical antenna beampattens of non-subarray and subarray structures. Non-subarray: 2λ spacing, Hamming window; Subarray: $K_1 = 4$, d_1=λ, $K_2 = 84$, d_2=2λ, Hamming / Hamming weights.

ment weights, element spacing $d = 1.4\lambda$, 60 ring-shaped cells and 2-cell frequency reuse plan (30 cells/channel) provides a significantly better coverage performance: 22.5 dB for 95% coverage. However, for $d = 1.4\lambda$, grating lobes appear outside the coverage area at angles $|\theta| > 73.4°$. This may be undesirable in some scenarios when other communications using similar frequency are conducted in the region outside of the HAP coverage area. To avoid the grating lobes, we use $d = \lambda$ and $K = 170$ (1.4 times more elements are required to support the same number of cells); in this case, the SIR of 23 dB is provided for 95% coverage. Finally, when applying the subarray technique with $d_1 = \lambda$, $d_2 = 2\lambda$, $K_1 = 4$, and $K_2 = 84$ to an antenna array with 170 elements, so that two neighboring subarrays share two antenna elements, and Hamming windows are used as element weights w_{k_1} and w_{k_2} for the primary and secondary arrays, the coverage performance is further improved (23.9 dB SIR for 95% coverage). However, the main benefit of the subarray technique is that the beamforming becomes simpler due to a smaller number of subarrays ($K_2 = 84$) in the array antenna, as opposed to $K = 170$ elements in the conventional array; i.e., the reduction in (real-time) computations is approximately two times.

Thus, a better coverage performance is achieved with vertical linear antenna arrays compared with aperture antennas and planar antenna arrays. If grating lobes outside the coverage area are acceptable, this is achieved with the same number of omnidirectional elements as the number of highly directive aperture antennas. Thus, a significant reduction in the antenna weight can also be achieved. If grating lobes outside the coverage area are undesirable, a vertical linear antenna array with 170 elements can be used, i.e., as little as 1.4 elements per aperture antenna.

Although for the downlink scenario with equal powers transmitted to cells, SIR may be high enough for reliable communications, in other scenarios a higher SIR performance is desirable. For example, these are the uplink scenario without power control or a downlink scenario with non-equal powers transmitted to cells. In these cases, a significant margin in the SIR performance is desirable. The coverage performance can be significantly improved by slightly increasing the number of antenna elements and optimizing the weights w_{k_1} and w_{k_2} of the primary and secondary arrays.

Fig.4.8 shows simulation results for different subarray antennas. The communications scenario is the same as that in Fig.4.7. The subarrays contain $K_1 = 4$ omnidirectional elements with element spacing $d_1 = \lambda$, and with Hamming window weights applied to the elements. The secondary array element spacing is $d_2 = 2\lambda$, i.e., neighboring subarrays share two antenna elements. Several window functions have been respectively used and the number of elements K_2 in the secondary array is slightly increased in order to keep the same number of cells per frequency channel. The case of the Hamming

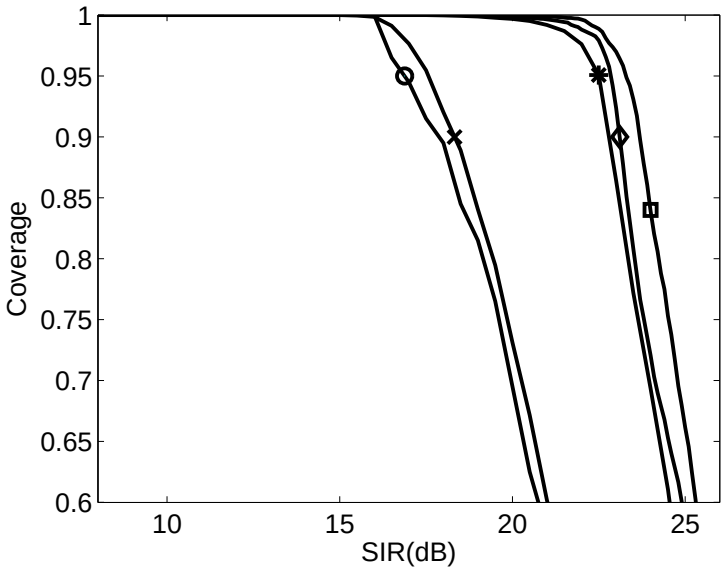

Figure 4.7: Coverage performance comparison: $\circ$ 424 planar antenna array [17]; $\times$ 121 aperture antennas [13]; $*$ 121-element vertical antenna array, 1.4 λ spacing, Hamming weights; $\diamond$ 170-element vertical antenna array, 1 λ spacing, Hamming weights; $\square$ 170-element vertical subarray antenna, $k_1 = 4$, $d_1 = 1\lambda$, $K_2 = 84$, $d_2 = 2\lambda$, Hamming / Hamming weights

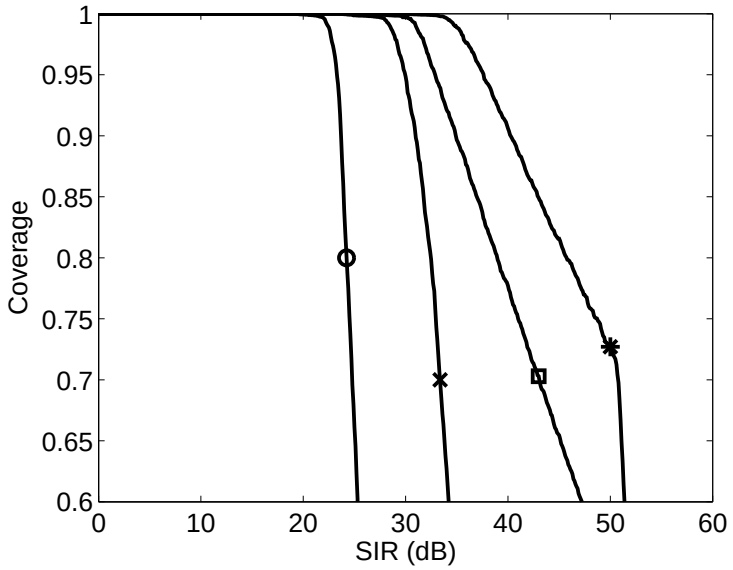

Figure 4.8: Coverage performance of vertical subarray antennas, $d_1 = \lambda$, $d_2 = 2\lambda$: $\circ$ 170-element, Hamming / Hamming; $\times$ 186-element, Hamming / Chebyshev; $\square$ 210-element, Hamming / Chebyshev; $*$ 216-element, Hamming / Blackman .

window has been already considered, which provides 23.9 dB SIR for 170 antenna elements and 84 subarrays. With the Chebyshev window for the secondary array and a slightly bigger antenna (186 elements, 92 subarrays), 30 dB SIR is achieved, while for a 210-element subarray antenna, the SIR is 32.9 dB. Finally, with the Blackman window, the SIR is 37.6 dB for 216 elements.

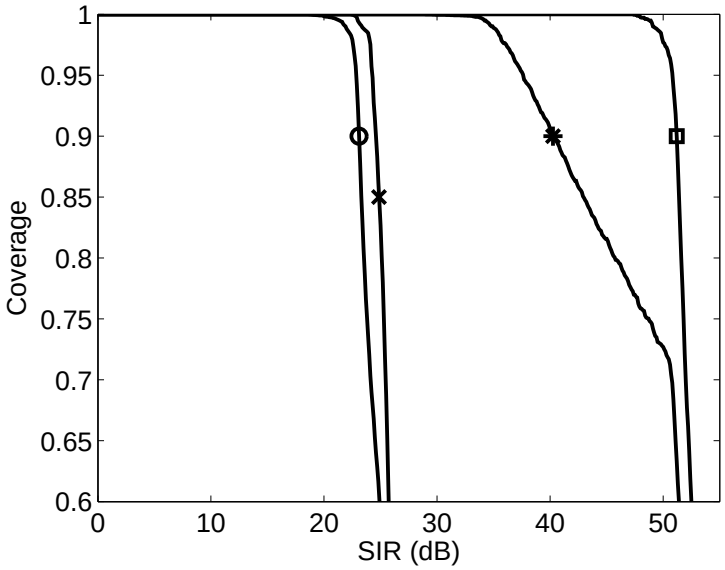

Figure 4.9: Coverage performance of subarray antennas using 2 and 3 spectral reuse factors: ∘ 170-element, 60 cells with 2 frequency reuse, Hamming / Hamming; × 170-element 90 cells with 3 frequency reuse, Hamming / Hamming; ∗ 216-element, 60 cells with 2 frequency reuse, Hamming / Blackman; □ 216-element, 90 cells with 3 frequency reuse, Hamming / Blackman

In Fig.4.8, the slopes of the last two curves from the left are low, which means users at some co-channel cells suffer relatively higher interference than others and lead to significant fluctuation of SIR values. This is caused by beamwidth and sidelobe properties of different window functions. Compared with Hamming window, Chebyshev (control to -80 dB sidelobe level) and Blackman have wider beamwidth. So users that positioned close to the main lobe may receive relatively high interference when Blackman or Chebyshev windows are applied, which limits the coverage performance to some extend. The problem can be solved by increasing the spectral reuse factor. In order to keep the number of cells per channel unchanged (for the convenience of comparison), cell sizes have to be reduced in order to form more cells. In this case, we use the spectral reuse factor 3 and make 1.4 dB main lobe beamwidth of each beampattern to cover the corresponding cell (instead of using 3 dB beamwidth in the previous scenario). Coverage performance of subarray vertical linear antennas is shown in Fig.4.9. Square and star

lines respectively representing 60 cells Hamming/Hamming and Hamming/Blakman subarrays have already been considered in Fig.4.8. For Hamming window weights, the effect of increasing the spectral reuse factor is limited, about 2 dB improvement for 95% coverage, while a significant 13 dB improvement can be achieved in the case of applying Blackman window weights.

From the simulation results above, it is found that a linear vertical antenna array, even using the simplest window functions as antenna element weights can provide much better coverage performance than the planar antenna arrays while requiring approximately 2.5 times less antenna elements. When compared with the distinct aperture antennas, the vertical antenna array with window weights requires 1.4 times more antenna elements in order to support the same number of cells per frequency channel as that of aperture antennas. Considering the bulky weight and size of the aperture antennas, described in the previous chapters, vertical antenna arrays show significant advantages in simplification of antenna design. In the later chapters, more sophisticated antenna weights optimization methods will be investigated using the linear vertical antenna array to further improve the coverage performance for HAPs communications.

It should be noted that in such an antenna array and cellular system, it is difficult to provide communications for the center cell since the antenna array is steered to its endfire, which is the most disadvantage of using vertical antenna array. One aperture antenna can be especially applied for the 'blind' (center) cell. Another disadvantage is that the proposed ring-shaped cellular structure may result in unequal cell size. The size outside cells could be larger than the inner cells. Therefore, in order to achieve equal sized cellular communications, array thinning methods should be applied to further reduce the mainlobe beamwidth when the beam is steered to the outside cells with narrow width. However, considering the significant improvement of coverage performance and antenna payload reduction, the vertical antenna array and ring-shaped cellular configuration can be still considered as a possible antenna solution for HAPs communications. The implementation issue will be considered as one of the future work.

4.5 Summary

In this chapter, we have proposed the use of a linear vertical antenna array for ring-shaped cellular coverage from high altitude platforms (HAPs). We have shown that for a fixed number of cells per frequency channel, using a proper frequency re-use factor, the linear vertical antenna arrays with ring-shaped cellular configuration are capable of pro-

viding a significantly better coverage performance than that of the narrowbeam aperture antennas or planar antenna arrays. More specifically, using simple Hamming weights, a 170-element linear vertical antenna array achieves 6 dB better coverage performance than 121-element aperture antenns or 424-element planar antenna array. Therefore, the linear array provides further benefits in terms of antenna design and implementation simplification, weight and size reduction. The improvement is even more significant when subarry structure is applied, which reduces the effect of grating lobes and reduces the number of output antenna elements. The improvement mentioned above is crucial for the payload limited stratospheric platforms.

Chapter 5

Modified Null-Broadening Adaptive Beamforming for HAPs Communications: A Constrained Optimization Approach

Contents

5.1 Introduction

In the last two chapters, several cellular beamforming methods have been investigated for HAPs applications. These methods aim to optimize beampattern footprints to cover the corresponding cells while reducing the sidelobe levels. In the downlink scenario, interference users are located at the sidelobes area and receive relatively low power from the array antenna. Therefore an overall high SIR performance can be achieved.

Adaptive beamforming is another possible solution to system capacity improvement. It

achieves maximum reception in a specified direction by estimating the signal from a desired direction (in the presence of noise) while signals of the same frequency from other directions are rejected. Therefore, the beampatterns generated by adaptive beamforming methods are optimized only at the direction of desired signal and interferers, which leads to high SINR performance. The MVDR beamformer [66] is one of the most well known methods, which has significant interference rejection capability, provided that the array steering vector is accurately known. However, its performance degrades significantly if the knowledge of the steering vector is imprecise. Diagonal loading is a popular approach to improve the robustness of the MVDR beamformer [85–87]. However, these optimal weights are derived by maximizing uplink SINR. In our downlink scenario, where there are multiple users and the weights are required to optimize simultaneously, diagonal loading formed weights, to our best knowledge from the literature, can not be derived. Previous work on downlink robust beamforming are found in [88, 89]. However, these methods achieve quite low performance (in terms of extremely high transmit power in total) when users are closely separated. Moreover, the selection of the constrained parameter is still in an *ad hoc* way. Null-broadening is another robust beamforming method [90]. The underlying concept of null-broadening is to distribute equal-strength artificial sources around each interference user to generate trough like beampatterns. Therefore, instead of placing sharp nulls in the directions of interferers as in the traditional MVDR beamformer, the null-broadening method provides significant robustness against inaccuracy of steering information. The method requires DoA estimation to obtain steering knowledge, although the accuracy of the DoA estimation is not required to be high. However, the most advantages of the null-broadening method is its robustness and simple implementation, especially for a linear antenna array. Because of these, the null-broadening method can be considered as a solution to robust beamforming for downlink HAPs communications.

On the other hand, the null-broadening method proposed in [90] can be further improved. For instance, the mainlobe is not broadened. This may result in poor coverage performance when the system is suffering high steering errors while the beampattern is narrow. Furthermore, arranging an equal number of additive sources for each interferer evidently limits coverage performance. In this chapter, the linear vertical antenna array described in the previous chapter is applied in order to reduce the system complexity. First we investigate the MVDR and diagonal loading robust beamforming in both uplink and downlink scenarios. Then we propose an improved null-broadening method. In particular, the following refinements are introduced to improve the robustness of the null-broadening technique: (i) a new constrained optimization problem is formulated to broaden both nulls and mainlobe; (ii) the optimization problem is solved using semidefinite programming (SDP) [106, 107]; (iii) a non-equal number of additive sources

are assigned to different users to reduce the total number of optimization parameters, which makes the SDP solution more efficient. The proposed approach is compared with the traditional MVDR beamformer and the conventional null-broadening technique proposed in [90] for downlink HAPs communications. Performance improvement due to the modified null-broadening approach is significant. The related material has been published in [108].

5.2 Adaptive Beamforming and Diagonal Loading Techniques

In this section, we begin by reviewing the MVDR beamformer and investigate the diagonal loading robust beamforming method for both uplink and downlink.

Consider a linear antenna array of K omnidirectional elements. Assume that there are L users randomly distributed on the ground. Using the matrix representation, the output of a narrowband beamformer is given by

$$y(t) = \mathbf{w}^H \mathbf{x}(t), \tag{5.1}$$

where t is the time index; $\mathbf{x}(t) = [x_1(t), \cdots, x_K(t)]^T \in C^{K\times 1}$ is the array observations and $\mathbf{w} = [w_1, \cdots, w_K]^T \in C^{K\times 1}$ is the array weights. $(\cdot)^H$ denotes the conjugate transpose and $(\cdot)^T$ denotes the transpose. The uplink SIR is represented at [85]:

$$\eta(\theta_m) = \frac{\mid \mathbf{w}_m^H \mathbf{u}(\theta_m) \mid^2}{\mathbf{w}_m^H \mathbf{R} \mathbf{w}_m}, \tag{5.2}$$

where $\mathbf{u}(\theta_m)$ is the $K \times 1$ steering vector pointing θ_m degrees from the broadside and $\mathbf{R}$ represents the theoretical $K \times K$ covariance matrix. In practical applications, $\mathbf{R}$ is unavailable and is substituted by sample covariance matrix $\hat{\mathbf{R}}$,

$$\hat{\mathbf{R}} = \frac{1}{N} \mathbf{X}\mathbf{X}^H, \tag{5.3}$$

where $\mathbf{X} = [\mathbf{x}_1(t), \cdots, \mathbf{x}_N(t)] \in C^{K\times N}$ represents the received snapshots, N the number of snapshots. The MVDR beamforming is designed to solve the following constrained quadratic problem [66],

$$\min_{\mathbf{w}_m} \mathbf{w}_m^H \hat{\mathbf{R}} \mathbf{w}_m \quad \text{subject} \quad \text{to} \quad \mathbf{w}_m^H \mathbf{u}(\theta_m) = 1. \tag{5.4}$$

More generally, we investigate the following problem,

$$\min_{\mathbf{w}_m} \mathbf{w}_m^H \hat{\mathbf{R}} \mathbf{w}_m \quad \text{subject} \quad \text{to} \quad \mathbf{w}_m^H \mathbf{u}(\theta_m) = g, \tag{5.5}$$

where g is a complex constant. (5.5) is referred to Linear Constraint Minimum Variance (LCMV) beamformer [109]. It linearly constraints the weights, such that any signal coming from the angle direction θ_m is passed to the output with response (gain) g. Comparing (5.4) and (5.5), we see that the MVDR beamformer is indeed a special case of the LCMV beamformer for $g = 1$.

The problem (5.5) is solved by the method of Lagrangian multipliers. The Lagrangian for (5.4) is

$$\zeta(\mathbf{w}_m) = \mathbf{w}_m^H \hat{\mathbf{R}} \mathbf{w}_m + \lambda[\mathbf{u}^H(\theta_m)\mathbf{w}_m - g], \tag{5.6}$$

where λ is the Lagrangian multiplier. Taking the gradient with respect to $\mathbf{w}_m$ and setting the result equal to zero, we get

$$\nabla_{\mathbf{w}_m}(\zeta) = \hat{\mathbf{R}}\mathbf{w}_m + \lambda \mathbf{u}(\theta_m) = 0, \tag{5.7}$$

and

$$\mathbf{w}_m = \lambda \hat{\mathbf{R}}^{-1} \mathbf{u}(\theta_m). \tag{5.8}$$

From (5.5), we have $\mathbf{u}^H(\theta_m)\mathbf{w}_m = g^*$, where $(\cdot)^*$ denotes the conjugate. Therefore, from the left multiply $\mathbf{u}^H(\theta_m)$ on both sides of (5.8), we obtain

$$\lambda = \frac{g^*}{\mathbf{u}^H(\theta_m)\hat{\mathbf{R}}^{-1}\mathbf{u}(\theta_m)}. \tag{5.9}$$

Substituting (5.9) in (5.8), the solution to (5.4) is derived:

$$\mathbf{w}_m = \frac{g^* \hat{\mathbf{R}}^{-1}\mathbf{u}(\theta_m)}{\mathbf{u}^H(\theta_m)\hat{\mathbf{R}}^{-1}\mathbf{u}(\theta_m)}. \tag{5.10}$$

In order to improve the robustness of the MVDR beamformer, diagonal loading optimum weights are widely used, which are solved by the method of Lagrange multiplier. A random error α is added onto the accurate steering vector $\mathbf{u}(\theta_m)$ and (5.4) is modified as [86]

$$\begin{aligned} \min_{\mathbf{w}_m} \mathbf{w}_m^H \hat{\mathbf{R}} \mathbf{w}_m \quad \text{subject} \quad \text{to} \quad & \mathbf{w}_m^H[\mathbf{u}(\theta_m) + \alpha] = g \\ & \text{and} \quad \|\alpha\|^2 \leq \epsilon, \end{aligned} \tag{5.11}$$

where ϵ is the constraint of α. The Lagrangian for (5.11) is

$$\begin{aligned} \zeta(\{\mathbf{w}_m, \alpha\}, \lambda_1, \lambda_2) = \mathbf{w}_m^H \hat{\mathbf{R}} \mathbf{w}_m + \lambda_1[(\mathbf{u}(\theta_m) + \alpha)^H \mathbf{w}_m - g] \\ + \lambda_2(\epsilon - \|\alpha\|^2), \end{aligned} \tag{5.12}$$

where λ_1 and λ_2 are Lagrangian multipliers. We solve (5.12) by taking the gradients with respect to $\mathbf{w}_m$ and α and setting the results equal to zeros,

$$\nabla_{\mathbf{w}_m}(\zeta) = \hat{\mathbf{R}}\mathbf{w}_m + \lambda_1[\mathbf{u}(\theta_m) + \alpha] = 0, \tag{5.13}$$

and

$$\nabla_{\alpha}(\zeta) = \lambda_1 \mathbf{w}_m - \lambda_2 \alpha = 0. \tag{5.14}$$

From (5.14), we have

$$\alpha = \frac{\lambda_1}{\lambda_2} \mathbf{w}_m. \tag{5.15}$$

By applying (5.15) into (5.13), the optimum weight is found

$$\mathbf{w}_m = -\lambda_1 (\hat{\mathbf{R}} + \frac{\lambda_1^2}{\lambda_2} \mathbf{I})^{-1} \mathbf{u}(\theta_m), \tag{5.16}$$

where $\mathbf{I} \in C^{K \times K}$ is the identity matrix.

The weights (5.16) are designed for an uplink scenario. For a downlink scenario, we aim to optimize downlink SIR, which can be represented as [110],

$$\eta'(\theta_m) = \frac{\mid \mathbf{w}_m^H \mathbf{u}(\theta_m) \mid^2}{\sum_{l=1, l \neq m}^{L} \mid \mathbf{w}_l^H \mathbf{u}(\theta_m) \mid^2}. \tag{5.17}$$

From the literature, there are two major optimization problems that are considered for a downlink scenario [110]:

A: $\max(\min_{1 \leq m \leq L}(\eta'(\theta_m)/\gamma_m))$ under a total power constraint, where γ_m is the SIR target for the mth user,

or

B: Minimize the total transmission power while fulfilling $\eta'(\theta_m) \geq \gamma_m \quad m = 1 \cdots L$.

However, we show in Appendix I that the diagonal loading formed optimum weights can not be derived for either of the optimization problem in a downlink scenario.

5.3 Null-broadening Adaptive Beamforming

Diagonal loading is an extension to the MVDR beamformer, considering the uncertainty of the accurate steering knowledge. Null-broadening is another extension in order to improve the robustness of the MVDR beamformer. The MVDR beamformer places sharp nulls in the directions of interferers. Therefore, it is extremely sensitive to inaccurate steering knowledge. If one can generate wide nulls at the location of cochannel interferers, such beamforming method is robust to the steering errors. The idea is first proposed

by Mailloux in 1995 [90]. He proposed to distribute a cluster of equal-strength incoherent artificial interferers around each original interferer. The method can be considered as the conventional MVDR beamformer with close formed additive interferers. The beampattern can therefore be generated with the wide nulls at the original interferers location. More specifically, Mailloux showed that the method is equivalent to modify the covariance matrix **R**. Let's first rewrite **R** in an analytical form [93]

$$R_{qp} = N_c\delta_{qp} + \sum_{m=1}^{L} P_m e^{jk_0(x_q - x_p)\sin\theta_m}, \quad q, p = 1 \cdots K, \tag{5.18}$$

where N_c is the noise variance, δ_{qp} the Kronecker delta function, P_m the received power of the mth user and x_q represents the element location. To produce a trough pattern in each of the interference directions, U equal-strength incoherent sources around each original interference source are distributed. Fig.5.1 illustrates the null-broadening approach in the scenario of HAPs communications with a vertical linear antenna array mounted on a HAP at an altitude H, providing the coverage over a circular area of radius R. In this case, the

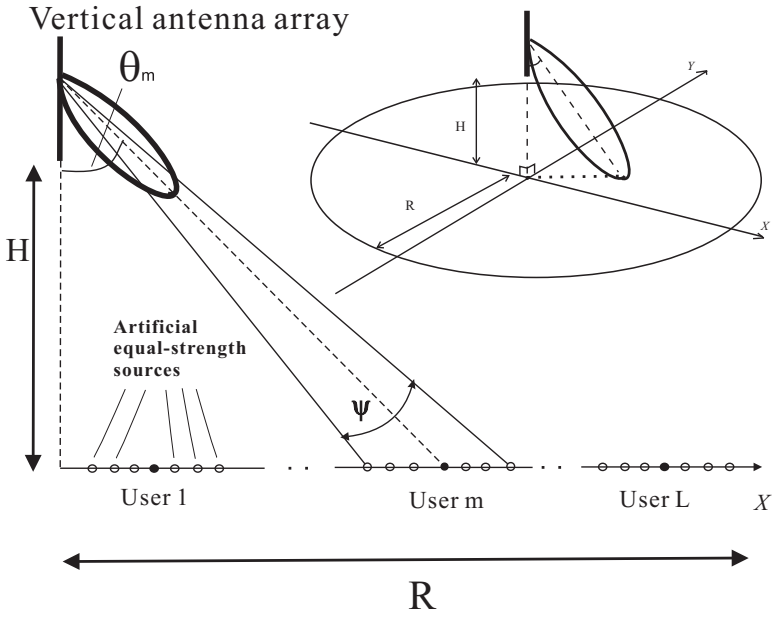

Figure 5.1: The use of null-broadening approach for HAPs communications.

modified covariance matrix $\hat{R}_{qp}$ has entries [90]

$$\hat{R}_{qp} = \frac{\sin(U\Lambda_{qp})}{U\sin(\Lambda_{qp})} R_{qp}, \quad q, p = 1 \cdots K, \tag{5.19}$$

where

$$\Lambda_{qp} = \pi(x_q - x_p)\xi/\lambda, \tag{5.20}$$

and

$$\xi = \Psi/(U-1), \tag{5.21}$$

where Ψ represents the trough width, shown in Fig.5.1.

Mailloux's method increases the number of interference users and puts these additive users in a close form to broaden the nulls. However, the method fails to broaden the mainlobe. This may result in poor coverage performance when the mainlobe beamwidth is relatively narrow, compared with the amount of steering error for the desired user, since the beamwidth varies with the number of antenna elements and steering location. Therefore, we propose a modified null-broadening method to broaden the mainlobe in addition to the nulls. Denote

$$\Theta = [\Theta_1, \Theta_2, \cdots, \Theta_L] \tag{5.22}$$

and

$$\Theta_m = [\theta_m^{(-\frac{U-1}{2})}, \theta_m^{(-\frac{U-1}{2}+1)}, \cdots, \theta_m^{(0)}, \cdots, \theta_m^{(\frac{U-1}{2}+1)}, \theta_m^{(\frac{U-1}{2})}], \quad m = 1, \cdots, L, \tag{5.23}$$

where $\theta_m^{(0)} = \theta_m$ represents the original user position. The set Θ contains all user positions including the additive sources around each original user. We denote $\overline{\Theta}_m$ as the complementary set of Θ_m with respect to Θ, that is

$$\overline{\Theta}_m \cup \Theta_m = \Theta. \tag{5.24}$$

The improved null-broadening approach is based on minimizing the total power of all original interferers and their respective additive sources, while assigning unity received power to the desired user and its additive sources. Then, the beamformer weight vector $\mathbf{w}_m = [w_m^{(1)}, \cdots, w_m^{(K)}]^T$ providing a beampattern for the mth user can be found by solving the following constrained optimization problem

$$\mathbf{w}_m = \arg\min_{\mathbf{w}} \sum_{\theta_i \in \overline{\Theta}_m} \left|\mathbf{w}^H \mathbf{u}(\theta_i)\right|^2 \text{ subject to } \frac{1}{U} \sum_{\theta_n \in \Theta_m} \left|\mathbf{w}^H \mathbf{u}(\theta_n)\right|^2 = 1, \tag{5.25}$$

where $i = 1, \cdots, (L-1)U, \quad n = 1, \cdots, U$. Different from assigning a unit power to the desired user, as in the case of the MVDR beamformer [66] or the Mailloux's null-broadening method [90], the problem (5.25) sets a constraint to the total received power of a cluster of 'desired users' in order to broaden the mainlobe.

The problem (5.25) can be described as a minimization problem, consisting of an objective function and one equality constraint function. Such optimization problem is especially appropriate for a semidefinite programming (SDP) solver (by using the interior point method) [111]. SDP creates a smooth convex nonlinear barrier function for the constraints and makes it practical to solve convex problems of large size [106, 107]. However, the performance of SDP is affected by the total number of optimization parameters, i.e. $L \times U$ in the problem (5.25). Therefore, to obtain more efficient SDP

solutions, the total number of optimization parameters should be reduced and this can be achieved by assigning a non-equal number of additive sources for different users. In particular, the number of additive sources required can be made inversely proportional to the beamwidth of the beampattern projected to the desired user. For a vertical linear array, it can be found that the number of additive sources for the mth original user U_m can be made proportional to $\sin(\theta_m)$. We now rewrite (5.24) as

$$\Theta = [\Theta_1^{(U_1)}, \Theta_2^{(U_2)}, \cdots, \Theta_L^{(U_L)}], \tag{5.26}$$

and

$$U_m = \lfloor a \sin(\theta_m) + b \rfloor, \tag{5.27}$$

where $\lfloor \cdot \rfloor$ denotes the rounding integer. Therefore the total number of optimization parameters could be much smaller than that of the scenario of uniformly distribution, $\sum_{m=1}^{L} U_m < L \times U$.

In our simulation scenario, we propose to use 170-element vertical antenna array to provide communications for 60 users on the ground. Every user is suffering a 60 m maximum position error. Suppose the antenna array is steered to a user at $\theta_m = 0$, it is found that $U_m = 3$ is enough to broaden the 3 dB mainlobe beamwidth to cover the predefined error range. Therefore $b = 3$. Then we assume that there is a user located at ($\theta_m = 58.5°$). It is found that we should use $U_m = 7$ or $U_m = 8$ ($U_m = 7$ is not enough while 8 is too more) to cover the error range. Therefore, we determine $a = 5$ and $b = 3$ to estimate the required number of additive users according to (5.27).

5.4 Numerical Results

Coverage performance estimation is similar to those in Chapters 3 and 4. Assume that L users are randomly distributed over the coverage area, sharing the same frequency channel. The mth user receives powers $\{P_1, \cdots, P_L\}$ from all L beams of the HAP antenna. Downlink SIR for the mth user is given by

$$SIR_m = \frac{P_m}{\sum_{i=1, i \neq m}^{L} P_i}. \tag{5.28}$$

The coverage performance is represented by the cumulative distribution function $C(\rho) = Pr\{SIR_m > \rho\}$. Fig.5.2 and Fig.5.3 compare the coverage performance of the following four adaptive beamforming methods in the downlink HAPs communications scenario: (i) the MVDR beamformer; (ii) Mailloux's null-broadening method [90]; (iii) proposed null-broadening method using an equal number of additive sources for all users;

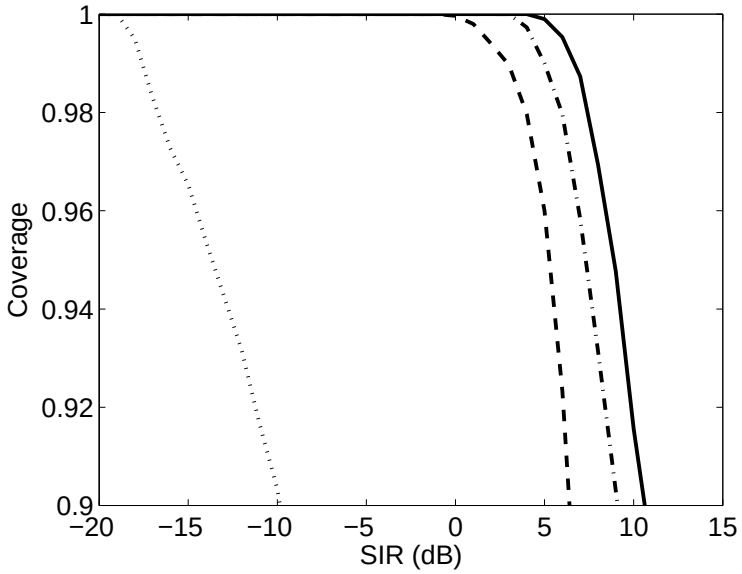

Figure 5.2: Coverage performance comparison of MVDR beamformer, Mailloux's method [81] and the improved null-broadening method, $K = 170$, $L = 60$, 60m maximum user position error: dotted, MVDR beamformer; dashed, Mailloux's method [81]; dash-dotted, improved null-broadening approach, using uniform distribution for number of additive sources; solid, improved null-broadening approach, using non-uniform distribution for number of additive sources.

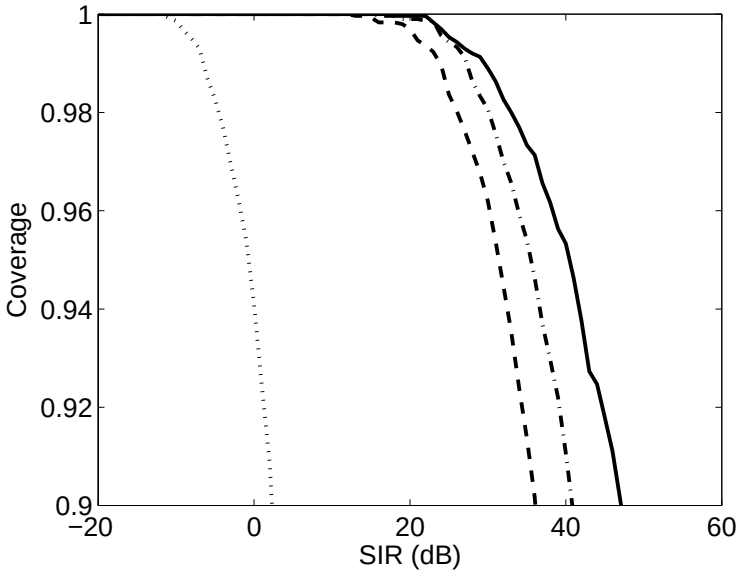

Figure 5.3: Coverage performance comparison of MVDR beamformer, Mailloux's method [81] and the improved null-broadening method, $K = 170$, $L = 20$, 60m maximum user position error: dotted, MVDR beamformer; dashed, Mailloux's method [81]; dash-dotted, improved null-broadening approach, using uniform distribution for number of additive sources; solid, improved null-broadening approach, using non-uniform distribution for number of additive sources.

(iv) proposed null-broadening method using a non-equal number of additive sources (5.27).

The communications scenario is defined as: the coverage radius $R = 32.7$ km; the HAP altitude $H = 20$ km; the number of antenna elements $K = 170$. The users position errors are random with uniform distribution within the interval [-60 m, +60 m]. Coefficients in (5.27) are set to $a = 5$ and $b = 3$. Fig.5.2 shows the comparison results when there are 60 users sharing the same frequency channel. It can be seen that the MVDR beamformer has poor performance in the scenario of existence of steering errors. Mailloux's null-broadening method [90] significantly improves performance when compared with the MVDR beamformer. Method (iii), using constrained optimization, however, can achieve approximately 3 dB better SIR performance for 95% coverage. Further 2 dB improvement is obtained by method (iv), using non-equal number of additive sources. In Fig.5.3, the total co-channel users are reduced to 20. Again, the MVDR beamformer achieves the worst coverage performance, since it is extremely sensitive to any steering errors. The improvement of the proposed null-broadening methods are more significant than that in Fig.5.2, compared with the Mailloux's method. For a given number of antenna elements, the reduction in the number of co-channel users provides more optimization freedom for the problem (5.25). This implies that the performance of the proposed constrained optimization method can be significantly improved by increasing the number of antenna elements or increasing the frequency reuse factor.

5.5 Summary

A constrained optimization approach is proposed to improve the performance of null-broadening adaptive beamforming. This approach broadens the beampattern at the directions of the desired user as well as the interferers. The constrained optimization problem is solved by semidefinite programming and its efficiency and performance are further improved when a non-equal number of additive sources are distributed among users to reduce the total number of optimization parameters. Simulations results are obtained under the downlink HAPs communications scenario. The proposed approach achieves significant improvement in coverage performance, compared with the traditional MVDR beamformer and the previously reported null-broadening method.

Chapter 6

Antenna Array Optimization Using Semidefinite Programming for Cellular Communications From HAPs

Contents

6.1 Introduction

Cellular beamforming methods for HAPs communications have been described in Chapters 3 and 4. In Chapter 3, a footprint optimization method is proposed using a planar antenna array, which can be used to generate equal-sized circular hexagonal cells on the ground. The method requires 4 times more antenna elements than aperture antennas to achieve the same coverage performance. In Chapter 4, a configuration of using vertical antenna array forming ring-shaped cells is proposed. In such an antenna and cellular configuration, complicated footprint optimization is avoided. Therefore, the antenna design complexity is reduced. We also show that even using the simple window weights, the coverage performance is significantly improved. This requires 1.4 times more antenna elements, compared with the aperture antennas. The linear

vertical antenna array shows significant advantages in antenna payload and system complexity reduction. The coverage performance is expected to be further improved by using more sophisticated optimization techniques. From the literature, most work has been focused on beampattern synthesis (generating pencil beam and reducing sidelobes) [42, 45], asymmetric beampatterns optimization (obtain optimal element spacing for a non-uniform spaced array) [47–52] or generating beampatterns with arbitrary 2-dimensional footprints [53–59]. However, from the literature, there are rarely work that optimize beampatterns taking into account the cellular configuration on the ground. In Chapter 5, adaptive beamforming techniques are investigated in the downlink HAPs communications scenario. In the case of traditional MVDR beamformer [66], the antenna steers unit power to the desired user while steering nulls to the interferers in order to maximize the SIR performance. However, the idea can be extended to design a cellular beamformer. That is steering the unit power to the desired cell while steering nulls to the other co-channel cells. Therefore, only a part of the beampattern is optimized according to the cellular configuration, which is the key difference from the previous cellular beamforming techniques. Much better coverage performance is expected, since the optimization freedom is increased.

In this chapter, we propose a cellular beamformer based on constrained optimization for HAPs applications. The method, combining the property of the MVDR adaptive beamformer, optimizes the beampattern for the location of co-channel cells only. In particular, we show that this optimization, when applied to a linear vertical array of omnidirectional antenna elements, achieves 3 dB better SIR performance for 95$\%$ coverage compared with that of an array of the same number of narrowbeam aperture antennas. Thus, our design shows significant advantages in both coverage performance improvement and HAPs antenna payload weight reduction. The related material has been published in [112].

6.2 Constrained Optimization for Cellular Beamforming

Fig.6.1 illustrates the communications scenario with a vertical antenna array mounted on a HAP at altitude H, providing coverage over a circular area of radius R. The coverage area is divided into M ring-shaped cells.

The conventional beampattern optimization aims to constrain the mainlobe to cover the corresponding cell while suppressing sidelobes; this results in low intercell interference. Coverage performance can be significantly improved if the beampattern is optimized at

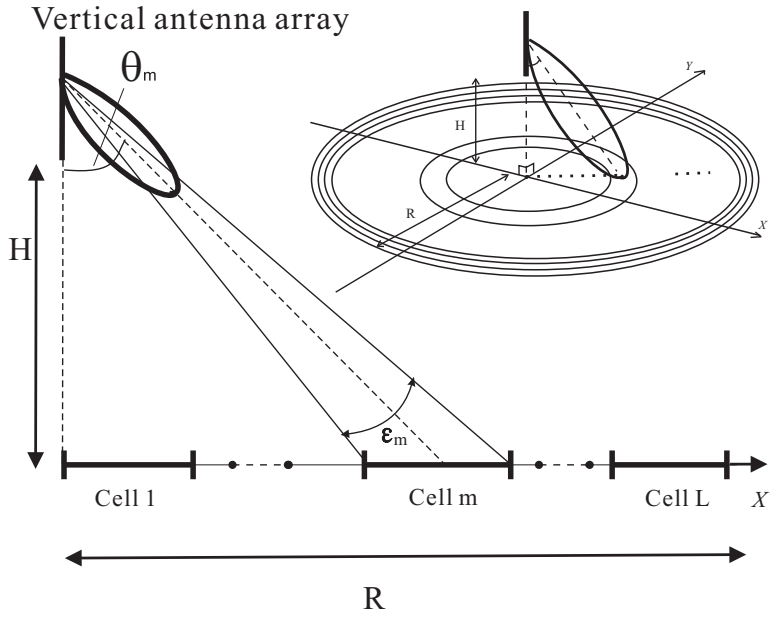

Figure 6.1: Steering the beampattern of a vertical antenna array to the m th cell from the HAP.

the location of co-channel cells instead of the whole coverage area. It is shown in [90] and [108] that wide nulls and mainlobe can be generated by placing artificial users closely around the original user. The idea can be simply extended to the scenario of cellular beamforming. Artificial users can be placed within all the co-channel cells and the beampattern, after optimization, has a wide mainlobe to cover the desired cell and wide nulls for the other co-channel interfering cells.

Let $\Theta = [0, \theta_{max}]$ represent the interval of complementary elevation angles θ corresponding to the coverage area. The steering vector for an angle $\theta \in \Theta$ is given by

$$\mathbf{u}(\theta) = [1 \quad e^{-jk_0 d\cos\theta} \quad \cdots \quad e^{-jk_0(K-1)d\cos\theta}]^T, \tag{6.1}$$

where $k_0 = 2\pi/\lambda$ is the wave number, λ the wavelength, d the element spacing and K the number of antenna elements. The coverage area is divided into ring-shaped cells. Therefore, the position of every cell can be determined by a set of angles θ. Suppose that the mth antenna array beam is steered to the mth cell. Let Θ_m be the set of angles θ corresponding to the mth cell and $\tilde{\Theta}_m$ be the set of angles θ corresponding to the other cells sharing the same channel of the frequency reuse plan as the mth cell. The cell positions are pre-defined according to the variation of beamwidth when the antenna array is steered from its broadside to the endfire, as described in section 4.3. The beamformer weight vector $\mathbf{w}_m = [w_m^{(1)}, \cdots, w_m^{(K)}]^T$ providing a beampattern for covering the mth cell

can be found by solving the following constrained optimization problem

$$\mathbf{w}_m = \arg\min_{\mathbf{w}} \sum_{\theta_i \in \tilde{\Theta}_m} \left|\mathbf{w}^H \mathbf{u}(\theta_i)\right|^2 \text{ subject to } \frac{1}{N_m} \sum_{\theta_n \in \Theta_m} \left|\mathbf{w}^H \mathbf{u}(\theta_n)\right|^2 = 1, \quad i = 1, \cdots, I_m \quad , \quad n = 1, \cdots, N_m. \tag{6.2}$$

Here, we suppose there are N_m samples of θ in the desired cell and totally I_m samples of θ in the other co-channel cells. The optimization minimizes the sum of the power steered to I_m set of θ in the interference cells and keeps the sum of the average power to the unit for the N_m set of θ in the desired cell. The constrained optimization problem can be simply solved by the semidefinite programming (SDP) solver [111].

It can be found that the constrained optimization (6.2) is similar to (5.20). However, there are still some difference between these two methods. The null broadening optimization (5.20) is an adaptive beamforming method, which means direction of arrival (DoA) should be estimated from time to time to obtain the steering knowledge. In the cellular beamforming scenario, such steering knowledge corresponds to the cell positions, represented by a cluster of close elevation angles, which are fixed for a cellular communication system. For the null-broadening method, the amount of the null width $|\theta_m^{(U-1)/2} - \theta_m^{-(U-1)/2}|$ (see section 5.3) depends on the estimated maximum steering errors of a communication system and is uniformly distributed for all the users. In the case of cellular beamforming, non-equal size cells are defined on the ground according to the variation of the footprint size of the beampattern. In the case that the number of co-channel cells in the cellular beamforming scenario is the same as that of the co-channel users in the adaptive beamforming scenario and the total optimization parameters are the same for both scenarios, the cellular beamforming method (6.2) and the null-broadening method (5.20) should result in similar coverage performance. However, for a random user distribution, the situation may frequently occur that more than one user are positioned in one cell. The cellular beamforming system can not distinguish multiple users within a cell. In this case, more access resources are required in a cellular beamforming system (i.e. applying different frequency or orthogonal codes to distinguish users as the FDMA and CDMA techniques). In the next Chapter, a methodology is introduced to compare the coverage performance of cellular beamforming (6.2) and the modified null-broadening method (5.20) in the HAPs communications scenario, taking into account the random user distribution.

6.3 Numerical Results

Assume that there are N_c cells that share the same channel and users are randomly positioned within these co-channel cells, with one user per cell. The HAP antenna steers N_c beams to these co-channel cells. The user of interest at the position θ (defined by the complementary elevation angle) receives powers $P_i(\theta), i = 1, \cdots, N_c$, from these beams, one forms the cell with the user of interest, the power of which is denoted by $P_m(\theta)$. For the user of interest, the SIR can be defined by:

$$SIR(\theta) = \frac{P_m(\theta)}{\sum_{i=1, i\neq m}^{N_c} P_i(\theta)}. \tag{6.3}$$

Coverage performance is represented by the cumulative distribution function $C(\rho) = Pr\{SIR > \rho\}$.

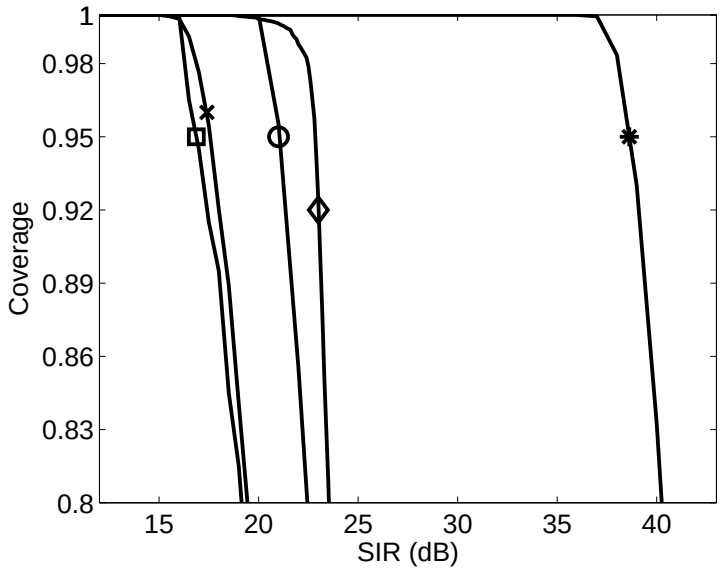

Figure 6.2: Coverage performance of aperture antennas, a planar antenna array and vertical linear antenna arrays: □ 424-element planar antenna, 121 hexagonal cells, reuse factor 4 [17]; × 121-element aperture antennas, 121 hexagonal cells, reuse factor 4 [13]; ○ 121-element vertical antenna, 61 ring-shaped cells, reuse factor 2, constrained optimization; ◇ 170-element vertical antenna, 61 ring-shaped cells, reuse factor 2, Hamming weights [95]; ∗ 170-element vertical antenna, 61-ring-shaped cells, reuse factor 2, constrained optimization.

Fig.6.2 compares the coverage performance of four antenna configurations: (i) a

set of narrowbeam aperture antennas forming hexagonal cells [23]; (ii) a planar antenna array forming hexagonal cells [27]; (iii) a vertical linear antenna array forming ring-shaped cells, using Hamming window as antenna element weights [103]; and (iv) a vertical linear antenna array forming ring-shaped cells, using constrained optimization.

The respective communication scenario is defined as: 121 hexagonal cells for antenna configurations (i) and (ii); 61 ring-shaped cells for antenna configuration (iii) and (iv); coverage radius $R = 32.7$ km; HAP altitude $H = 20$ km; 30 cells / channel. In Fig.6.2 it can be seen that the planar antenna array requires almost four omnidirectional antenna elements per cell to provide similar 95% coverage performance as that of aperture antennas employed in [23]. Our proposed approach (antenna configuration (iv)), however, can achieve about 3 dB better coverage performance using the same number of (omnidirectional, hence, physically simple) antenna elements as (narrowbeam, hence, physically large) aperture antennas, i.e. the optimization shows significant coverage performance improvement while reducing antenna payload. This is desirable, particularly in regard to light, unmanned aeroplane HAPs (e.g. NASA Pathfinder [113]). In [103], Hamming weights are applied for each vertical antenna array element and they provide 5 dB better coverage performance than aperture antennas or planar array. However, this requires 1.4 times more antenna elements in order to support the same number of cells per frequency channel. When compared with this result, our proposed beampattern optimization improves coverage performance by 15 dB. This is due to the increase of the SDP optimization freedom, which could be achieved by increasing the number of antenna elements or increasing the frequency reuse factor.

6.4 Summary

In this chapter, we have described a cellular beamforming approach for antenna array optimization that takes into account the frequency reuse plan and is based on semidefinite programming. In particular, the method combines the idea of the MVDR adaptive beamformer by optimizing the beampattern for the position of co-channel cells only. Therefore, the optimization freedom is increased, which makes it different from the traditional cellular beamformers and significantly improves the system capacity. In the HAPs cellular communications scenario, it is shown that for a fixed number of cells per frequency channel, a linear vertical antenna array achieves approximately 3 dB better SIR performance for 95% coverage compared with that of using narrowbeam aperture antennas or planar antenna arrays. This requires the same number of antenna elements as that of aperture antennas or approximately four times less number of elements than that of a planar array.

Therefore, besides the coverage performance improvement, the proposed approach could simplify antenna implementation and reduce HAPs payload.

Chapter 7

Coverage Performance Comparison of Cellular Beamforming and Adaptive Beamforming for HAPs Communications

Contents

7.1 Introduction

In Chapters 3, 4 and 6, cellular beamforming methods have been investigated for communications from HAPs. An antenna array is mounted on the HAP, providing communications over a coverage area on the ground divided by cells. This reduces system payload and makes it more flexible for system configuration. The best coverage performance of cellular beamforming is achieved by a linear vertical antenna array forming ring-shaped cellular structure, using constrained optimization [112] described in Chapter 6. The method constrains the mainlobe to cover the desired cell while minimizing the power steered to the co-channel cells. Using the same number of antenna

elements, the method allows a linear vertical antenna array to achieve better coverage performance than that of using distinct aperture antennas [23]. Considering the bulky size and weight of the aperture antennas, the proposed method shows significant advantages in antenna payload reduction. Compared with the planar antenna array solution [27] described in Chapter 3, the constrained optimization method using vertical antenna array requires 4 times less antenna elements. In Chapter 5, a modified null-broadening adaptive beamforming method is described [108]. The method improves the robustness of Mailloux's null-broadening method [90] by broadening the mainlobe as well as the nulls. Moreover, the proposed method distributes non-equal number of additive sources for each co-channel user in order to reduce the total number of optimization parameters. Simulation results show that the modified null-broadening method is robust and provides significantly better coverage performance than the Mailloux's method. Although a lot of DBF schemes (both conventional and adaptive) have been developed in the literature, there has not been much work done in evaluating and comparing the conventional and adaptive beamformers in the same communications scenario. The only work we find from the literature is the DBF performance evaluation for satellite communications [26]. However, the random user distribution is not taken into account. In the conventional beamforming scenario, multiple users could be positioned in a single cell due to a random distribution. A conventional beamformer can not distinguish users in one cell and more multiple access resources are required than that is the case in (non-cellular based) adaptive beamforming scenario. Therefore, in order to achieve accurate coverage performance comparison between conventional and adaptive beamformers, the random user distribution should be taken into account.

In this chapter, a novel methodology is proposed to evaluate and compare the performance of cellular beamforming and adaptive beamforming methods. Taking into account the random user distribution, the methodology allows the two kinds of beamformers occupying the same amount of access resources in order to improve the accuracy of the coverage performance comparison. The constrained optimization method [112] described in Chapter 6 and the modified null-broadening method [108] described in Chapter 5 are respectively selected as the cellular and adaptive beamformers. Simulation results suggest the conditions, at which the coverage performance of adaptive beamformer is better or worse than that of the cellular beamformer.

7.2 Cellular and Adaptive Beamforming Comparison Methodology

The proposed methodology is composed of the following 4 steps. Steps $1 \sim 3$ evaluate the coverage performance of the cellular beamformer and Step 4 evaluates the performance of the adaptive beamformer and compare the result with that of the cellular beamformer.

(i) Step 1 : The coverage area is divided into M cells. Users are positioned into the coverage area according to a random distribution. We denote $S(m), m = 1, \cdots, M$ as the number of users in the mth cell . A spreading factor ν is pre-defined. It determines the maximum number of users the communication system can support simultaneously in one cell. For the mth cell, the number of rejected users $S_r(m)$ can be obtained,

$$S_r(m) = \begin{cases} S(m) - \nu & S(m) > \nu \\ 0 & otherwise. \end{cases} \tag{7.1}$$

We define Υ as the communication quality, which shows the percentage of the non-rejected users,

$$\Upsilon = \frac{-\sum_{m=1}^{M} S_r(m) + \sum_{m=1}^{M} S(m)}{\sum_{m=1}^{M} S(m)}. \tag{7.2}$$

In order to achieve a high communication quality Υ, a large value of spreading factor ν is require to reduced the number of rejected users. Here, a mapping relationship $\{\Upsilon, \nu\}$ is obtained.

(ii) Step 2: Assign frequency channels for the cells according to the spectrum reuse factor β. Users that share the same frequency channel and spreading factor are obtained. They are selected to estimate the coverage performance of the cellular beamformer.

(iii) Step 3: Assume that there are N_c users that share the same frequency channel and spreading factor. The HAP antenna steers N_c beams to the cells the users are located, using a conventional beamforming optimization method. A user at the position θ (defined by the complementary elevation angle) receives powers $P_i(\theta), i = 1, \cdots, N_c$, from these beams, one forms the cell with the user of interest, the power of which is denoted by $P_m(\theta)$ and the others are interference. For this user, the SIR can be defined by:

$$SIR(\theta) = \frac{P_m(\theta)}{\sum_{i=1, i \neq m}^{N_c} P_i(\theta)}. \tag{7.3}$$

We do several trials and a number of SIR values are obtained. The function representing the coverage performance is estimated by

$$C(\rho) = Pr\{SIR > \rho\}. \tag{7.4}$$

In order to compare the performance between cellular beamformer and adaptive beamformer, we define SIR value ρ_0 at the level of 95% coverage to represent the estimated coverage performance, that is

$$\rho_0 = C^{-1}(0.95). \tag{7.5}$$

(iv) Step 4: In the non-cellular based adaptive beamforming system, we reject the worst case users (users that having closest relative distances) to achieve the same level of Υ as in the cellular beamforming system, defined in (7.2). For instance, if $\Upsilon = 0.95$, 5% most closely distributed users are rejected. According to the the mapping relationship $\{\Upsilon, \nu\}$, the value of the spreading factor ν is obtained. The co-channel users are selected from every $\nu \times \beta$ users (β has been pre-defined in Step 2). Therefore, during the coverage performance comparison, the cellular and adaptive beamforming systems always occupy the same amount of access resources and provide the same level of communication quality Υ. Again (5.23), (7.4) and (7.5) are used to estimate the coverage performance of adaptive beamformer and obtain the SIR value for 95% coverage, represented as ρ_1. Compare the 95% coverage performance of cellular and adaptive beamformer,

$$\Delta\rho(\Upsilon, e_0) = \rho_1(\Upsilon, e_0) - \rho_0(\Upsilon), \tag{7.6}$$

where $\rho_1(\Upsilon, e_0)$ and $\rho_0(\Upsilon)$, respectively, represent the 95% coverage performance of adaptive and cellular beamformer for a given Υ level and a constant level of maximum user position error e_0. The communication quality level Υ' is obtained when the two kinds of beamformers achieve similar coverage performance, which is also the 'turning point' of the two beamformers' performance, as we will find in the numerical results.

$$\Upsilon' = \arg\min_{\Upsilon} |\Delta\rho(\Upsilon, e_0)|. \tag{7.7}$$

7.3 Numerical Results

In this section, using the methodology described in Section 7.2, we compare the coverage performance of the following two beamformers in the HAPs communications scenario: (i) cellular beamforming using vertical antenna array and constrained optimization [112], described in Chapter 6; (ii) modified null-broadening adaptive beamforming [108], described in Chapter 5.

A 170-element linear vertical antenna array is mounted on the HAP, 20 km above the ground, providing communications for a circular coverage area with the radius

$R = 32.7$ km. The operation frequency is 30 GHz and the element spacing is 1 λ. For method (i), the coverage area is divided into 61 ring-shaped cells and the frequency reuse factor is $\beta = 2$. For both methods, 190 users are supported.

Firstly, users are randomly positioned into the coverage area. In the vertical antenna array and ring-shaped cellular system, users are distinguished with each other only by their distance to the center of the coverage. Therefore, users can be positioned according to either a 1-dimensional or 2-dimensional random distribution. In the simulation, we respectively use 4 kind of distributions: 1D uniform, 1D Gaussian, 2D uniform and 2D Gaussian distributions.

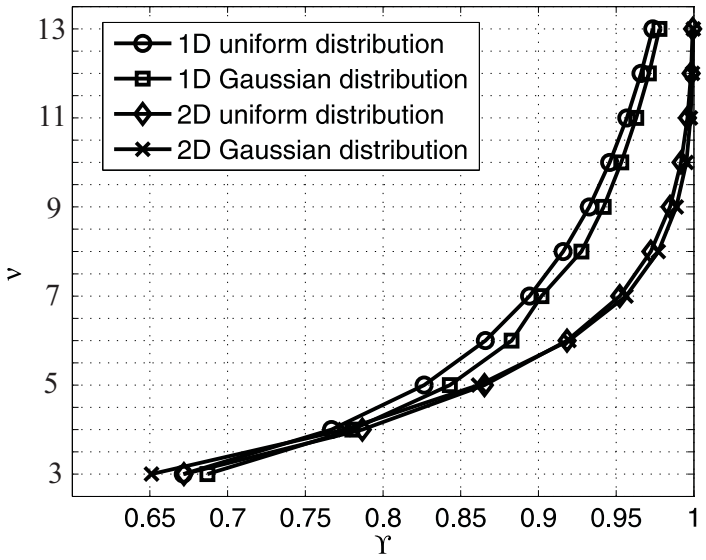

Figure 7.1: Mapping relationship of spreading factor ν and the communications quality factor Υ.

In the cellular beamforming scenario, 61 ring-shaped cells are supported with a frequency reuse factor $\beta = 2$. For a random user distribution, the communication quality factor Υ is obtained by (7.2), according to the values of the spreading factor ν. Fig.7.1 shows such a mapping relationship with ν varying from 3 to 13 when four kinds of random user distributions are respectively applied. For an efficient communication system, a high Υ level is required. In our scenario, i.e. if $\Upsilon = 0.95$, $\nu = 10$ is required for 1D users distribution while $\nu = 7$ for 2D distribution. In the adaptive beamforming scenario, we then reject the same number of users as the conventional beamforming to achieve the same Υ level and obtain the co-channel interference users according to the values of β and ν, as has been described in Step 4, Section 7.2.

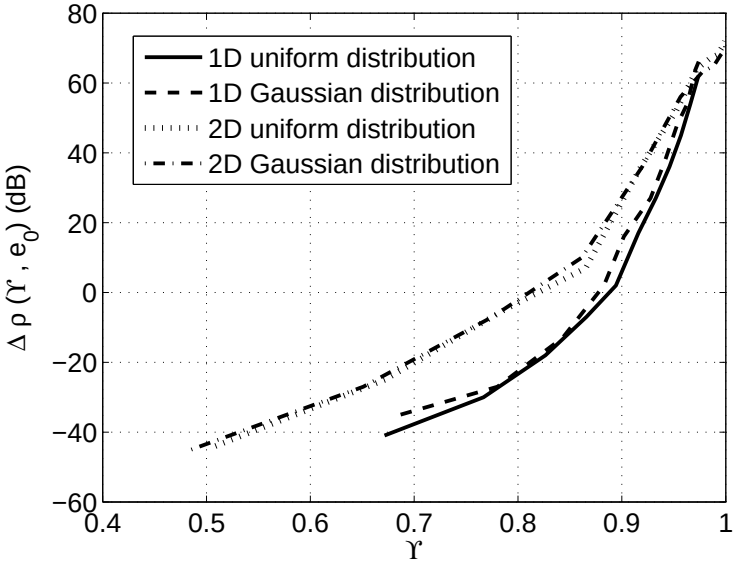

Figure 7.2: Compare the 95% coverage performance of cellular beamforming method (Chapter 6) and the modified null-broadening method (Chapter 5) with various communications quality level Υ and a constant maximum user position error $e_0 = 0.2$ km.

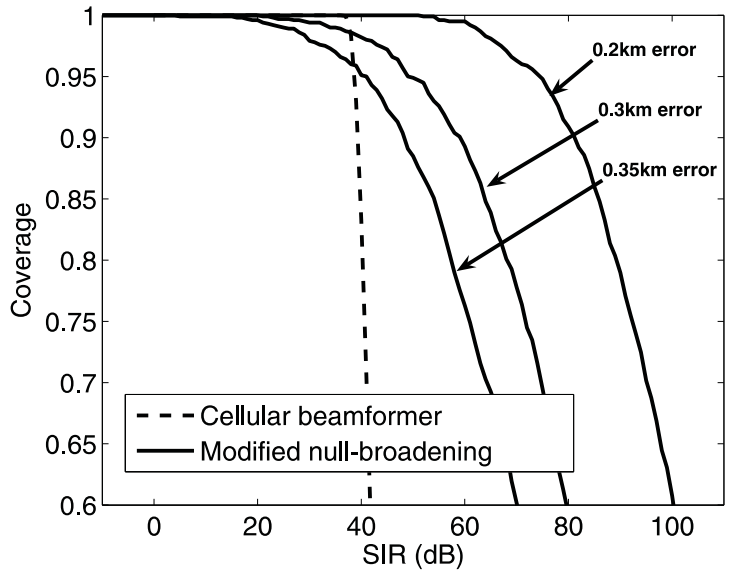

Figure 7.3: Compare coverage performance of cellular beamformer (Chapter 6) and the modified null-broadening method (Chapter 5) with a constant communications quality level $\Upsilon_0 = 0.95$ and various user position errors, 1D uniform user distribution.

Fig.7.2 gives the comparison results of $\Delta\rho(\Upsilon, e_0)$ in (7.6) with Υ varying from 0.48 to 1. For the current most popular communication systems, user position errors are estimated as below 0.2 km for GSM [114] and 0.14 km for UMTS system [115]. Here, we choose $e_0 = 0.2$ km. It is found that the higher the Υ, the more advantages the modified null-broadening adaptive beamformer shows. High Υ level implies that a large frequency reuse factor ν is applied, which means there are less co-channel interferers and the optimization freedom of the modified null-broadening beamformer is significantly increased. Fig.7.2 also suggests the benchmark values of Υ when $\Delta\rho(\Upsilon, e_0) = 0$. They are 0.82 for 2D user distribution scenario and 0.88 for 1D user distribution scenario. Therefore, the modified null-broadening adaptive beamforming method can provide better coverage performance if the communications quality level is higher than the benchmark level. Alternatively, using the mapping relationship in Fig.7.1, for the case $\Upsilon = 0.88$, $\nu = 6$. This corresponds to 16 co-channel users in the adaptive beamforming scenario. It shows that, for a 1D user distribution with a maximum 0.2 km position errors and the HAPs communications scenario, a 170-element vertical antenna array using the modified null-broadening adaptive beamforming provides worse coverage performance than that of the cellular beamforming using constrained optimization when the number of co-channel users are more than 16 (approximately 10% of the number of antenna elements). In Fig.7.2, the performance of the 4 kinds of user distribution are quite similar, which, on the other hand, shows the robustness of the proposed comparison methodology.

In the simulations above, we have defined the maximum user position errors as a constant value $e_0 = 0.2$ km. In the end, we investigate the robustness of the modified null-broadening method. Fig.7.3 shows the coverage performance of the two kinds of beamformers when $\Upsilon = 0.95$ and the maximum user position error varying from 0.2 km to 0.35 km. 1D uniform distribution is applied in this scenario. The maximum user position error is found to be 0.35 km for the modified null-broadening method when it's coverage performance degrades to the similar level as the cellular beamformer for 95% coverage. It can be seen that, in a high communication quality level (Υ), the modified null-broadening method can provide sufficient robustness for downlink HAPs applications.

7.4 Summary

In this chapter, we propose a methodology to compare the coverage performance of cellular beamformer and adaptive beamformer. In particular, a variable of communications quality is introduced, which shows the probability that a user is allowed accessing into

the communications service. Its value depends on the pre-defined spreading factor, which determines the maximum number of users the communication system can support simultaneously in a single cell. The methodology allows an adaptive beamformer occupying the same amount of access resources as that of a cellular beamformer in order to make their coverage performance comparable. We compare the coverage performance of the cellular beamformer using constrained optimization and the modified null-broadening adaptive beamformer in the HAPs communications scenario. Simulation results show the communications quality level at which the two beamformers achieve the same coverage performance. The modified null-broadening method provides much better coverage performance than the cellular beamformer when a high communications quality is provided (this requires a large number of spreading factor or frequency reuse factor). This also implies that for a access resource limited system, the proposed cellular beamforming method could be more effective and economic, considering the complicated real-time signal processing that is required by the adaptive beamformer.

Chapter 8

Space-Time Signal Processing of OFDM Transmission in the Fast-Varying Underwater Acoustic Channel

Contents

8.1 Introduction

In the previous chapters, several digital beamforming (DBF) techniques using antenna arrays have been described in applications to HAPs communications. These methods significantly improve the coverage performance while reducing the antenna payload and simplifying the system. In Chapter 8 and Chapter 9, we focus on another application of array signal processing. That is orthogonal frequency division multiplexing (OFDM) transmission in fast-varying underwater acoustic channels.

The underwater acoustic channel is a challenging environment for reliable coherent communications [29]. The underwater channel is non-stationary due to the moving

transmitting and receiving antennas, and multiple reflections of sound waves off the bottom and moving water surface. Communications in a time-varying multipath channel suffer from the intersymbol interference (ISI) which causes severe signal distortion and results in performance degradation in high data rate systems. OFDM [30] has been adopted in radio communication systems as an efficient technique for high data rate transmission in frequency-selective channels. In the underwater acoustic channel, multiple experiments with data transmission using OFDM signals were carried out by the Acoustics Institute (Moscow) in 1987-1989 [32, 33]. The use of OFDM signals has been considered as a promising technique for high data rate transmission in the underwater acoustic channel [34–36].

In OFDM systems, a guard interval is introduced to reduce the ISI due to multipath propagation. This is most often based on insertion of a cyclic prefix (CP). However, with a long channel delay spread (typical for underwater channels), the CP will consume a significant transmitted power and time. The CP insertion can be replaced by zero-padding [116]. However, any guard interval (CP or zero-padding) reduces the spectral efficiency of a communication system. In experiments that we consider below, the guard interval is not used.

In fast varying fading channels, the superimposed training allows accurate channel estimation and compensation for the signal distortion [32, 117]. In particular, it allows mitigation of the intercarrier interference (ICI) due to Doppler scattering. In our experiments, a pseudo-random pilot signal is (arithmetically) added to the transmitted data. As the period of the pilot signal is the same as the duration of the OFDM symbol, we have a periodic pilot signal. The periodicity simplifies the channel estimation and synchronization in the receiver.

We use the experimental data obtained by the Acoustics Institute in the Pacific Ocean in 1989 [33, 36]. Several space-time processing techniques are investigated in application to OFDM signals transmitted by a fast moving (at a speed of 5 m/s) underwater transducer at a depth of 250 m. A linear vertical antenna array of omnidirectional elements, positioned at a depth of 420 m, is used for receiving the signals. In this chapter, the signal processing in the receiver is described including time synchronization, coarse Doppler compensation, channel estimation and frequency-domain linear equalization. An adaptive Doppler filter (ADF) is designed in the frequency domain to provide fine compensation for the residual ICI. Experiments have been carried out in the Pacific Ocean at distances around 30 km with transmission at data efficiency of 0.5 bit/s/Hz and 1 bit/s/Hz. In this chapter, experimental results of using a single antenna element and combining signals from multiple antennas are respectively shown. In chapter 9,

adaptive beamforming methods using antenna array are applied to further improve the bit-error-rate (BER) performance. The related material has been published in [118].

8.2 Transmitted OFDM Signal

The transmitted OFDM signal is given by [36]

$$s(t) = A \sum_{k=0}^{N-1} \cos[2\pi f_k + \varphi(k)], \tag{8.1}$$

where A is an amplitude, N is the number of subcarriers ($N = 1024$), $f_k = f_c - F/2 + k/T_s$, f_c is the central transmitted frequency ($f_c = 3072$ Hz), $F = N/T_s$ is the frequency bandwidth ($F = 1024$ Hz), and T_s is the OFDM symbol duration ($T_s = 1$ s). The phase modulation $\varphi(k)$ of the subcarriers is given by

$$\sqrt{2}e^{j\varphi(k)} = a(k)M_2(k) + jM_1(k), \tag{8.2}$$

where $M_1(k)$ is the spectrum of a superimposed pilot signal used by the receiver for channel estimation. The spectrum of the data signal is $a(k)M_2(k)$, where $a(k)$ is a BPSK data symbol transmitted at kth subcarrier, and $M_2(k)$ is a pseudo-random binary sequence that provides randomization of the transmitted signal. The sequences $a(k)$, $M_1(k)$ and $M_2(k)$ are binary with values ± 1. Thus, the transmitted pilot signal is orthogonal to the data signal. Below, two scenarios are considered: (1) transmission without frequency diversity, and (2) transmission with frequency diversity, as follows. For frequency diversity, each data bit $d_m, \quad m = 0, \cdots, N/Q - 1$, is interleaved and simultaneously transmitted at Q subcarriers: $a(m + iN/Q) = d_m, i = 0, \cdots, Q - 1$ with $Q = 1$ and $Q = 2$, respectively.

8.3 Signal Processing in the Receiver

Fig.8.1 shows the receiver block diagram in the single antenna scheme and Fig.8.2 shows the receiver block diagrams in the scheme of combining signals from the multiple antennas. The received signal is analyzed to find the beginning of the OFDM symbol (symbol timing estimation) and Doppler channel (frequency estimation). This information is further used for a coarse Delay-Doppler compensation. The output of this stage is a set of samples that approximately present an OFDM symbol. They are sent to a frequency-domain linear equalizer to compensate for the residual multipath distortion. An adaptive

Doppler filter (ADF) is used to cancel the residual ICI. The output of the ADF is further combined according to the frequency diversity at the transmitter and, finally, mapped to the BPSK constellation. In Fig.8.2, signals received from every antenna element are parellelly processed and linearly combined before they are sent to the ADF.

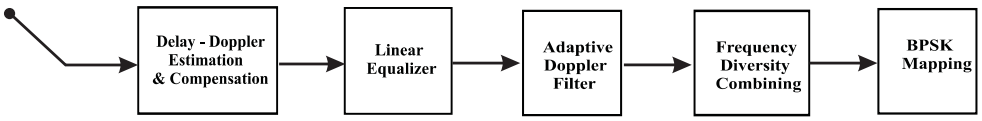

Figure 8.1: Receiver block diagram using single omnidirectional antenna.

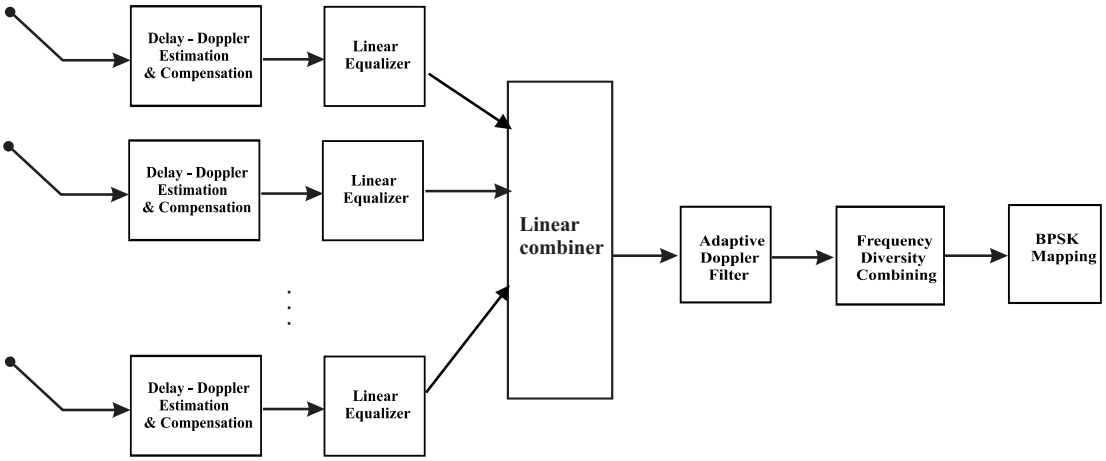

Figure 8.2: Receiver block diagram using multiple antenna combining.

8.3.1 Doppler and delay estimation

The received signal $x(t)$ is filtered in the frequency band $[f_c - F/2, f_c + F/2]$, sampled at the frequency $f_s = 1/T = 4f_c$ and, over each interval of duration T_s, the samples are used for calculation of complex envelopes

$$z_q(n) = \sum_i x(iT) e^{j2\pi f_c iT/\eta_q} g[nT_s\eta_q/N - iT], \tag{8.3}$$

where $g(t)$ is the impulse response of a discrete lowpass filter with a frequency bandwidth of $F/2$ and $n = 0, \cdots, N-1$. The frequencies $f_c(q) = f_c/\eta_q$ cover the Doppler frequency range $[f_c - F_D, f_c + F_D]$: $f_c(q) = f_c + q\Delta f/2$, where $q = -N_D, \cdots, N_D$, $(2N_D+1)$ is the number of Doppler channels in the receiver; $\Delta f = 1/T_s$ is the frequency resolution of the signal, and $F_D = \Delta f N_D/2$.

In order to estimate the delays and Doppler parameters, the cross-ambiguity function is calculated. The envelopes $z_q(n)$ are correlated with the pilot signal described by the spectral sequency $M_1(n)$,

$$Z_q(k) = \sum_{n=0}^{N-1} z_q(n) e^{-j2\pi kn/N}, \tag{8.4}$$

$$y_q(n) = \frac{1}{N} \sum_{k=0}^{N-1} Z_q(n) M_1(k) e^{j2\pi kn/N}. \tag{8.5}$$

The Doppler coefficient η and the delay τ are found according to

$$[\eta, \tau] = \arg \max_{q,n} \{|y_q(n)|\}, \tag{8.6}$$

These estimates are used for coarse compensation of the delay and Doppler shifts. For this compensation, linear interpolation is used.

8.3.2 Linear equalization

For linear equalization, we use estimates of the channel frequency response based on its approximation by the complex exponential series:

$$H(k) = \sum_{p=1}^{L_0} h^*(p) e^{-j2\pi k\hat{\tau}_p/N}, \tag{8.7}$$

where the delays $\hat{\tau}_1, \cdots, \hat{\tau}_{L_0}$ are found as the first L_0 maxima of the sequence $|\hat{y}(n)|$ given by

$$Y(k) = \sum_{n=0}^{N-1} y_\eta(n-\tau) e^{-j2\pi kn/N}, \tag{8.8}$$

$$\hat{y}(n) = \frac{1}{N} \sum_{k=0}^{N-1} Y(k) M_1(k) e^{j2\pi kn/N}. \tag{8.9}$$

The expansion coefficients $h(p)$ are found as

$$h(p) = \hat{y}(\hat{\tau}_p). \tag{8.10}$$

The output of the linear equalizer in the frequency domain is given by

$$C(k) = \frac{Y(k)}{H(k)}. \tag{8.11}$$

In the scenario of combing signals from multiple antennas, for the signal snapshot received by every antenna element, $(8.3) - (9.26)$ are processed in parellel and the output of the linear equalizer can be represented as $C_i(k), i = 0, \cdots, K-1$. These outputs from the K branches are linearly combined,

$$\hat{C}(k) = \sum_{i=0}^{K-1} C_i(k). \tag{8.12}$$

8.3.3 Adaptive Doppler filter (ADF)

After the linear equalizer, the signal still contains a residual ICI. It can be efficiently reduced by using an adaptive Doppler filter (ADF). The ADF is applied in the frequency domain; it makes a weighted sum of Doppler-shifted versions of the signal in the frequency domain. Its non-adaptive structure is presented in [119]. Here, we use the ADF with the filter weights updated by the normalized least mean square (NLMS) algorithm:

$$\begin{aligned} G(k) &= \sum_{b=0}^{B-1} \hat{C}(k-b)\hat{w}_b(k) \\ e(k) &= M_1(k) - G(k) \\ \hat{w}_b(k+1) &= \hat{w}_b(k) + \frac{\varrho \hat{C}^*(k-b)e(k)}{\sum_{b=0}^{B-1} |\hat{C}(k-b)|^2}, \end{aligned} \tag{8.13}$$

where B is the filter order, $G(k)$ is the filter output, $\hat{w}_b(k)$ is the weight of the bth filter tap at kth subcarrier, and ϱ is the step-size parameter; we use $\varrho = 0.05$ in the experiment.

8.3.4 Frequency diversity combining and BPSK mapping

The combining of Q frequency diversity signals is performed as

$$G_c(k) = \sum_{i=0}^{Q-1} G(k + iN/Q) M_2(k + iN/Q). \tag{8.14}$$
$$k = 0, \ldots, N/Q - 1,$$

Finally, the estimated data bits $\hat{d}_k$ are found as

$$\hat{d}_k = \text{sign}\{\Re[G_c(k)]\}, \;\; k = 0, \ldots, N/Q - 1, \tag{8.15}$$

where $\Re\{\cdot\}$ denotes the real part of a complex number.

8.4 Experimental Results

During the experiment, the transmit antenna moved at a depth of 250 m with a speed of 5 m/s. The duration of the communication session was approximately 380 s. Fig.8.3 shows the spectral and time envelopes. In the figure of filtered time envelope, it can be seen that the noise level is about 77 dB and lasts for about 20 sec. We discard the first 50 s received signals, which exhibit extremely low SNR (0 - 3 dB). For the rest of the received signals, the signal plus noise level varies approximately from 84 to 88 dB. Therefore, the SNR of the processed signals varies from 7 to 11 dB.

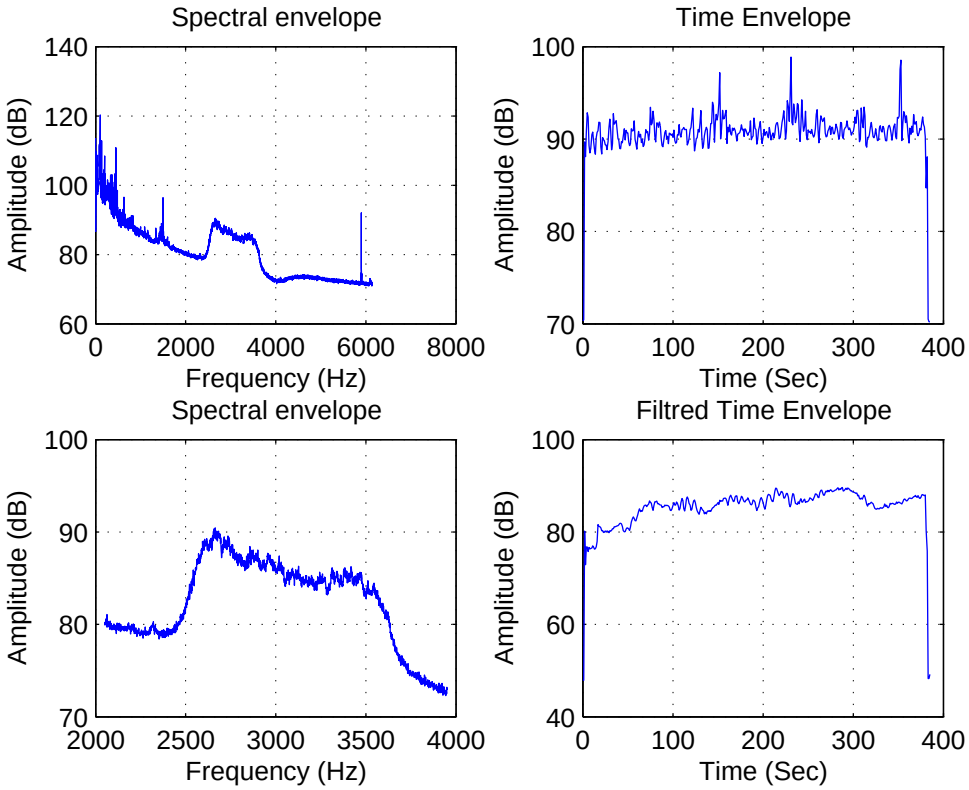

Figure 8.3: Measured spectral and time envelope: depth 250 m; transmit antenna speed 5 m/s; communication duration 380 s.

Fig.8.4 shows the channel impulse response measured at a single omnidirectional antenna; the delay unit is 0.5 ms in the figure. There are three groups of multipaths with a total delay spread of 32 ms. Fig.8.5 shows amplitude variations of the three multipath components. It is seen that the variations are fast with respect to the symbol duration (1 s).

In Table.8.1, the bit-error-rate (BER) performance for data efficiency 1 bit/s/Hz

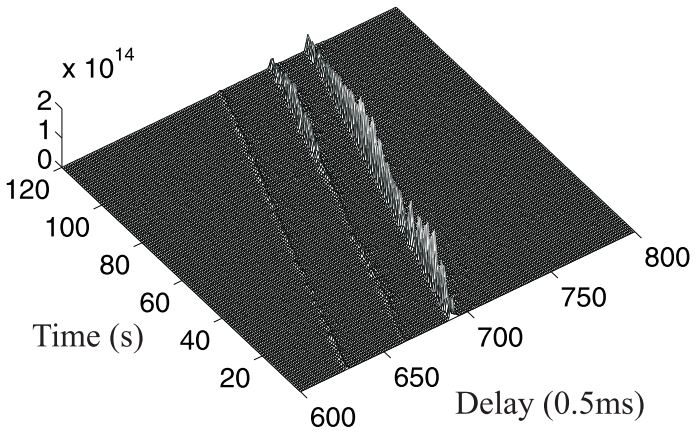

Figure 8.4: Impulse response measured at one element of the vertical antenna.

and 0.5 bit/s/Hz are compared between the schemes of using a single antenna element and combining signals from 14 omnidirectional antennas. The use of the only antenna element does not provide a high detection performance. The use of signal combining from multiple antennas improves the diversity and leads to a better BER performance. However, without the ADF, this improvement is not significant. The application of ADF does not help a lot in the case of the single antenna element. However, it allows significant improvement in the detection performance when using the combing techniques of 14 omnidirectional antenna elements. It is seen that the proposed space-time processing in the receiver achieves the BER 2.1×10^{-2} and 6.7×10^{-3} for the data efficiency 1 bit/s/Hz and 0.5 bit/s/Hz, respectively.

Table 8.1: Average BER versus data efficiency (bit/s/Hz).

Techniques		1bit/s/Hz	0.5bit/s/Hz
1 element	no ADF	2.3×10^{-1}	1.6×10^{-1}
	ADF	1.1×10^{-1}	6.1×10^{-2}
14 elements signal combining	no ADF	1.7×10^{-1}	9.6×10^{-2}
	ADF	2.1×10^{-2}	6.7×10^{-3}

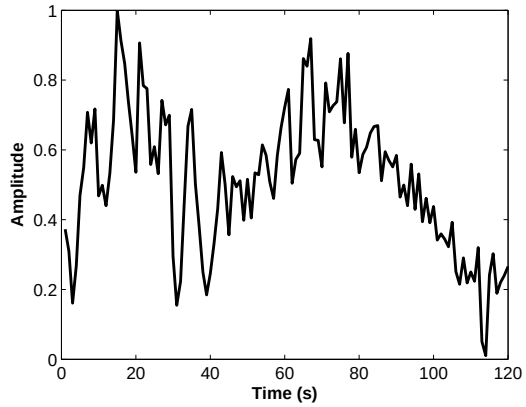

(a)

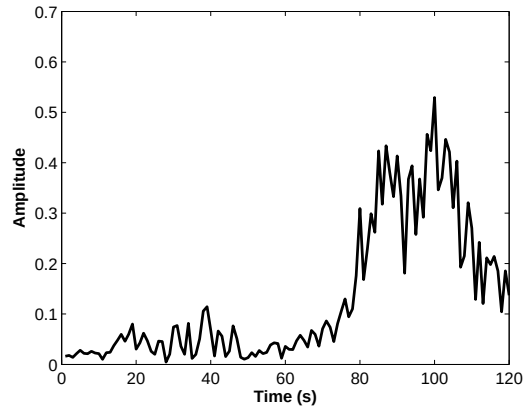

(b)

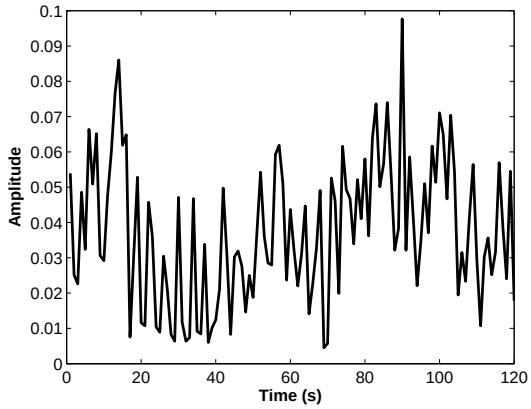

(c)

Figure 8.5: Amplitude variation of the three multipath components: (a) first multipath component; (b) second multipath component; (c) third multipath component. The amplitudes are shown relatively to the maximum among all the amplitudes.

8.5 Summary

Several different space-time processing techniques have been investigated in application to OFDM signal transmitted through a fast-varying underwater acoustic channel. This channel is characterized by the intersymbol and intercarrier interference that make a high data rate transmission complicated. In application to experimental data obtained at a distance of 30 km, it has been shown that the proposed space-time processing based on time and Doppler compensation, frequency-domain linear equalization, multiple antenna, frequency diversity and adaptive Doppler filtering achieves the BER of 2.1×10^{-2} and 6.7×10^{-3} for the transmission data efficiency 1 bit/s/Hz and 0.5 bit/s/Hz, respectively.

Chapter 9

Application of Adaptive Beamforming to OFDM Transmission in Fast-Varying Underwater Acoustic Channel

Contents

9.1 Introduction

High data rate communications over underwater acoustic channel is challenging due to time-varying multipath propagation. The orthogonal frequency-division multiplexing (OFDM) is a promising technique for increasing the transmission data rate. However, this requires accurate channel estimation; this can be achieved by using pilot signals superimposed with the data signals. We have described some basic space-time signal processing techniques for underwater OFDM transmission in the Chapter 8 in order to reduce the intersymbol interference (ISI) due to multipath propagation. The techniques include time and Doppler compensation, channel estimation, frequency-domain linear equalization and adaptive Doppler filtering. The receiver structure using single omnidirectional antenna element and using multiple antennas are respectively described.

In this chapter, we aim to apply adaptive beamforming techniques to improve the bit-error-rate (BER) performance in underwater OFDM signal transmission. In particular, three direction-of-arrival (DoA) estimation techniques are considered. The techniques use signal interpolation, the modified MVDR beamformer and the superimposed pilot signal. The DoA estimates are used for angle-separation of signals. We apply the MVDR beamforming, due to its strong capability of interference rejecting, to generate the output signal according to every detected arriving angle. The multiple output branches, after synchronization, Doppler compensation, channel estimation and linear equalization, are linearly combined and filtered by the adaptive Doppler filter (ADF). Due to the fast-varying channel, the estimated DoA information could be inaccurate. As we have discussed in the previous chapters, the inaccurate DoA estimation could make the performance of the MVDR beamformer even worse than that of the conventional beamformer. The null-broadening method proposed in Chapter 5 is applied to improve the robustness of the traditional MVDR beamformer. We still use the experimental data obtained in the Pacific Ocean in 1989 [33, 36]. We show that the proposed DoA estimation and adaptive beamforming methods allow further improvement of the BER performance for high data rate OFDM transmission in such a fast-varying underwater acoustic channel. The related material has been published in [118].

9.2 Signal Processing in the Receiver

The transmitted OFDM signal is the same as that has been described in Chapter 8. Fig.9.1 shows the receiver block diagram. The DoA estimator provides a set of angles $\theta_m, m = 1, \cdots, L$, corresponding to L directions; further processing in the receiver is performed in L branches. In every branch, a modified MVDR beamforming is implemented for selection of signals arriving from the direction θ_m and cancelling signals arriving from the other directions. Time and Doppler compensation, channel estimation and frequency-domain linear equalization are implemented for the output signals of the modified MVDR beamformer. The outputs of the equalizers from the L branches are linearly combined; the combining provides a multipath diversity. An ADF is used to cancel the residual intercarrier interference (ICI). The output of the ADF is further combined according to the frequency diversity at the transmitter and, finally, mapped to the BPSK constellation.

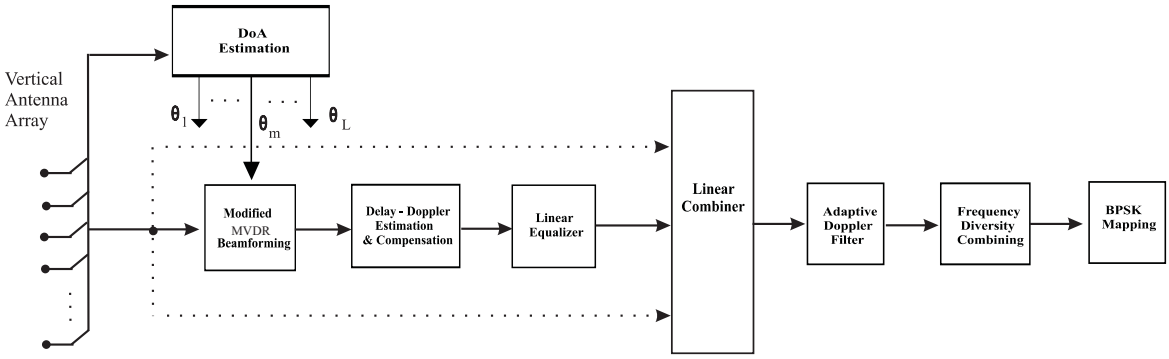

Figure 9.1: Receiver block diagram using a vertical linear antenna array.

9.2.1 DoA estimation

Consider a linear array of K omnidirectional antenna elements with arbitrary element spacing. In out experiment, $K = 14$ and the total antenna array length is 8.1 m, with distances between antenna elements - 0.3 m, 0.6 m and 0.9 m. We denote $x_k(t)$ as a signal received by the kth antenna element at time index t. The time delay of a signal arriving at the kth element with respect to the first element is given by

$$\varsigma(k,\theta) = \frac{D(k)\sin(\theta)}{c}, \tag{9.1}$$

where $D(k)$ is the distance between the first and kth antenna elements and c is the sound speed ($c \approx 1500$ m/s). Three DoA estimation techniques are considered below. All the techniques are based on delay compensation (instead of phase rotation) for synchronizing the signals arriving at different antenna elements from a direction θ. This is due to the reason that in the underwater acoustic environment, when receiving wideband signals, the phase rotation is no more accurate. For the delay compensation, the linear time-domain interpolation of the sampled signals from the antenna elements is used. The sampled signal is $x_k(iT)$ and the sampling frequency is $f_s = 1/T = 4f_c = 12288$ Hz.

1) Modified MVDR DoA estimation: In this DoA estimation technique, the snapshot matrix $\mathbf{X} \in C^{K\times N}$ is used for calculating the diagonally loaded sample covariance matrix

$$\mathbf{R}(\theta) = \mathbf{X}(\theta)\mathbf{X}^H(\theta) + \kappa\mathbf{I}_K, \tag{9.2}$$

and

$$[\mathbf{X}(\theta)]_{k,n} = x_k(nT - \varsigma(k,\theta)), \quad n = 1, \cdots, N, \tag{9.3}$$

where $(\cdot)^H$ denotes the conjugate transpose, $\mathbf{I}_K$ is the $K \times K$ identity matrix, and κ is a loading factor. The solution to the MVDR beamforming results in the estimated signal power from the direction θ:

$$P(\theta) = \frac{1}{\mathbf{v}^H \mathbf{R}^{-1}(\theta)\mathbf{v}}. \tag{9.4}$$

Note that in the classical MVDR beamforming [66], the vector $\mathbf{v}$ is a steering vector which depends on a direction of arrival θ:

$$\mathbf{v} = \left[1, \ldots, e^{-j\sin(\theta)D(u)}, \ldots, e^{-j\sin(\theta)D(U)}\right]^T, \tag{9.5}$$

where $(\cdot)^T$ denotes the transpose. The use of the steering vector implies that the delays between signals at the antenna elements can be compensated by the phase rotation: $e^{-j\sin(\theta)D(u)}$. However, in the underwater acoustics environment, when receiving wideband signals, this approximation is not accurate, and direct delay compensation is required. In our case, the linear interpolation is used to steer the antenna in the direction θ, as has been described in (9.3). After the steering, the phase rotation is not required and, thus in (9.4), we have

$$\mathbf{v} = [1, \ldots, 1]^T. \tag{9.6}$$

Therefore (9.4) can be rewritten as

$$P(\theta) = \frac{1}{\sum_{\mu=1}^{K}\sum_{\nu=1}^{K}[\mathbf{R}^{-1}(\theta)]_{\mu,\nu}}. \tag{9.7}$$

This makes the method different from the traditional MVDR DoA estimation. The directions of arrival $\Theta = [\theta_1, \ldots, \theta_m, \ldots, \theta_L]$ are found as the first L maxima of the function $P(\theta)$:

$$\Theta = \arg\max_{\theta}\{P(\theta)\}. \tag{9.8}$$

Every time when one DoA θ_m is obtained, before searching for the next, we ignore the angle directions close to θ_m with a range $[\theta_m - \psi, \theta_m + \psi]$ by setting $P(\theta) = 0, \theta \in [\theta_m - \psi, \theta_m + \psi]$.

2) Angle-Delay-Doppler search for DoA estimation: This DoA estimation method is based on selecting a signal received from a θ-direction and calculation of cross-correlation of the signal with the superimposed pilot signal for all possible time delays (within the OFDM symbol duration) and Doppler coefficients. The Doppler coefficient η_q indicates the time compression of the received signal [120] for a qth Doppler channel. The angle selection is given by

$$\mathbf{z}(\theta) = \mathbf{w}^H \mathbf{X}(\theta), \tag{9.9}$$

where $\mathbf{z}(\theta)$ is an N-length column vector with elements $z_q(\theta, n)$, $n = 1, \ldots, N$. $\mathbf{X}(\theta)$ is the delay compensated snapshot matrix, defined in (9.3), $\mathbf{w}$ is a $K \times 1$ vector of antenna element weights, which is given by

$$\mathbf{w}(\theta) = [1/K \; 1/K \; \ldots \; 1/K]^T. \tag{9.10}$$

The cross-correlation between the signal $z_q(\theta, n)$, which is obtained by correcting the initial sampling period T according to $T_q = \eta_q T$, $q = -N_D, \ldots, N_D$, and the pilot sequence $M_1(n)$ is obtained in the frequency domain as

$$Z_q(\theta, k) = \sum_{n=0}^{N-1} z_q(\theta, n) e^{-j2\pi kn/N}, \tag{9.11}$$

$$y_q(\theta, n) = \frac{1}{N} \sum_{k=0}^{N-1} Z_q(\theta, k) M_1(k) e^{j2\pi kn/N}. \tag{9.12}$$

For the Doppler compensation, when calculating the cross-correlation, the linear interpolation is used. The directions of arrival $\Theta = [\theta_1, \ldots, \theta_m, \ldots, \theta_L]$ are found according to the first L maxima of the function $|y_q(\theta, n)|$:

$$\Theta = \arg \max_{\theta} \{|y_q(\theta, n)|\}. \tag{9.13}$$

The maxima selection is similar to that described in (9.8). The only difference is that (9.13) is 2-dimensional selection. Every time when one DoA θ_m is obtained, before searching for the next, we ignore the angle directions within a circular area around (θ_m, n_m) with the radius ψ.

3) Joint MVDR & Delay-Doppler-search DoA estimation: The third DoA estimation technique is similar to the second technique. The only difference is in the antenna weight vector $\mathbf{w}(\theta)$, which now depends on the direction θ. Specifically, the modified MVDR beamforming is used for calculating the weight vector. The reason of using the MVDR weights is that the weight vector in (9.10) does not cancel strong interfering signals arriving from the other directions. Better results can be obtained when using the weight vector for the modified MVDR beamformer:

$$\mathbf{w}(\theta) = \frac{\mathbf{R}^{-1}(\theta)\mathbf{v}}{\mathbf{v}^H \mathbf{R}^{-1}(\theta)\mathbf{v}}, \tag{9.14}$$

where the sample covariance matrix $\mathbf{R}$ and the modified steering vector $\mathbf{v}$ have been respectively defined in (9.2) and (9.6). Then the same computations as described in (9.11)-(9.13) are performed to find the DoA estimates Θ.

9.2.2 Beamforming output

After DoA estimation, the modified MVDR beamformer is used to generate the beamforming output signals by steering the antenna to every detected arriving angle $\theta_m, m = 1, \cdots, L$, while cancelling the other interferers. As in (9.9), the output signal can be written as

$$\mathbf{z}(\theta_m) = \mathbf{w}^H(\theta_m)\mathbf{X}(\theta_m), \tag{9.15}$$

where

$$\mathbf{w}(\theta_m) = \frac{\mathbf{R}^{-1}(\theta_m)\mathbf{v}}{\mathbf{v}^H\mathbf{R}^{-1}(\theta_m)\mathbf{v}}, \tag{9.16}$$

and $\mathbf{R}$ and $\mathbf{v}$ have been defined in (9.2) and (9.6) respectively.

However, the MVDR beamforming is sensitive to any errors in the steering knowledge. The performance could degrade when the DoA estimation is not accurate enough. The null-broadening method described in Chapter 5 can be applied to improve the robustness of the traditional MVDR beamformer. This is implemented by placing U artificial users closely around each detected angle. Denote

$$\widetilde{\Theta} = [\Theta_1, \Theta_2, \cdots, \Theta_L] \tag{9.17}$$

and

$$\Theta_m = [\theta_m^{(-\frac{U-1}{2})}, \theta_m^{(-\frac{U-1}{2}+1)}, \cdots, \theta_m^{(0)}, \cdots, \theta_m^{(\frac{U-1}{2}+1)}, \theta_m^{(\frac{U-1}{2})}], \quad m = 1, \cdots, L, \tag{9.18}$$

where $\theta_m^{(0)} = \theta_m$ represents the estimated direction. The set $\widetilde{\Theta}$ contains all directions including the additive angles around each original one. We denote $\overline{\Theta}_m$ as the complementary set of Θ_m with respect to $\widetilde{\Theta}$, that is

$$\overline{\Theta}_m \cup \Theta_m = \widetilde{\Theta}. \tag{9.19}$$

The null-broadening approach is based on minimizing the total power of all original interferers and their respective additive ones, while assigning unity received power to the desired angle direction and its additive ones. Therefore a beampattern with broad mainlobe and broad nulls is generated. Such beamformer weight vector can be found by solving the following constrained optimization problem

$$\mathbf{w}(\theta_m) = \arg\min_{\mathbf{w}} \sum_{\theta_i \in \overline{\Theta}_m} \left|\mathbf{w}^H\mathbf{v}(\theta_i)\right|^2 \text{ subject to } \sum_{\theta_n \in \Theta_m} \left|\mathbf{w}^H\mathbf{v}(\theta_n)\right|^2 = 1, \tag{9.20}$$

where $i = 1, \cdots, (L-1)U, \quad n = 1, \cdots, U$ and $\mathbf{v}$ is the steering vector defined in (9.5).

9.2.3 Doppler and delay estimation

In mth (due to the estimated directions θ_m, $m = 1, \ldots, L$) branch of the receiver, the Doppler coefficient η_m and the delay τ_m are found according to

$$[\eta_m, \tau_m] \quad = \quad \arg\max_{q,n}\{|y_q(\theta_m, n)|\}, \tag{9.21}$$

where $|y_q(\theta_m, n)|$ is the cross-correlation function of the beamformer output and the superimposed pilot sequence, defined in (9.12). These estimates are used for coarse compensation of the delay and Doppler shifts. For this compensation, linear interpolation is used.

9.2.4 Linear equalization

For linear equalization for a direction θ_m, we use estimates of the channel frequency response based on its approximation by the complex exponential series:

$$H(k) = \sum_{p=1}^{L_0} h^*(p) e^{-j2\pi k\hat{\tau}_p/N} \tag{9.22}$$

where the delays $\hat{\tau}_1, \ldots, \hat{\tau}_{L_0}$ are found as the first L_0 maxima of the sequence $|\hat{y}_m(n)|$ given by

$$Y_m(k) \quad = \quad \sum_{n=0}^{N-1} y_{\eta_m}(\theta_m, n - \tau_m) e^{-j2\pi kn/N}, \tag{9.23}$$

$$\hat{y}_m(n) \quad = \quad \frac{1}{N} \sum_{k=0}^{N-1} Y_m(k) M_1(k) e^{j2\pi kn/N}. \tag{9.24}$$

The expansion coefficients $h(p)$ are found as

$$h(p) = \hat{y}_m(\hat{\tau}_p). \tag{9.25}$$

The output of the linear equalizer in the frequency domain is given by

$$C_m(k) = \frac{Y_m(k)}{H(k)}. \tag{9.26}$$

The equalizer outputs $C_m(k)$ from all L branches are weighted by $p_m = \max_{q,n}\{|y_q(\theta_m, n)|\}$ and linearly combined,

$$C(k) = \sum_{m=1}^{L} p_m C_m(k). \tag{9.27}$$

9.2.5 Adaptive Doppler filter (ADF)

The combined signal $C(k)$ is then sent to the ADF to reduce the residual ICI, as it has been described in the Chapter 8. Mathematically, it is represented as:

$$\begin{aligned} G(k) &= \sum_{b=0}^{B-1} C(k-b)\hat{w}_b(k) \\ e(k) &= M_1(k) - G(k) \\ \hat{w}_b(k+1) &= \hat{w}_b(k) + \frac{\varrho C^*(k-b)e(k)}{\sum_{b=0}^{B-1}|C(k-b)|^2}, \end{aligned} \tag{9.28}$$

where B is the filter order, $G(k)$ is the filter output, $\hat{w}_b(k)$ is the weight of the bth filter tap at kth subcarrier, and ϱ is the step-size parameter; we use $\varrho = 0.05$ in the experiment.

9.2.6 Frequency diversity combining and BPSK mapping

The combining of Q frequency diversity signals is performed as

$$G_c(k) = \sum_{i=0}^{Q-1} G(k+iN/Q)M_2(k+iN/Q). \tag{9.29}$$
$$k = 0, \ldots, N/Q-1,$$

Finally, the estimated data bits $\hat{d}_k$ are found as

$$\hat{d}_k = \text{sign}\{\Re[G_c(k)]\}, \;\; k = 0, \ldots, N/Q-1.$$

where $\Re\{\cdot\}$ denotes the real part of a complex number.

9.3 Experimental Results

We still use the experimental data obtained from the Pacific Ocean in 1989 [33, 36]. The OFDM signals are transmitted by a fast moving (at a speed of 5 m/s) underwater transducer at a depth of 250 m. A 14-element vertical antenna array of omnidirectional elements, positioned at a depth of 420 m, is used for receiving the signals. The duration of the communication session was 2 minutes. The measured spectral & time envelope and impulse response have been shown in Fig.8.3 - Fig.8.5 in the Chapter 8. The SNR of the received signals varies approximately from 7 to 11 dB.

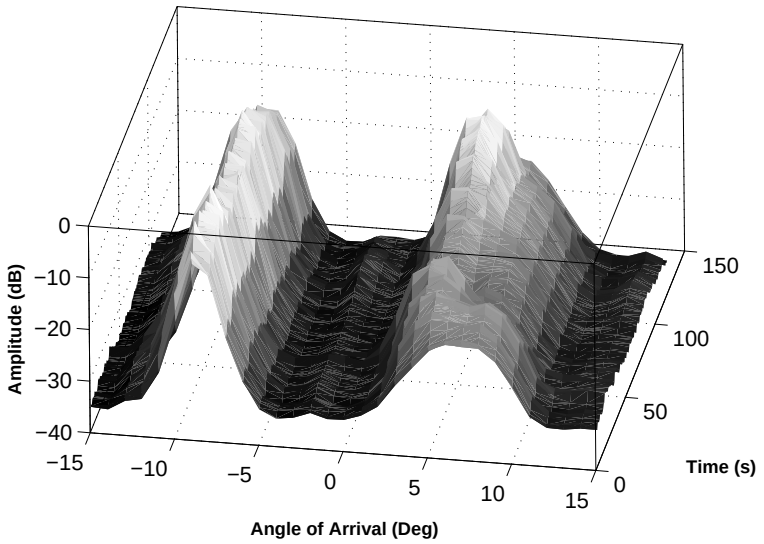

(a)

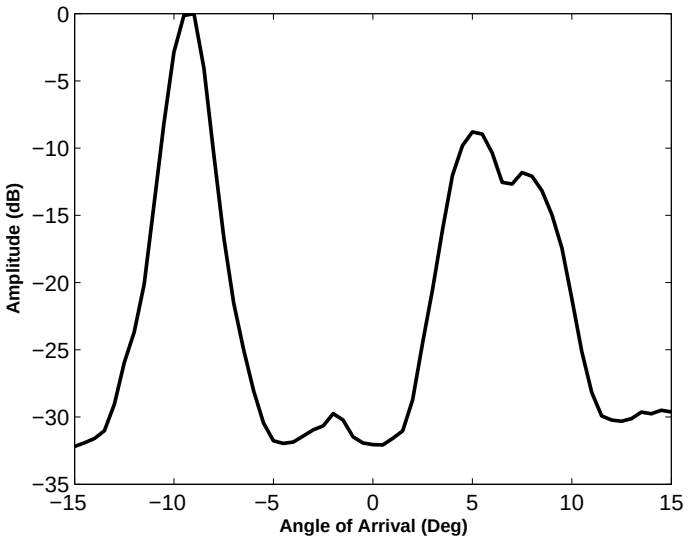

(b)

Figure 9.2: 2D and 1D section time-angle structure of the received signal obtained, using the modified MVDR method.

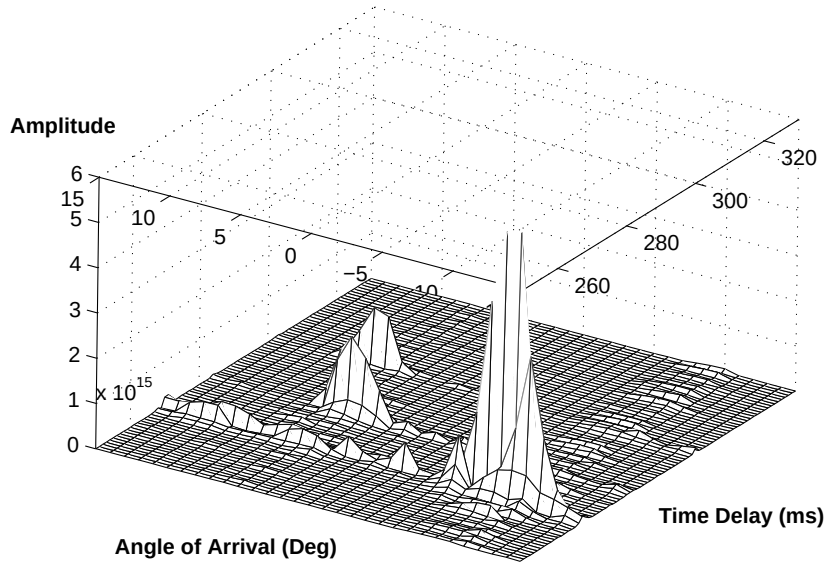

Figure 9.3: Time-angle structure of the received signal using the Angle-Delay-Doppler multipath search.

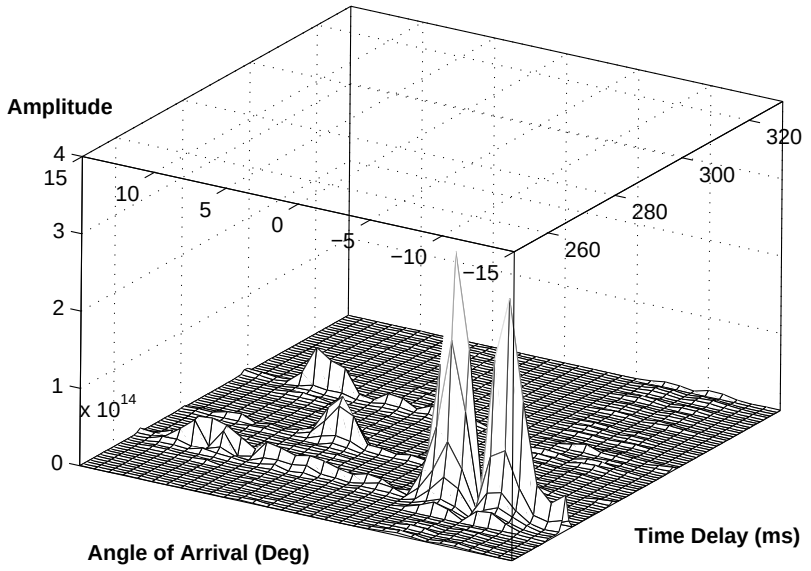

Figure 9.4: Time-angle structure of the received signal using the MVDR method & Delay-Doppler multipath search.

Fig.9.2 - Fig.9.4 show the angle-delay structure of the received signal for the three DoA estimation techniques. Fig.9.2 shows the angle distribution of the received signal for the first technique: the Modified MVDR DoA estimates. There can be seen two DoAs: $\theta_1 \approx +6^\circ$ and $\theta_2 \approx -10^\circ$. For the other two DoA estimation methods, DoAs are obtained by searching the multiple peaks in the three-dimensional time-angle structure. In Fig.9.3, the second DoA estimation techniques (Angle-Delay-Doppler search) finds three DoAs: $\theta_1 \approx +9^\circ$, $\theta_2 \approx +4^\circ$ and $\theta_3 \approx -10^\circ$. A more accurate angle structure is obtained by using the third technique (joint MVDR $\&$ Delay-Doppler-search) as seen in Fig.9.4; there are four DoAs: $\theta_1 \approx +9^\circ$, $\theta_2 \approx +4^\circ$, $\theta_3 \approx -8^\circ$ and $\theta_4 \approx -11^\circ$. Thus, the third technique finds 4 DoAs, while the other two techniques failed to separate some directions.

The bit-error-rate (BER) performance for data efficiency 1 bit/s/Hz and 0.5 bit/s/Hz is compared in Table.9.1 with respect to the three DoA estimation techniques. The use of a simple omnidirectional antenna element does not provide a high detection performance. The use of DoA estimation and adaptive beamforming techniques significantly improves the detection performance, compared with that of using one antenna element and using multiple antenna combining. Within the three DoA estimation techniques, the joint MVDR $\&$ Delay-Doppler search (Table.9.1(c)) provides the best detection performance. By applying the adaptive Doppler filter (ADF), it achieves the BER 10^{-2} and 1.4×10^{-3} for the data efficiency 1 bit/s/Hz and 0.5 bit/s/Hz, respectively. Based on this DoA estimation technique, when null-broadening method is used (Table.9.1(d)), the BER performance is significantly improved, especially in the non-ADF scenario, which improves approximately 50%.

9.4 Summary

Several DoA estimation and adaptive beamforming methods are investigated in application to OFDM signals transmitted through a fast-varying underwater acoustic channel, which is characterized by the intersymbol and intercarrier interference that make a high data rate transmission complicated. The DoA estimates are used for angle-separation of signals from the multipath by applying the modified MVDR beamforming. Other space-time signal processing techniques include time and Doppler compensation, channel estimation, frequency-domain linear equalization and adaptive Doppler filtering. The null-broadening adaptive beamformer can be applied to improve the robustness of the traditional MVDR beamformer. In application to experimental data obtained from the Pacific Ocean at a distance of 30 km, it has been shown that the proposed DoA estimation, adaptive beamforming and other space-time signal processing achieves the BER 10^{-3} and

10^{-2} for the transmission data efficiency 0.5 bit/s/Hz and 1 bit/s/Hz, respectively.

Table 9.1: Average BER versus data efficiency (bit/s/Hz).

(a) Modified MVER DoA estimation.

Techniques		1bit/s/Hz	0.5bit/s/Hz
1 element	no ADF	2.3×10^{-1}	1.6×10^{-1}
	ADF	1.1×10^{-1}	6.1×10^{-2}
14 elements signal combining	no ADF	1.7×10^{-1}	9.6×10^{-2}
	ADF	2.1×10^{-2}	6.7×10^{-3}
14-element array	no ADF	1.9×10^{-1}	1.1×10^{-1}
	ADF	1.8×10^{-2}	4.5×10^{-3}

(b) Angle-Delay-Doppler search for DoA estimation.

Techniques		1bit/s/Hz	0.5bit/s/Hz
1 element	no ADF	2.3×10^{-1}	1.6×10^{-1}
	ADF	1.1×10^{-1}	6.1×10^{-2}
14 elements signal combining	no ADF	1.7×10^{-1}	9.6×10^{-2}
	ADF	2.1×10^{-2}	6.7×10^{-3}
14-element array	no ADF	1.4×10^{-1}	3.9×10^{-2}
	ADF	1.7×10^{-2}	3.2×10^{-3}

(c) Joint MVDR & Delay-Doppler search for DoA estimation.

Techniques		1bit/s/Hz	0.5bit/s/Hz
1 element	no ADF	2.3×10^{-1}	1.6×10^{-1}
	ADF	1.1×10^{-1}	6.1×10^{-2}
14 elements signal combining	no ADF	1.7×10^{-1}	9.6×10^{-2}
	ADF	2.1×10^{-2}	6.7×10^{-3}
14-element array	no ADF	1.2×10^{-1}	3.8×10^{-2}
	ADF	1.0×10^{-2}	1.4×10^{-3}

(d) Joint MVDR & Delay-Doppler search for DoA estimation, using null-broadening beamforming technique.

Techniques		1bit/s/Hz	0.5bit/s/Hz
1 element	no ADF	2.3×10^{-1}	1.6×10^{-1}
	ADF	1.1×10^{-1}	6.1×10^{-2}
14 elements signal combining	no ADF	1.7×10^{-1}	9.6×10^{-2}
	ADF	2.1×10^{-2}	6.7×10^{-3}
14-element array	no ADF	6.3×10^{-2}	2.1×10^{-3}
	ADF	1.2×10^{-2}	1.3×10^{-3}

Chapter 10

Conclusions And Future Work

Contents

10.1 Summary of the Work

In this thesis, we have investigated various digital beamforming (DBF) techniques in application to high altitude platforms (HAPs) communications (Chapters 3 - 7) and high data rate transmission in fast-varying underwater acoustic channel (Chapters 8 - 9).

The DBF techniques using antenna array for HAPs communications can be divided into fixed beamforming (cellular based) and adaptive beamforming (non-cellular based). In Chapter 3, we start from the most traditional scenario, that is using a planar antenna array to provide communications for a hexagonal cellular structure on the ground. The beampattern of the antenna array should be optimized to have equal-sized circular footprints to cover every hexagonal cell within the coverage area. Simultaneously, sidelobe levels are required to be suppressed in order to reduce co-channel interference and improve the signal-to-interference ratio (SIR). A three-step footprint optimization technique is proposed, which achieves a good compromise among mainlobe beamwidth, footprint shape and sidelobe levels. We compare its coverage performance with that of using aperture antennas with one spot beam per cell. The proposed footprint optimization technique using a planar antenna array requires 4 times more antenna elements than that of using aperture antennas in order to achieve a similar coverage performance. However,

the use of aperture antennas results in bulky antenna size and weight. Even though requiring 4 times more antenna elements, the proposed beampattern optimization using planar antenna array still shows an expected reduction in mass payload [23, 27]. The related work has been published in [27, 121].

In Chapter 4, we propose to use a linear vertical antenna array to form ring-shaped cells for HAPs communications. Such antenna configuration generates symmetric cylinder footprints and therefore get rid of the footprint distortion problem, which saves the optimization freedom for sidelobe suppression. As a result, such antenna and cellular configuration using simple window weights requires only 1.4 times more antenna elements to achieve the same coverage performance as that of using distinct aperture antennas. Therefore, the antenna payload and system complexity are significantly reduced. Moreover, it shows the potential ability of the vertical antenna array for further coverage performance improvement when more sophisticated beampattern optimization techniques are applied. The related work has been published in [103].

In Chapter 5, adaptive beamforming techniques are investigated for HAPs applications. We start from the traditional MVDR beamformer and its diagonal loaded form. Then, Mailloux's null-broadening method is applied in the downlink HAPs communications scenario, which significantly improves the robustness of the traditional MVDR beamformer. We show that the performance of Mailloux's method can be significantly improved by broadening the mainlobe as well as the nulls. It is shown that the modified null-broadening method can be expressed as a constrained optimization problem. Taking into account the varying beamwidth for various steering positions, the total number of fictitious sources is reduced to improve the optimization freedom, which is another advantageous over the Mailloux's method and provides further improvement of coverage performance. The related work has been published in [108].

Based on the methods proposed in Chapter 5, the constrained optimization is applied in the cellular beamforming scenario in Chapter 6. The method, taking advantages of both cellular and adaptive beamforming, optimizes the beampattern only at the co-channel cells to improve the optimization freedom, which is the key difference from the traditional cellular beamformers. Since the method optimizes the beampatterns for fixed cellular configuration, the complicated real-time signal processing is not required. Simulation results show that the method allows a linear vertical antenna array achieving better coverage performance than that of using a set of distinct aperture antennas with the same number of (omnidirectional, therefore, simple) antenna elements. Besides the coverage performance improvement, its advantages in antenna payload reduction and system simplification are even more significant. The related work has been published

in [112, 122].

In Chapter 7, the coverage performance of cellular beamforming and adaptive beamforming are compared in the downlink HAPs communications scenario. A comparison methodology is proposed. In particular it allows the two kind of beamformers occupying the same amount of access resources and make their performance to be comparable. We compare the cellular beamforming method proposed in Chapter 6 with the adaptive beamforming method proposed in Chapter 5. Numerical results suggest the conditions at which the the adaptive beamforming method is better or worse than that of the cellular beamforming method.

In Chapters 8 and 9, we have investigated the antenna array and DBF techniques in the application to OFDM signal transmission in fast-varying underwater acoustic channel. The work is based on the experimental data obtained by the Acoustic Institute (Moscow) from the Pacific Ocean in 1989. In Chapter 8, the receiver structure using one omnidirectional antenna element and using multiple antennas are respectively described. Several space-time signal processing techniques are described in order to reduce inter-symbol interference (ISI) and intercarrier interference (ICI). The techniques include time and Doppler compensation, frequency-domain linear equalization and adaptive Doppler filtering. In Chapter 9, a receiver based on an adaptive beamforming is proposed for high data rate transmission in underwater acoustic channel. Several direction of arrival (DoA) estimation methods are investigated, which based on signal interpolation and modified MVDR beamforming. The DoA estimation is used to separate arriving angles from the multipath and therefore time-delay and Doppler can be accurately compensated. The modified null-broadening method, proposed in Chapter 5 in the HAPs communications scenario, is applied to improve the robustness of the MVDR beamformer. Experimental results show that the proposed adaptive beamforming based signal processing techniques significantly improve the bit-error-rate (BER) performance, compared with using one omnidirectional antenna or using the techniques based on combining signals from multiple antennas. The related work has been published in [118].

10.2 Future Work

Some suggestions for future work, based on this thesis, are given below.

1) In Chapter 6, a constrained optimization method is proposed to improve the performance of cellular beamforming for HAPs applications. This method is based

on using a linear vertical antenna array forming ring-shaped cellular structure. This method can be applied in the scenario of using a planar array forming hexagonal cells. Therefore, optimization freedom can be saved for those co-channels cells. A better coverage performance is expected than that is obtained in Chapter 3.

2) In the scenario of HAPs communications, we assume the HAP is static and parallel to the ground. However, this may not happen in the real situation. In most cases, the HAPs antenna arrays suffer from rotation errors and pitch errors. Therefore, it is worth investigating how these errors affect the coverage performance and whether the proposed beamforming methods are still robust to these errors. It could be useful to develop some methods to compensate for these random errors.

3) In Chapter 9, we show that it is effective to use DoA estimation to separate arriving angles from the multipath. This makes time-delay and Doppler to be accurately compensated. It is seen that different DoA estimates result in different angle structures, different number of detected angles and final detection performance. From the literature, there are many DoA estimation methods. The classical ones include linear prediction method (LPM), maximum likelihood method (MLM), eigen-structure method, multiple signal classification (MUSIC) and estimation of signal parameters via rotational invariance technique (ESPRIT). It is worth comparing the angle structure and the final detection performance by applying these DoA estimation methods.

Appendix A

The Nonexistence of Diagonal Loaded Optimum Weights for Downlink Scenario

In this appendix, we show that the optimum weights with the form of diagonal loading can not be derived for downlink scenario A and B as described in Chapter 5.

First Let's rewrite the expression of downlink SIR, considering transmission power $\mathbf{p} = [p_1, p_2, \cdots p_L]^T$ and a random steering error α

$$\eta''(\theta_m) = \frac{p_m \mid \mathbf{w}_m^H[\mathbf{u}(\theta_m) + \alpha] \mid^2}{\sum_{l=1, l\neq m}^{L} p_l \mid \mathbf{w}_l^H[\mathbf{u}(\theta_m) + \alpha] \mid^2}. \tag{A.1}$$

The downlink optimum problem A can be described as: $\max(\min_{1\leq m\leq L}(\eta''(\theta_m)/\gamma_m))$ under a total power constraint, where γ_m is the SIR target for the mth user. Mathematically, it can be written as

$$\begin{aligned} &\max_{\mathbf{w}_1 \cdots \mathbf{w}_L, \mathbf{p}} (\min_{1\leq m\leq L} \frac{\eta''(\theta_m)}{\gamma_m}) \quad \text{subject to} \\ &\mid \mathbf{w}_m^H[\mathbf{u}(\theta_m) + \alpha] \mid^2 = 1 \quad \text{and} \\ &\|\alpha\|^2 \leq \epsilon \quad \text{and} \quad \|\mathbf{p}\|_1 = 1. \end{aligned} \tag{A.2}$$

However, the max-min problem is difficult to handle. In [123], it is shown that instead of solving (A.2), one can achieve such max-min fairness by minimizing the sum of weighted

inverse SIR:

$$\begin{aligned}&\min_{\mathbf{w}_1\cdots\mathbf{w}_L,\mathbf{p}} \sum_{m=1}^{L} \beta_m \frac{\gamma_m}{\eta''(\theta_m)} \quad \text{subject to} \\ &\mid \mathbf{w}_m^H[\mathbf{u}(\theta_m)+\alpha] \mid^2 = 1 \quad \text{and} \quad \|\alpha\|^2 \le \epsilon \\ &\text{and} \quad \|\mathbf{p}\|_1 = 1. \end{aligned} \tag{A.3}$$

Provided that β_m is properly selected, (A.3) leads to optimal max-min fairness. In order to simplify the problem, we consider the two-user scenario in our derivation and in such scenario, $\beta_m = 1$ [124, 125]. The objective function can be rewritten as

$$\min_{\mathbf{w}_1,\mathbf{w}_2,\mathbf{p}} \sum_{m=1}^{2} \frac{\gamma_m \mathbf{de}(\eta''(\theta_m)}{\mathbf{nu}(\eta''(\theta_m))}, \tag{A.4}$$

where $\mathbf{de}(\cdot)$ and $\mathbf{nu}(\cdot)$ are respectively the denominator and numerator of a fraction. From the first constraint in (A.3), we have $\mathbf{nu}(\eta''(\theta_m)) = 1$. Therefore, the Lagrange multiplier function is written as

$$\begin{aligned}&\zeta'(\{\mathbf{w}_1, \mathbf{w}_2, p_1, p_2, \alpha\}, \lambda_1, \lambda_2, \lambda_3, \lambda_4) = \\ &\gamma_1 p_2 |\mathbf{w}_2^H[\mathbf{u}(\theta_1)+\alpha]|^2 + \gamma_2 p_1 |\mathbf{w}_1^H[\mathbf{u}(\theta_2)+\alpha]|^2 \\ &+\lambda_1\{\mid \mathbf{w}_1^H[\mathbf{u}(\theta_1)+\alpha] \mid^2 -1\} + \lambda_2\{\mid \mathbf{w}_2^H[\mathbf{u}(\theta_2)+\alpha] \mid^2 -1\} \\ &+\lambda_3(\epsilon - \|\alpha\|^2) + \lambda_4(|p_1| + |p_2| - 1). \end{aligned} \tag{A.5}$$

If we solve the gradient of (A.5) with respect to $\mathbf{w}_1$ and take it to zero, we have

$$\nabla_{\mathbf{w}_1}(\zeta') = 2\gamma_2 p_1 [\mathbf{u}(\theta_2)+\alpha]\mathbf{w}_1 + 2\lambda_1[\mathbf{u}(\theta_1)+\alpha]\mathbf{w}_1 = 0, \tag{A.6}$$

which leads to $\mathbf{w}_1 = 0$ and similarly $\mathbf{w}_2 = 0$ when taking the gradient to zero with respect to $\mathbf{w}_2$. These results do not satisfy the constraint in (A.3). Therefore, the diagonal loading formed optimum weights can not be derived in this downlink scenario.

Then we show that diagonal loading optimum weights can neither be derived for the downlink scenario B. The optimisation problem is described as: minimize the total transmission power while fulfilling $\eta''(\theta_m) \ge \gamma_m \quad m = 1 \cdots L$. Mathematically, it is written as

$$\begin{aligned}&\min_{\mathbf{w}} \sum_{l=1}^{L} \|\mathbf{w}_l\|^2 \quad \text{subject to} \\ &\frac{\mid \mathbf{w}_m^H[\mathbf{u}(\theta_m)+\alpha] \mid^2}{\sum_{l=1, l\neq m}^{L} \mid \mathbf{w}_l^H[\mathbf{u}(\theta_m)+\alpha] \mid^2} \ge \gamma_m \quad \text{and} \\ &\|\alpha\|^2 \le \epsilon. \end{aligned} \tag{A.7}$$

This optimizes downlink beamforming by minimizing the total transmitted power under the constraint that the received SIR at each user is above a certain threshold ϵ. Alternatively, (A.7) can be rewritten as

$$\begin{aligned}
&\min_{\mathbf{w}}(\|\mathbf{w}_m\|^2 + \sum_{l=1,l\neq m}^{L} \|\mathbf{w}_l\|^2) \quad \text{subject} \quad \text{to} \\
&\mid \mathbf{w}_m^H[\mathbf{u}(\theta_m) + \alpha] \mid^2 \geq \gamma_m \sum_{l=1,l\neq m}^{L} \mid \mathbf{w}_l^H[\mathbf{u}(\theta_m) + \alpha] \mid^2 \quad \text{and} \\
&\|\alpha\|^2 \leq \epsilon. \qquad \text{(A.8)}
\end{aligned}$$

The Lagrange function for (A.8) is

$$\begin{aligned}
&\zeta''(\{\mathbf{w}_1 \cdots \mathbf{w}_L, \delta\}, \lambda_1, \lambda_2) = \|\mathbf{w}_m\|^2 + \sum_{l=1,l\neq m}^{L} \|\mathbf{w}_l\|^2 \\
&+\lambda_1\{\mid \mathbf{w}_m^H[\mathbf{u}(\theta_m) + \alpha] \mid^2 - \gamma_m \sum_{l=1,l\neq m}^{L} \mid \mathbf{w}_l^H[\mathbf{u}(\theta_m) + \alpha] \mid^2\} \\
&+\lambda_2[\epsilon - \|\alpha\|^2]. \qquad \text{(A.9)}
\end{aligned}$$

Theoretically the $L + 1$ parameters in (A.9) can be solved by respectively taking their gradients to zero. For the weight of desired user $\mathbf{w}_m$, we have

$$\nabla_{\mathbf{w}_m}(\zeta'') = 2\mathbf{w}_m + 2\lambda_1[\mathbf{u}(\theta_m) + \alpha]\mathbf{w}_m = 0, \qquad \text{(A.10)}$$

which again leads to $\mathbf{w}_m = 0$ and the same results are obtained for $\mathbf{w}_{l,l\neq m} = 0$. So we can neither derive the diagonal loading optimum weighting for the downlink scenario B.

Bibliography

[1] A. Molisch, *Wireless Communications*, John Wiley & Sons, 2005.

[2] J. Litva and T.K. Lo, *Digital beamforming in wireless communications*, Artech House, Inc. Norwood, MA, USA, 1996.

[3] J.C. Liberti and T.S. Rappaport, *Smart Antennas for Wireless Communications: IS-95 and Third Generation CDMA Applications*, Prentice Hall PTR Upper Saddle River, NJ, USA, 1999.

[4] R. Prasad, *CDMA for Wireless Personal Communications*, Artech House, Inc. Norwood, MA, USA, 1996.

[5] M. Barrett and R. Arnott, "Adaptive antennas for mobile communications", *Electronics & Communication Engineering Journal*, vol. 6, no. 4, pp. 203–214, 1994.

[6] A.F. Naguib, A. Paulraj, and T. Kailath, "Capacity improvement with base-station antenna arrays in cellular CDMA", *IEEE Transactions on Vehicular Technology*, vol. 43, no. 3 Part 1, pp. 691–698, 1994.

[7] C. Farsakh and JA Nossek, "Channel allocation and downlink beamforming in an SDMA mobile radiosystem", *Personal, Indoor and Mobile Radio Communications, 1995. PIMRC'95.'Wireless: Merging onto the Information Superhighway'., Sixth IEEE International Symposium on*, vol. 2, 1995.

[8] HP Lin, SS Jeng, I. Parra, G. Xu, WJ Vogel, and GW Torrence, "Experimental studies of SDMA schemes for wireless communications", *Acoustics, Speech, and Signal Processing, 1995. ICASSP-95., 1995 International Conference on*, vol. 3, 1995.

[9] C. Farsakh and JA Nossek, "Spatial covariance based downlink beamforming in an SDMA mobileradio system", *Communications, IEEE Transactions on*, vol. 46, no. 11, pp. 1497–1506, 1998.

[10] M. Rim, "Multi-user downlink beamforming with multiple transmit and receive antennas", *Electronics Letters*, vol. 38, no. 25, pp. 1725–1726, 2002.

[11] D. Bartolome and AL Pirez-Neira, "Performance analysis of scheduling and admission control for multiuser downlink SDMA", *Acoustics, Speech, and Signal Processing, 2004. Proceedings.(ICASSP'04). IEEE International Conference on*, vol. 2, 2004.

[12] D. Hammarwall, M. Bengtsson, and B. Ottersten, "Beamforming and user selection in SDMA systems utilizing channel statistics and instantaneous SNR feedback", *Proc. IEEE Int. Conf. on Acoustics, Speech, and Signal Processing*, 2007.

[13] T.E. Curtis and R.J. Ward, "Digital beam forming for sonar systems", *IEE Proc*, vol. 127, no. 4 Pt F, 1980.

[14] P. Barton, "Digital beam forming for radar", *IEE Proceedings, Part F-Communications, Radar*, vol. 127, no. 4 pt F, pp. 266–277, 1980.

[15] W.L. Stutzman and G.A. Thiele, *Antenna theory and design*, Wiley New York, 1981.

[16] R.E. Collins and F.J. Zucker, *Antenna Theory, Part I*, McGraw-Hill, New York, 1969.

[17] J.H. Justice, N.L. Owsley, J.L. Yen, and A.C. Kak, *Array signal processing*, Prentice-Hall, NJ. 1st edition, 1985.

[18] A.D. Craig, *Study on Digital Beamforming Networks*, Technical Report TP8721, British Aerospace Ltd., Stevenage, England, 1990.

[19] M. Barrett, "Digital beamforming network technologies for satellite communicaitons", *in ESA Workshop on Advanced Beamforming Networks for Space Applications, Noordjwijk, Netherlands*, 1991.

[20] T.C. Tozer and D. Grace, "High-altitude platforms for wireless communications", *Electronics & Communication Engineering Journal*, vol. 13, no. 3, pp. 127–137, 2001.

[21] D. Grace, N.E. Daly, T.C. Tozer, and A.G. Burr, "LMDS from high altitude aeronautical platforms", *Global Telecommunications Conference, 1999. GLOBECOM'99*, vol. 5, 1999.

[22] D. Grace, NE Daly, T.C. Tozer, A.G. Burr, and D.J. Pearce, "Providing multimedia communications services from high altitude platforms", *International Journal of Satellite Communications*, vol. 19, no. 6, pp. 559–580, 2001.

[23] J. Thornton, "A low sidelobe asymmetric beam antenna for high altitude platform communications", *Microwave and Wireless Components Letters, IEEE*, vol. 14, no. 2, pp. 59–61, 2004.

[24] J. Thornton and D. Grace, "Effect of antenna aperture field on co-channel interference, capacity, and payload mass in high altitude platform communications", *ETRI Journal*, vol. 26, no. 5, 2004.

[25] T. Gebauer and H.G. Gockler, "Channel-individual adaptive beamforming for mobile satellitecommunications", *IEEE Journal on Selected Areas in Communications*, vol. 13, no. 2, pp. 439–448, 1995.

[26] W. Li, X. Huang, and H. Leung, "Performance evaluation of digital beamforming strategies for satellite communications", *IEEE Transactions on Aerospace and Electronic Systems*, vol. 40, no. 1, pp. 12–26, 2004.

[27] Z. Xu, G. White, and Y. Zakharov, "Optimisation of beam pattern of high-altitude platform antenna using conventional beamforming", *IEE Proceedings-Communications*, vol. 153, pp. 865, 2006.

[28] "Stratospheric Broadband", *http://www.capanina.org/*, 2004.

[29] D.B. Kilfoyle and A.B. Baggeroer, "The state of the art in underwater acoustic telemetry", *IEEE Journal on Oceanic Engineering*, vol. 25, no. 1, pp. 4–27, 2000.

[30] J.C. Bingham, "Multicarrier modulation for data transmission: an idea whose time has come", *Communications Magazine, IEEE*, vol. 28, no. 5, pp. 5–14, 1990.

[31] A.G. Burr, *Modulation and coding for wireless communications*, Prentice Hall, 2001.

[32] Y.V. Zakharov and V.P. Kodanev, "Experimental study of an underwater acoustic communication system with pseudonoise signals", *Acoustical Physics*, vol. 40, pp. 707–715, 1994.

[33] V.P. Kodanev and Y.V. Zakharov, "Experimental research of underwater acoustic long-range transmission of high-rate data", *Journal de physique. IV*, vol. 4, no. 5, pp. C5–1105–1108, 1994.

[34] E. Bejjani and J.C. Belfiore, "Multicarrier coherent communications for the underwater acoustic channel", *OCEANS'96. MTS/IEEE.'Prospects for the 21st Century'. Conference Proceedings*, vol. 3, pp. 1125–1130, 1996.

[35] W.K. Lam and R.F. Ormondroyd, "A coherent COFDM modulation system for a time-varying frequency-selective underwater acoustic channel", *Electronic Engineering in Oceanography, 1997.'Technology Transfer from Research to Industry'., Seventh International Conference on*, pp. 198–203, 1997.

[36] Y.V. Zakharov and V.P. Kodanev, "Multipath-Doppler diversity of OFDM signals in an underwater acoustic channel", *Acoustics, Speech, and Signal Processing, 2000. ICASSP'00. Proceedings. 2000 IEEE International Conference on*, vol. 5, pp. 2941–2944, 2000.

[37] "Special issue on active and adaptive antennas", *IEEE Trans. Antennas Propagat.*, vol. AP-12, 1964.

[38] "Special issue on adaptive antennas", *IEEE Trans. Antennas Propagat.*, vol. AP-24, 1976.

[39] "Special issue on adaptive processing antenna systems", *IEEE Trans. Antennas Propagat.*, vol. AP-34, 1986.

[40] "Special issue on beamforming", *IEEE J. Oceanic Eng.*, vol. OE-10, 1985.

[41] L.C. Godara, "Application of antenna arrays to mobile communications. II. Beamforming and direction-of-arrival considerations", *Proceedings of the IEEE*, vol. 85, no. 8, pp. 1195–1245, 1997.

[42] F.J. Ares-Pena, J.A. Rodriguez-Gonzalez, E. Villanueva-Lopez, and S.R. Rengarajan, "Genetic algorithms in the design and optimization of antenna arraypatterns", *IEEE Transactions on Antennas and Propagation*, vol. 47, no. 3, pp. 506–510, 1999.

[43] D.E. Goldberg, *Genetic algorithms in search, optimization and machine learning*, Addison-Wesley Longman Publishing Co., Inc. Boston, MA, USA, 1989.

[44] S. Kirkpatrick, Gelatt J., and M.P. Vecchi, "Optimization by simulated annealing", *Science*, vol. 220, no. 4598, pp. 671, 1983.

[45] R.L. Flaupt, "Thinned arrays using genetic algorithms", *IEEE Transactions on Antennas and Propagation*, vol. 42, no. 7, pp. 993–999, 1994.

[46] H. Unz, "Linear arrays with arbitrarily distributed elements", *IEEE Transactions on Antennas and Propagation [legacy, pre-1988]*, vol. 8, no. 2, pp. 222–223, 1960.

[47] B.P. Kumar and G.R. Branner, "A new technique of analysis of unequally spaced planar arrays", *Antennas and Propagation Society International Symposium, 1996. AP-S. Digest*, vol. 3, 1996.

[48] C.C. Yu, "Sidelobe reduction of asymmetric linear array by spacing perturbation", *Electronics Letters*, vol. 33, no. 9, pp. 730–732, 1997.

[49] B.P. Kumar and G.R. Branner, "Design of unequally spaced arrays for performance improvement", *IEEE Transactions on Antennas and Propagation*, vol. 47, no. 3, pp. 511–523, 1999.

[50] A. Trucco, "Synthesizing asymmetric beam patterns", *IEEE Journal on Oceanic Engineering*, vol. 25, no. 3, pp. 347–350, 2000.

[51] T. Isernia, P. Di Iorio, and F. Soldovieri, "An effective approach for the optimal focusing of array fieldssubject to arbitrary upper bounds", *IEEE Transactions on Antennas and Propagation*, vol. 48, no. 12, pp. 1837–1847, 2000.

[52] T. Isernia, F.J.A. Pena, O.M. Bucci, M. DUrso, J.F. Gómez, and JA Rodríguez, "A hybrid approach for the optimal synthesis of pencil beams through array antennas", *IEEE Transactions on Antennas and Propagation*, vol. 52, no. 11, 2004.

[53] J.M. Cid, J.A. Rodriguez, F. Ares, and E. Moreno, "Synthesis of satellite footprints by perturbation of Woodward-Lawson solutions for planar array antennas", *Journal of electromagnetic waves and applications*, vol. 14, no. 1, pp. 3–10, 2000.

[54] R.S. Elliott and G.J. Stern, "Footprint patterns obtained by planar arrays", *Microwaves, Antennas and Propagation, IEE Proceedings H*, vol. 137, no. 2, pp. 108–112, 1990.

[55] F. Ares, R.S. Elliott, and E. Moreno, "Design of planar arrays to obtain efficient footprint patterns withan arbitrary footprint boundary", *IEEE Transactions on Antennas and Propagation*, vol. 42, no. 11, pp. 1509–1514, 1994.

[56] A. Trastoy, F. Ares, and E. Moreno, "Arbitrary footprint patterns from planar arrays with complexexcitations", *Electronics Letters*, vol. 36, no. 20, pp. 1678–1679, 2000.

[57] J. Fondevila-Gómez, J.A. Rodríguez-González, A. Trastoy, and F. Ares-Pena, "Synthesis of arbitrary footprint patterns from bidimensional arrays with optimal boundary", *Proc. JINA*, vol. 2, pp. 439–442, 2002.

[58] J. Fondevila-Gomez, J.A. Rodriguez-Gonzalez, A. Trastoy, and F. Ares-Pena, "Optimization of array boundaries for arbitrary footprint patterns", *IEEE Transactions on Antennas and Propagation*, vol. 52, no. 2, pp. 635–637, 2004.

[59] A. Rodriguez, R. Munoz, H. Estevez, E. Ares, and E. Moreno, "Synthesis of planar arrays with arbitrary geometry generating arbitrary footprint patterns", *IEEE Transactions on Antennas and Propagation*, vol. 52, no. 9, pp. 2484–2488, 2004.

[60] V.C. Anderson and P. Rudnick, "Rejection of a coherent arrival at an array", *The Journal of the Acoustical Society of America*, vol. 45, pp. 406, 1969.

[61] V.C. Anderson, "DICANNE, a Realizable Adaptive Process", *The Journal of the Acoustical Society of America*, vol. 45, pp. 398, 1969.

[62] Y. Bresler, V.U. Reddy, and T. Kailath, "Optimum beamforming for coherent signal and interferences", *IEEE Transactions on Acoustics, Speech, and Signal Processing*, vol. 36, no. 6, pp. 833–843, 1988.

[63] I.S. Reed, J.D. Mallett, and L.E. Brennan, "Rapid convergence rate in adaptive arrays", *IEEE Transactions on Aerospace and Electronic Systems*, pp. 853–863, 1974.

[64] L.E. Brennan and L.S. Reed, "Theory of adaptive radar", *IEEE Transactions on Aerospace and Electronic Systems*, pp. 237–252, 1973.

[65] H. Cox, "Resolving power and sensitivity to mismatch of optimum array processors", *The Journal of the Acoustical Society of America*, vol. 54, pp. 771, 1973.

[66] J. Capon, "High-resolution frequency-wavenumber spectrum analysis", *Proceedings of the IEEE*, vol. 57, no. 8, pp. 1408–1418, 1969.

[67] S. Haykin, *Adaptive filter theory*, Prentice-Hall, Inc. Upper Saddle River, NJ, USA, 1996.

[68] J.S. Blogh and L. Hanzo, *Third-generation systems and intelligent wireless networking: smart antennas and adaptive modulation*, IEEE, 2002.

[69] B. Farhang-Boroujeny, *Adaptive filters: theory and applications*, John Wiley & Sons, 1998.

[70] S.C. Douglas, "A family of normalized LMS algorithms", *Signal Processing Letters, IEEE*, vol. 1, no. 3, pp. 49–51, 1994.

[71] D. Slock, "On the convergence behavior of the LMS and the normalized LMSalgorithms", *IEEE Transactions on Signal Processing*, vol. 41, no. 9, pp. 2811–2825, 1993.

[72] M. Montazeri and P. Duhamel, "A set of algorithms linking NLMS and block RLS algorithms", *IEEE Transactions on Signal Processing*, vol. 43, no. 2, pp. 444–453, 1995.

[73] J.G. Proakis, C.L. Nikias, C.M. Rader, F. Ling, M. Moonen, and I.K. Proudler, *Algorithms for statistical signal processing*, Prentice Hall PTR Upper Saddle River, NJ, USA, 2001.

[74] B. Widrow and M.A. Lehr, "30 years of adaptive neural networks: perceptron, Madaline, and back propagation", *Proceedings of the IEEE*, vol. 78, no. 9, pp. 1415–1442, 1990.

[75] Y. Zakharov and T.C. Tozer, "Multiplication-free iterative algorithm for LS problem", *Electronics Letters*, vol. 40, no. 9, pp. 567–569, 2004.

[76] Y. Zakharov and F. Albu, "Coordinate descent iterations in fast affine projection algorithm", *Signal Processing Letters, IEEE*, vol. 12, no. 5, pp. 353–356, 2005.

[77] J. Liu, B. Weaver, and G. White, "FPGA implementation of the DCD algorithm", *Communications Symposium, London, UK*, Sept. 2006.

[78] J. Liu, B. Weaver, G. White, and Y. Zakharov, "An FPGA based MVDR beamformer using dichotomous coordinate descent iterations", *IEEE International Conference on Communications (ICC'2007), Glasgow, to be presented*, 2007.

[79] M. Er and A. Cantoni, "Derivative constraints for broad-band element space antenna array processors", *IEEE Transactions on Acoustics, Speech, and Signal Processing*, vol. 31, no. 6, pp. 1378–1393, 1983.

[80] K. Buckley and L. Griffiths, "An adaptive generalized sidelobe canceller with derivative constraints", *IEEE Transactions on Antennas and Propagation [legacy, pre-1988]*, vol. 34, no. 3, pp. 311–319, 1986.

[81] S. Zhang and I. Thng, "Robust presteering derivative constraints for broadband antennaarrays", *IEEE Transactions on Signal Processing*, vol. 50, no. 1, pp. 1–10, 2002.

[82] B.D. Carlson, "Covariance matrix estimation errors and diagonal loading inadaptive arrays", *IEEE Transactions on Aerospace and Electronic Systems*, vol. 24, no. 4, pp. 397–401, 1988.

[83] H. Cox, R.M. Zeskind, and M.M. Owen, "Robust adpative beamforming", *IEEE Trans. Acoust., Speech, Signal Processing*, vol. 35, no. 10, pp. 1365–1376, 1987.

[84] C.C. Lee and J.H. Lee, "Robust adaptive array beamforming under steering vector errors", *IEEE Transactions on Antennas and Propagation*, vol. 45, no. 1, pp. 168–175, 1997.

[85] S.A. Vorobyov and A. Luo, "Robust adaptive beamforming using worst-case performance optimization: a solution to the signal mismatch problem", *IEEE Transactions on Signal Processing*, vol. 51, no. 2, pp. 313–324, 2003.

[86] R.G. Lorenz and S.P. Boyd, "Robust minimum variance beamforming", *IEEE Transactions on Signal Processing*, vol. 53, no. 5, pp. 1684–1696, 2005.

[87] J. Li, P. Stoica, and Z. Wang, "On robust Capon beamforming and diagonal loading", *IEEE Transactions on Signal Processing*, vol. 51, no. 7, pp. 1702–1715, 2003.

[88] M. Bengtsson and B. Ottersten, "Optimal downlink beamforming using semidefinite optimization", *Proc. 37th Annual Allerton Conference on Communication, Control, and Computing*, pp. 987–996, 1999.

[89] B.K. Chalise and A. Czylwik, "Robust downlink beamforming based upon minimum outage probability criterion", *Global Telecommunications Conference, 2004. GLOBECOM'04. IEEE*, vol. 6.

[90] R.J. Mailloux, "Covariance matrix augmentation to produce adaptive array patterntroughs", *Electronics Letters*, vol. 31, no. 10, pp. 771–772, 1995.

[91] M. Zatman, "Production of adaptive array troughs by dispersion synthesis", *Electronics Letters*, vol. 31, no. 25, pp. 2141–2142, 1995.

[92] J.R. Guerci, "Theory and application of covariance matrix tapers for robustadaptive beamforming", *IEEE Transactions on Signal Processing*, vol. 47, no. 4, pp. 977–985, 1999.

[93] H. Song, W.A. Kuperman, W.S. Hodgkiss, and P. Gerstoft, "Null broadening with snapshot-deficient covariance matrices in passive sonar", *IEEE Journal on Oceanic Engineering,*, vol. 28, no. 2, pp. 250–261, 2003.

[94] H.L. Van Trees, *Optimum array processing*, Wiley-Interscience New York, 2002.

[95] R.J. Mailloux, *Phased array antenna handbook*, Artech House Boston, 1994.

[96] R.S. Elliott, *Antenna theory and design*, Prentice-Hall Englewood Cliffs, NJ, 1981.

[97] J. Thornton, D. Grace, M.H. Capstick, and T.C. Tozer, "Optimizing an array of antennas for cellular coverage from a high altitude platform", *IEEE Transactions on Wireless Communications*, vol. 2, no. 3, pp. 484–492, 2003.

[98] "Preferred characteristics of systems in the FS using high altitude platforms operating in the Bands 47.2–47.5 GHz and 47.9–48.2 GHz ", *International Telecommunications Union, 2000, Also ITU-R S*, vol. 672.

[99] "Resolution 145 (WRC-03) and radio regulations footnotes 5.537 A and 5.543 A", *World Radiocommunication Conference, WRC-03, Geneva*, 2003.

[100] M. Nofal, M. Hadhood, M. Dessouky, and Y. Albagory, "A novel cellular structure for stratospheric platform mobile communications", *Radio Science Conference, 2002.(NRSC 2002). Proceedings of the Nineteenth National*, pp. 354–362, 2002.

[101] S. Faruque, *Cellular mobile systems engineering*, Artech House Boston, 1996.

[102] R. Prasad, *Universal wireless personal communications*, Artech House, Inc. Norwood, MA, USA, 1998.

[103] Z. Xu, Y. Zakharov, and G. White, "Vertical antenna array and spectral reuse for ring-shaped cellular coverage from high altitude platform", *the Loughborough Antennas and Propagation Conference (LAPC), Loughborough, UK.*, April 2006.

[104] A. Abbaspour-Tamijani and K. Sarabandi, "An affordable millimeter-wave beam-steerable antenna using interleaved planar subarrays", *IEEE Transactions on Antennas and Propagation*, vol. 51, no. 9, pp. 2193–2202, 2003.

[105] G.L. Stuber, *Principles of mobile communication*, Kluwer Academic Publishers Norwell, MA, USA, 1996.

[106] M.S. Lobo, L. Vandenberghe, S. Boyd, and H. Lebret, "Applications of second-order cone programming", *Linear Algebra and Its Applications*, vol. 284, no. 1-3, pp. 193–228, 1998.

[107] L. Vandenberghe and S. Boyd, "Semidefinite programming", *SIAM Review*, vol. 38, no. 1, pp. 49–95, 1996.

[108] Z. Xu and Y. Zakharov, "Modified null broadening adaptive beamforming: constrained optimisation approach", *Electronics Letters*, vol. 43, no. 3, pp. 145–146, 2007.

[109] S. Stergiopoulos, *Advanced signal processing handbook*, CRC Press Boca Raton, FL, 2000.

[110] M. Schubert and H. Boche, "Solution of the multiuser downlink beamforming problem with individual SINR constraints", *IEEE Transactions on Vehicular Technology*, vol. 53, no. 1, pp. 18–28, 2004.

[111] Z. Luo and W. Yu, "An introduction to convex optimization for communications and signal processing", *IEEE Sel. Area Commun.*, , no. 24 (8), pp. 1426–1438, 2006.

[112] Z. Xu, Y. Zakharov, and G. White, "Antenna array optimisation using semidefinite programming for cellular communications from HAPs", *Electronics Letters*, vol. 43, no. 2, pp. 67–69, 2007.

[113] S.D. Prince, S.N. Goward, and N.P. Hanan, "Estimation of global primary production using NOAA/NASA Pathfinder AVHRR land data set", *IGARSS 95*, vol. 2, pp. 1000–1002, July 1995.

[114] D. Zimmermann, J. Baumann, A. Layh, F. Landstorfer, R. Hoppe, and G. Wolfle, "Database correlation for positioning of mobile terminals in cellular networks using wave propagation models", *Vehicular Technology Conference, 2004. VTC2004-Fall. 2004 IEEE 60th*, vol. 7, 2004.

[115] H. Laitinen, J. Lahteenmaki, T. Nordstrom, and V.T.T.I. Technol, "Database correlation method for GSM location", *Vehicular Technology Conference, 2001. VTC 2001 Spring. IEEE VTS 53rd*, vol. 4, 2001.

[116] B. Li, S. Zhou, M. Stojanovic, and L. Freitag, "Pilot-tone based ZP-OFDM Demodulation for an Underwater Acoustic Channel", *OCEANS 2006*, pp. 1–5, 2006.

[117] T. Collins, P. Atkins, C. Bongiovanni, J.J. Davies, S. Dunn, and S.A. Pointer, "Using continuous additive training sequences for high rate, Doppler tolerant communications", *The Journal of the Acoustical Society of America*, vol. 109, pp. 2477, 2001.

[118] Z. Xu, Y. Zakharov, and V.P. Kodanev, "Space-time signal processing of OFDM signals in fast-varying underwater acoustic channel", *Oceans'07 IEEE Aberdeen, accepted*, Feb 2007.

[119] T.H. Eggen, A.B. Baggeroer, and J.C. Preisig, "Communication over Doppler spread channels. Part I: Channel andreceiver presentation", *Oceanic Engineering, IEEE Journal of*, vol. 25, no. 1, pp. 62–71, 2000.

[120] B.S. Sharif, J. Neasham, O.R. Hinton, and A.E. Adams, "A computationally efficient Doppler compensation system forunderwater acoustic communications", *Oceanic Engineering, IEEE Journal of*, vol. 25, no. 1, pp. 52–61, 2000.

[121] Z. Xu and G. White, "Optimizing the beam pattern of high altitude platform antenna arrays", *PostGraduate Symposium on the Convergence of Telecommunications, Networking and Broadcasting (PGNET2005), Liverpool, UK.*, June 2005.

[122] Z. Xu, Y. Zakharov, and G. White, "Beampattern optimization for downlink cellular communications from High Altutude Platforms", *First HAPCOS-COST297 Workshop, York, UK.*, Oct. 2006.

[123] H. Boche and M. Schubert, "Resource allocation in multiantenna systems-achieving max-min fairness by optimizing a sum of inverse SIR", *IEEE Transactions on Signal Processing*, vol. 54, no. 6 Part 1, pp. 1990–1997, 2006.

[124] D. Gerlach and A. Paulraj, "Adaptive transmitting antenna methods for multipath environments", *Global Telecommunications Conference, 1994. GLOBECOM'94.'Communications: The Global Bridge'., IEEE*, pp. 425–429.

[125] D. Gerlach and A. Paulraj, "Base station transmitting antenna arrays for multipath environments", *Signal Processing*, vol. 54, no. 1, pp. 59–73, 1996.

Publications

JOURNAL

1. Z. Xu and Y. Zakharov, "Modified null broadening adaptive beamforming: a constrained optimisation approach", *Electronics Letters*, vol. 43, no. 3, pp. 145-146, 2007.

2. Z. Xu, Y. Zakharov, and G. White, "Antenna array optimisation using semidefinite programming for cellular communications from HAPs", *Electronics Letters*, vol. 43, no. 2, pp. 67-69, 2007.

3. Z. Xu, G. White, and Y. Zakharov, "Optimisation of beam pattern of high-altitude platform antenna using conventional beamforming", *IEE Proceedings-Communications*, vol. 153, pp. 865, 2006.

CONFERENCE

1. Z. Xu, Y. Zakharov, and V.P. Kodanev, "Space-time signal processing of OFDM signals in fast-varying underwater acoustic channel", *Oceans'07 IEEE Aberdeen, accepted*, Feb 2007.

2. Z. Xu, Y. Zakharov, and G. White, "Beampattern optimization for downlink cellular communications from High Altitude Platforms", *First HAPCOS-COST297 Workshop*, York, UK., Oct. 2006.

3. Z. Xu, Y. Zakharov, and G. White, "Vertical antenna array and spectral reuse for ring-shaped cellular coverage from high altitude platform", *the Loughborough Antennas and Propagation Conference (LAPC)*, Loughborough, UK., April 2006.

4. Z. Xu and G. White, "Optimizing the beam pattern of high altitude platform antenna arrays", *PostGraduate Symposium on the Convergence of Telecommunications, Networking and Broadcasting (PGNET2005)*, Liverpool, UK., June 2005.